

የኢፌዴሪ የቴክኒክና ሙያ ስልጠና ኢንስቲትዩት
FDRE TECHNICAL & VOCATIONAL TRAINING INSTITUTE

TECHNICAL AND VOCATIONAL TRAINING INSTITUTION (TVTI)

School of Graduate Studies

FACULTY OF ELECTRICAL AND ELECTRONICS TECHNOLOGY

INFORMATION AND COMMUNICATION TECHNOLOGY

(DEPARTMENT OF ELECTRICAL AND ELECTRONICS TECHNOLOGY)

Performance Enhancement of Hexagonal Microstrip Antenna Arrays at 28 GHz Using Metamaterials for 5G Applications

A Thesis Submitted in Partial Fulfillment of the Requirements for the Degree of Master of Science (MSc) in Electronics Communication Technology

By:

Yonas Bizuayehu Kassa (TTMR/237/16)

Advisor:

Anand Anbalagan, PhD

June 2026

Addis Ababa, Ethiopia



የኢፌዴሪ የቴክኒክና ሙያ ስልጠና ኢንስቲትዩት
FDRE TECHNICAL & VOCATIONAL TRAINING INSTITUTE

Performance Enhancement of Hexagonal Microstrip Antenna Arrays at 28 GHz Using Metamaterials for 5G Applications

A Thesis submitted to

TECHNICAL AND VOCATIONAL TRAINING INSTITUTION (TVTI)

FACULTY OF ELECTRICAL AND ELECTRONICS TECHNOLOGY AND INFORMATION AND COMMUNICATION TECHNOLOGY
(DEPARTMENT OF ELECTRICAL AND ELECTRONICS TECHNOLOGY)

In partial fulfillment of the requirements for the degree

Masters of Science in Electronics Communication Technology

By:

Yonas Bizuayehu Kassa (TTMR/237/16)

Advisor:

Anand Anbalagan, PhD

DECLARATION

I hereby declare that this thesis entitled "Performance Enhancement of Hexagonal Microstrip Antenna Arrays at 28 GHz Using Metamaterials for 5G Applications" is my original work, has not been submitted for a degree in this or any other university and all sources of material used for this thesis work have been duly acknowledged.

Name: - Yonas Bizuayehu Kassa (TTMR/237/16)

Signature: - _____

Place: - Addis Ababa

Date of submission: - _____

This thesis has been, submitted for examination with approval as a TVTI advisor.

Advisor Name	Signature	Date
Dr. Anand Anbalagan		_____
Name of Co−Advisor	Signature	Date
_____	_____	_____

TECHNICAL AND VOCATIONAL TRAINING INSTITUTION (TVTI)

FACULTY OF ELECTRICAL, ELECTRONICS TECHNOLOGY, INFORMATION, AND COMMUNICATION TECHNOLOGY

(DEPARTMENT OF ELECTRICAL AND ELECTRONICS TECHNOLOGY)

Final Thesis on

Performance Enhancement of Hexagonal Microstrip Antenna Arrays at 28 GHz Using Metamaterials for 5G Applications

By:

Yonas Bizuayehu Kassa (TTMR/237/16)

APPROVED BY EXAMINING BOARD

Advisor Name	Signature	Date
Dr. Anand Anbalagan		
Name of Co−Advisor	Signature	Date
Name of the Internal Examiner	Signature	Date
Yosef Kefyalew (Ph.D.)		July 30, 2026
Name of the External Examiner	Signature	Date
Dr. Muluneh Meknonnen		July 30, 2026
Name of the Chairperson	Signature	Date

Abstract

5G wireless systems aim to provide high data rates and low latency, which has increased the use of the millimeter-wave band where large bandwidth is available. However, antenna design at millimeter-wave frequencies is challenging because the antenna must be compact while still providing high gain and wide bandwidth. For this reason, this thesis designs and investigates a 28 GHz hexagonal microstrip patch antenna array for 5G applications. The design is developed step by step: first a single hexagonal patch, then a 1×2 array and finally a 1×4 array. The 1×4 array is excited using an inset microstrip-line feed and a corporate microstrip feed network with quarter-wave impedance transformers is employed to achieve 50 Ω matching and in-phase power division. The main focus is the final 1×4 design, where a Complementary Split-Ring Resonator is etched into the ground plane to improve bandwidth while maintaining high realized gain. The antenna is built on Rogers RT/duroid 5880 ($\varepsilon_r = 2.2, \tan\delta = 0.0009, h = 0.254$ mm) with copper metallization and is simulated using ANSYS HFSS 2024. The final 1×4 CSRR-integrated array has a compact size of 21 mm $\times$ 30 mm. Around 28 GHz, the simulated antenna achieves a realized gain of 12.88 dBi, and a minimum reflection coefficient of approximately -25 dB ($S_{11} \approx -25$ dB) at 28 GHz. The achieved -10 dB impedance bandwidth is 1.638 GHz ($27.04 - 28.68$ GHz), and the total efficiency reaches 98.83%. These results show that etching a CSRR into the ground plane can significantly increase bandwidth without reducing realized gain, indicating the potential suitability of the proposed antenna for 28 GHz 5G millimeter-wave communication systems.

Keywords: millimeter-wave, Complementary Split-Ring Resonator (CSRR), microstrip patch antenna, Rogers RT/duroid 5880, 5G

Acknowledgment

First, I would like to thank Almighty God for giving me the strength, wisdom, and guidance to complete this thesis.

I Would like to express sincere thanks to my thesis advisor, **Dr. Anand Anbalagan**, for his assistance in choosing the thesis title, ongoing support, wise academic counsel, and direction throughout this thesis effort. He has taught many things, not only has he taught academic knowledge but also critical thinking, dedication, and motivation in all spheres. Really, appreciate his understanding of LaTeX and the way he presents the study technique. Also, want to thank all of the postgraduate communication systems technology teachers in the subject of ECT for their excellent instruction and development of research insight. Finally, want to express appreciation to friends and family for their support as worked on thesis and for their love.

Table of Contents

Abstract iii

Acknowledgment iv

List of Figures viii

List of Tables x

List of Acronyms xi

CHAPTER ONE 1

Introduction 1

1.1. Background of the study 1

1.1.1. 5G Millimeter Wave Communication 1

1.1.2. Microstrip Patch Antennas for 5G 2

1.1.3. Metamaterial for Enhanced Microstrip Antenna Performance 2

1.2. Statement of the problem 3

1.3. Objective of thesis 3

1.3.1. General Objective 3

1.3.2. Specific Objective 3

1.4. Methodology 4

1.5. Scope of the thesis 5

1.6. Significance of the study 6

1.7. Thesis contribution 7

1.8. Thesis organization 7

CHAPTER TWO 9

Literature Review 9

2.1. Summary of literature reviews 17

CHAPTER THREE 19

Microstrip Array Antenna 19
3.1. Microstrip Antenna Basics 19
3.1.1. Advantages and Disadvantages 19
3.1.2. Working Principle of Single Element Rectangular MPA 20
3.1.3. Feeding Techniques 20
3.2. Antenna parameters 24
3.3. Metamaterials 31
3.3.1. Classification of Metamaterial 31
3.3.2. Basic Properties of Metamaterial 32
3.3.3. Different types of Metamaterial Structures 34
3.3.4. The effects of applying metamaterials in antenna design 35
CHAPTER FOUR 36
Design Hexagonal Microstrip antenna 36
4.1. Antenna Design Specification 36
4.2. Design Procedure 36
4.2.1. Design Calculations of Single Hexagonal Microstrip Patch Antenna 36
4.2.2. Design Calculations of 1×2 Hexagonal Microstrip Patch Antenna Array 42
4.2.3. Design 1×4 Hexagonal Microstrip Patch Antenna Array without CSRR 44
4.2.4. Design 1×4 Hexagonal Microstrip Patch Antenna Array with Circular CSRR 46
4.3. Optimization Algorithm (HFSS Optimetrics) 48
CHAPTER FIVE 50
Simulation Result and Discussion 50
5.1. Antenna Design Simulation Result and Discussion 50
5.1.1. Hexagonal Single Microstrip Patch Antenna 50
5.1.2. Hexagonal $\mathbf{1 \times 2}$ microstrip patch antenna array 54

5.1.3. Hexagonal 1 × 4 microstrip patch antenna array 58

5.1.4. Hexagonal $\mathbf{1 \times 4}$ microstrip patch antenna with CSRR 63

5.1.5. Comparison of Single, $\mathbf{1 \times 2}$, and $\mathbf{1 \times 4}$ Hexagonal Arrays with and Without CSRR 70

5.2. Performance Comparison with Related Works 71

CHAPTER SIX 72

Conclusion and Future Work 72

6.1. Conclusion 72

6.2. Future Work 73

Reference 74

Appendix A 82

Appendix B 86

List of Figures

Figure 1. 1 flow chart of the thesis work 5
Figure 3. 1 Types of microstrip line feed. 21
Figure 3. 2 Coaxial (Probe) feed method 22
Figure 3. 3 Proximity coupling feed method 22
Figure 3. 4 Aperture coupled aperture feeding. 23
Figure 3. 5 Radiation Pattern. 24
Figure 3. 6 Bandwidth of an Antenna. 28
Figure 3. 7 polarization schemes. 29
Figure 3. 8 Classification of materials based on the value of effective medium parameters. 32
Figure 3. 9 Left: Right-Handed System and Right: Left-Handed System 34
Figure 3. 10 Topology of SRR and Its Equivalent Circuit. 35
Figure 3. 11 Double circular CSRR and equivalent circuit. 35
Figure 5. 1 The proposed design of single hexagonal patch antenna 51
Figure 5. 2 The return loss **S11** of the single band hexagonal single patch antenna 52
Figure 5. 3 The radiation bandwidth of the single band hexagonal single patch antenna 52
Figure 5. 4 The standing wave ratio of the single band hexagonal single patch antenna 53
Figure 5. 5 The radiation efficiency of the single band hexagonal single patch antenna 53
Figure 5. 6 The gain and directivity of the single band hexagonal single patch antenna 54
Figure 5. 7 The proposed design of single band hexagonal 1×2 MPA 55
Figure 5. 8 The return loss of single band hexagonal 1×2 MPA 56
Figure 5. 9 The Radiation bandwidth of single band hexagonal 1×2 MPA 56
Figure 5. 10 The radiation efficiency and total efficiency of the single band hexagonal 1×2 MPA 57
Figure 5. 11 The standing wave ratio of the single band hexagonal 1×2 MPA 57
Figure 5. 12 The gain of hexagonal 1×2 MPA polar and 3D plot 58
Figure 5. 13 The proposed design of single band hexagonal $\mathbf{1 \times 4}$ MPA 59
Figure 5. 14 The return loss of single band hexagonal $\mathbf{1 \times 4}$ MPA 60
Figure 5. 15 The Radiation bandwidth of single band hexagonal $\mathbf{1 \times 4}$ MPA 61
Figure 5. 16 The radiation efficiency and total efficiency of the single band hexagonal $\mathbf{1 \times 4}$ MPA 61

Figure 5. 17 The standing wave ratio of the single band hexagonal $\mathbf{1 \times 4}$ MPA 62
Figure 5. 18 The gain and directivity of hexagonal $\mathbf{1 \times 4}$ MPA polar and 3D plot..... 63
Figure 5. 19 The proposed design of single band hexagonal 1×4 MPA with a CSRR..... 65
Figure 5. 20 The return loss of single band hexagonal 1×4 MPA with CSRR..... 66
Figure 5. 21 The Radiation Bandwidth of single band hexagonal 1×4 MPA with CSRR 66
Figure 5. 22 The radiation efficiency and total efficiency of single band hexagonal 1×4 MPA with CSRR 67
Figure 5. 23 The standing wave ratio of single band hexagonal 1×4 MPA with CSRR 67
Figure 5. 24 The gain and directivity of hexagonal 1×4 MPA with CSRR polar and 3D plot..... 68
Figure 5. 25 Surface current distribution of the 1 × 4 hexagonal MPA array without CSRR at 28 GHz. 69
Figure 5. 26 Surface current distribution of the 1 × 4 hexagonal MPA array with CSRR at 28 GHz. 69
Figure 5. 27 Enlarged surface current distribution around the CSRR rings and split-gap region at 28 GHz. 69
Figure A. 1 Overall 3D model of the hexagonal MPA array (patch, substrate, ground, feed network, and CSRR) 82
Figure A. 2 Top view of the hexagonal MPA array (patch and feed network) 82
Figure A. 3 Bottom view of the antenna (ground plane and CSRR structure) 82
Figure A. 4 Global Mesh Distribution Over the Hexagonal Patch Geometry 83
Figure A. 5 Localized Mesh Refinement on the CSRR Unit Cells. 83
Figure A. 6 Parametric analysis of CSRR outer radius $\boldsymbol{rout}$ on the reflection coefficient $\mathbf{S11}$ of the proposed 1 × 4 CSRR-loaded hexagonal microstrip antenna array 84
Figure A. 7 HFSS adaptive mesh convergence result for the final 1 × 4 CSRR-loaded hexagonal microstrip antenna array 84
Figure A. 8 Fabrication tolerance analysis of the CSRR split gap g and its effect on the reflection coefficient $\mathbf{S11}$..... 85

List of Tables

Table 2. 1 Summary of literature reviews 18
Table 3. 1 Comparison of different feeding techniques based on different characteristics 23
Table 4. 1 Antenna design specification for Hexagonal Microstrip Antenna 36
Table 4. 2 summarizes the key geometric dimensions used to define the double circular CSRR etched into the ground plane. 48
Table 5. 1 Calculated dimension for hexagonal single patch antenna 51
Table 5. 2 Calculated dimension for hexagonal 1×2 microstrip patch antenna 55
Table 5. 3 Calculated dimension for hexagonal 1×4 microstrip patch antenna 59
Table 5. 4 Calculated dimension for hexagonal 1×4 microstrip patch antenna with a CSRR 64
Table 5. 5 Comparison of Single, 1×2, and 1×4 Hexagonal Arrays With/Without CSRR 70
Table 5. 6 Percentage Improvement of Single, 1×2, and 1×4 Hexagonal Arrays With/Without CSRR 71
Table 6. 1 HFSS Simulation Settings Used in This Work 86
Table 6. 2 Initial Calculated and Optimized Values of the Proposed Single Hexagonal MPA 86
Table 6. 3 Initial Calculated and Optimized Values of the Proposed 1×2 Hexagonal MPA Array. 87
Table 6. 4 Initial Calculated and Optimized Values of the Proposed 1×4 Hexagonal MPA Array. 87
Table 6. 5 Initial Calculated and Optimized Values of the Proposed 1×4 Hexagonal MPA Array with CSRR. 88

List of Acronyms

5G	Fifth Generation
AMC	Artificial Magnetic Conductor
ANSYS	ANSYS Simulation Platform
BW	Bandwidth
CST	Computer Simulation Technology (Microwave Studio/Studio Suite)
CSRR	Complementary split ring resonator
DBi	Decibels relative to isotropic radiator
DGS	defected Ground Structure
DNG	Double Negative
ECT	Electronics Communication Technology
e_o	Total Efficiency
e_c	Conduction Efficiency
e_{cd}	Radiation Efficiency
e_d	Dielectric Efficiency
e_r	Reflection (Mismatch) Efficiency
FR-4	Flame Retardant 4 (PCB substrate material)
GHz	Gigahertz
HFSS	High Frequency Structure Simulator
ISM	Industrial, Scientific and Medical
MIMO	Multiple Input Multiple Output
mm-Wave	Millimeter-Wave
MPA	Microstrip Patch Antenna
MRPA	Microstrip Rectangular Patch Antenna
MSc	Master of Science
MSPAs	Microstrip Patch Antennas
MTM	Metamaterial
PCB	Printed Circuit Board
Pin	Total Input Power
QoS	Quality of Service
S_{11}	Reflection Coefficient / Return Loss parameter

SRR	Split Ring Resonator
TM01	Transverse Magnetic Mode (01)
TM10	Transverse Magnetic Mode (10)
TVTI	Technical and Vocational Training Institution
UWB	Ultra-Wideband
$U(\theta_\varphi)$	Radiation Intensity
VSWR	Voltage Standing Wave Ratio
Z_o	Characteristic Impedance of Transmission Line
Z_{in}	Input Impedance
Γ (Gamma)	Voltage Reflection Coefficient

CHAPTER ONE

Introduction

1.1. Background of the study

As wireless communication continues to expand, there is a growing demand for compact and low-profile antenna systems, which has increased research interest in microstrip patch antennas [1]. Wireless communication remains one of the most actively studied fields as researchers work to enhance efficiency and reliability in modern systems. Since antennas are responsible for transmitting and receiving electromagnetic signals, they play a fundamental role in the overall performance of wireless networks [2]. With the emergence of fifth-generation (5G) technology, millimeter-wave communication has become particularly important due to its ability to support extremely high data rates and dense device connectivity. As communication technologies advance, the number of wireless devices continues to increase, further emphasizing the need for efficient antenna structures capable of operating effectively in the mm-wave spectrum [3].

1.1.1. 5G Millimeter Wave Communication

Fifth-generation (5G) mobile communication networks have significantly influenced modern wireless technology by promising multi-gigabit data rates, enhanced reliability, ultra-low latency, and overall improvements in network capacity and efficiency [4]. As one of the most advanced developments in wireless communication, 5G continues to drive intensive research activity within the field [5]. Antenna design plays a crucial role in enabling these capabilities, particularly at high-frequency mm-wave bands such as 28 GHz, which is the focus of the proposed antenna investigated in this study [6]. Furthermore, 5G aims to provide stable, seamless, and continuous global connectivity, supporting the rapidly growing number of wireless devices [7]. Current research efforts are increasingly centered on millimeter-wave frequencies due to limitations in available lower-band spectrum resource [8]. Consequently, antenna array design has become a key area of interest for improving gain, radiation performance, and overall transmission characteristics in 5G systems [9].

1.1.2. Microstrip Patch Antennas for 5G

A wide variety of antenna types exist, including microstrip patch antennas, conical antennas, and helical antennas [10]. Among these, microstrip patch antennas are especially attractive due to their simple structure, which typically consists of a radiating patch on the top layer, a dielectric substrate in the middle, and a ground plane on the bottom [11]. Microstrip Patch Antenna (MSPA) technology is considered one of the most promising solutions for modern 5G wireless networks because of its low profile, lightweight nature, planar geometry, and cost-effective fabrication process[12][13][14]. The radiating patch, commonly made from conductive materials such as copper or gold, can be designed in various shapes to meet specific performance goals [15]. To enhance bandwidth, traditional shapes like rectangular and hexagonal patches have been modified into ring structures, while other studies have explored circular and octagonal geometries. Since antennas play an essential role in wireless transmission and reception, patch antennas have become increasingly important, particularly in demanding 5G applications [16][17].

1.1.3. Metamaterial for Enhanced Microstrip Antenna Performance

The term metamaterial originates from the Greek word “meta,” meaning beyond or altered, reflecting the concept of engineered materials with properties not found in nature [18]. In antenna engineering, metamaterials have attracted significant interest due to their ability to manipulate electromagnetic behavior through artificially structured unit cells. Techniques such as Complementary Split-Ring Resonator (CSRR) have been applied to reduce antenna size and enhance performance [19]. Metamaterials typically exhibit unusual characteristics, such as negative permittivity or permeability at specific resonant frequencies, enabling new ways to improve antenna operation [20]. Their use in microstrip antenna design offers several advantages, including size reduction and improvements in key parameters such as bandwidth, gain, and return loss [21]. Since these materials do not occur naturally, they are deliberately engineered to achieve the desired electromagnetic response [22]. In this study, a hexagonal patch incorporating a Complementary Split-Ring Resonator (CSRR) ground plane is considered for operation beyond the 28 GHz 5G band [23]. Various metamaterial structures can be tailored for different applications, with classifications typically based on the effective permittivity and permeability produced by their unit cell arrangements [18].

1.2. Statement of the problem

5G communication systems operating in the millimeter-wave band, particularly around 28 GHz, need compact antenna arrays that can provide good impedance matching, sufficient bandwidth, high realized gain, and acceptable radiation performance. Microstrip patch antennas are widely used for such applications because they are low-profile, compact, low-cost, and easy to integrate with communication devices. However, their narrow impedance bandwidth remains one of the main challenges, especially for wideband 5G millimeter-wave communication systems.

A previous study showed that a hexagonal microstrip patch antenna array can operate effectively at 28 GHz [24]. However, the bandwidth of the conventional hexagonal array still needs further improvement while keeping the antenna compact and maintaining high gain. Therefore, the main problem addressed in this thesis is how to improve the impedance bandwidth and matching performance of a 28 GHz 1 × 4 hexagonal microstrip antenna array without significantly reducing its realized gain.

To address this problem, this thesis investigates the use of a Complementary Split-Ring Resonator (CSRR) etched into the ground plane of the 1 × 4 hexagonal microstrip antenna array. The proposed design is analyzed using HFSS simulation and compared with the same 1 × 4 hexagonal array without CSRR. The comparison is based on reflection coefficient, −10 dB impedance bandwidth, realized gain, efficiency, VSWR, and radiation characteristics.

1.3. Objective of thesis

1.3.1. General Objective

- The general objective of this thesis is to design a hexagonal microstrip antenna array at 28 GHz and enhance its performance using CSRR-based metamaterial techniques for 5G applications.

1.3.2. Specific Objective

- To design a hexagonal microstrip patch antenna (single element) operating at 28 GHz.
- To design and model 1 × 2 and 1 × 4 hexagonal antenna arrays at 28 GHz using the same substrate and feeding approach.

- To integrate a double circular CSRR into the ground plane of the 1×4 array to improve impedance bandwidth while maintaining high realized gain.
- To simulate and evaluate all designs in HFSS in terms of S_{11}, -10 dB impedance bandwidth ($|S_{11}| < -10$ dB), gain and total/radiation efficiency.
- To compare the results of the baseline arrays and the CSRR-integrated array using the above metrics to quantify the improvement**.**

1.4. Methodology

A structured, simulation-based method was used in this study. First, earlier research on 28 GHz microstrip antennas, CSRR-based metamaterials, and 5G millimeter-wave designs was reviewed. From the review, it was noted that patch antennas at millimeter-wave often have narrow bandwidth, and common ways to improve bandwidth include ground plane modifications (such as CSRR/DGS) and slot-based techniques. Next, the antenna was built step by step for fair testing and easy comparison. A single hexagonal patch was designed first, then expanded to a 1×2 array, and finally to a 1×4 array using the same substrate and design setup. This staged approach helps confirm that each upgrade is working correctly before moving to the next stage. After the baseline 1×4 array was ready, a double circular CSRR was added by etching it into the ground plane. The idea is that the CSRR creates a second resonance near the main 28 GHz resonance. When the two resonances overlap, the antenna achieves a wider -10 dB impedance bandwidth (the region where $|S_{11}| < -10$ dB while keeping high realized gain. All versions (single, 1×2 and 1×4 without CSRR) and 1×4 with CSRR were simulated in ANSYS HFSS 2024 around 28 GHz. The performance was evaluated using $S_{11} < -10$ dB bandwidth, realized gain, efficiency, and radiation pattern stability. Finally, the CSRR-loaded results were compared with the baseline designs to clearly show the improvement gained from CSRR-integration. The overall workflow of this research is depicted in Figure 1.1.

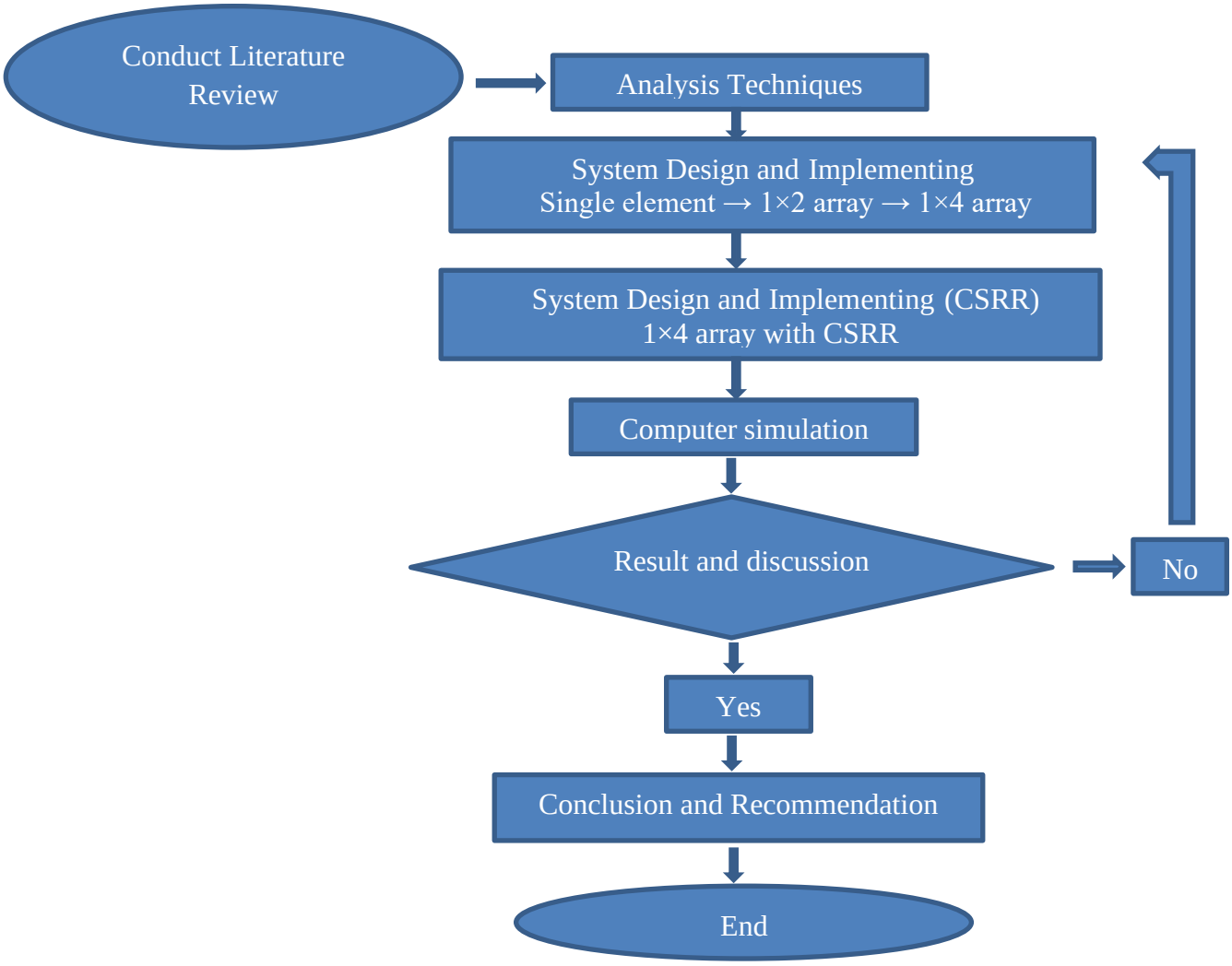


Figure 1. 1 flow chart of the thesis work

1.5. Scope of the thesis

This thesis focuses on designing, improving, and testing a compact hexagonal microstrip antenna for 5G operation at 28 GHz. The antenna is developed in clear stages starting from a single hexagonal element, then expanding to a 1×2 array, and finally a 1×4 array. The main goal is to achieve better bandwidth and compact footprint while still keeping a high gain. To do this, the study uses a metamaterial approach by adding circular CSRR (Complementary Split Ring Resonator) patterns, especially by etching them into the ground plane of the 1×4 array.

The scope includes

- Designing the antenna in stages single element $\longrightarrow 1 \times 2$ array $\longrightarrow 1 \times 4$ array for 28 GHz operation.
- Choosing a suitable low-loss substrate for millimeter-wave performance at 28 GHz.
- Designing the feeding structure needed to excite the array elements and achieve good matching.
- Adding circular CSRR structures (mainly in the ground plane) to support bandwidth improvement and miniaturization.
- Running full-wave simulations in ANSYS HFSS 2024 and evaluating S_{11}/return loss, bandwidth, realized gain, and radiation patterns.
- Comparing the conventional designs (without CSRR) against the CSRR-enhanced 1×4 design to clearly show what improvements CSRR provides.

This thesis is limited to simulation-based results and aims to prove that using CSRR metamaterial structures can produce a compact, high-performance antenna suitable for next-generation 5G millimeter-wave communication modules.

1.6. Significance of the study

The contribution of this thesis is creating a clear antenna design patch starting from a single hexagonal patch, then building it into 1×2 and 1×4 array and proving its performance through simulation at 28 GHz. It also shows how adding circular CSRR patterns etched in the ground plane of the 1×4 array can make the antenna smaller and give it a wider bandwidth, while still keeping a high realized gain. The findings of this research will benefit antenna designers and the telecommunication industry by helping them develop efficient, low-cost, and high-performance communication modules that can be used in next-generation mobile devices and other 5G millimeter-wave systems.

1.7. Thesis contribution

The contribution of this work is summarized as follows

- It develops a compact hexagonal microstrip antenna for 28 GHz 5G and shows its growth in stages single element $\longrightarrow 1 \times 2$ array $\longrightarrow 1 \times 4$ array.
- It introduces a metamaterial approach using circular CSRR patterns etched into the ground plane, which helps the antenna become smaller and achieve wide bandwidth, while still keeping high realized gain, compared to normal designs.
- It provides a complete design and testing workflow in ANSYS HFSS 2024, including substrate choice, geometry building, feed design, boundary setup and array configuration.
- It demonstrates that ground plane CSRR can improve impedance behavior and control resonance, which supports bandwidth improvement and compact design at 28 GHz.
- It analyzes and compares important antenna results S_{11}, bandwidth, gain, directivity, radiation efficiency, total efficiency and voltage standing wave ratio (VSWR) between the conventional antenna and CSRR-enhanced antenna to clearly show the benefits.
- It establishes a clear and practical design method that can guide future work and help industry build efficient, low-cost, high-performance 5G millimeter-wave antenna modules for next-generation devices.

1.8. Thesis organization

The next parts cover the remainder of the thesis:

- Chapter 2 gives the literature review. It talks about microstrip antennas, 5G millimeter-wave antennas at 28 GHz, and how metamaterials like CSRR and used to improve bandwidth, gain, and reduce antenna size. It also summarizes recent related research.
- Chapter 3 explains the theoretical background. It covers the basic ideas of microstrip antenna arrays, the key antenna parameters (like S_{11}, bandwidth, gain, directivity, efficiency), and the main concepts of metamaterial, especially how CSRR affects antenna performance.
- Chapter 4 describes the design work. It shows how the hexagonal antenna is built step by step: single element $\longrightarrow 1 \times 2$ array $\longrightarrow 1 \times 4$ array, and then improved by adding

circular CSRR etched into the ground plane. It includes the design procedure, feeding approach, and how the model is set up in HFSS.

- Chapter 5 presents the results and discussion. It shows the HFSS simulation results at 28 GHz and compares the normal designs with the CSRR-enhanced design using S_{11}, bandwidth, gain, directivity, efficiency and VSWR.
- Chapter 6 gives the summary, conclusion and recommendations. It wraps up the main findings, explains what was achieved, and suggests ideas for future improvements and further research.

CHAPTER TWO

Literature Review

This chapter reviews the literature most relevant to the enhancement of hexagonal microstrip antenna arrays operating at 28 GHz using metamaterials for 5G applications. The related works are described as follows.

In [25] Darboe et al. presented a compact rectangular microstrip patch antenna designed for 28 GHz 5G applications. Their study aimed to develop a low-profile, lightweight, and easily integrated antenna suitable for millimeter-wave communication systems. The simulated design resonated at about 27.954 GHz and achieved a return loss of −13.48 dB, bandwidth of 847 MHz, gain of 6.63 dB, VSWR of 1.5376, and radiation efficiency of 70.18 %.

In [26] Yusuf and Ali developed a compact rectangular microstrip patch antenna loaded with CSRRs for 26 GHz and 28 GHz 5G applications. The antenna was built on Rogers RT5880 substrate and simulated in CST Studio Suite. By adding CSRR slots to the ground plane, the researchers reduced the antenna size by about 20 % and improved the 28 GHz bandwidth from 0.81 GHz to 1.03 GHz. The CSRR-loaded antenna also achieved a gain of 9.79 dB, VSWR of 1.16, and efficiency of 92 %. This shows that CSRR loading is an effective technique for improving bandwidth and reducing antenna size without using a larger array structure. However, since the study was based only on simulation, practical fabrication and measurement are still required to confirm its real-world performance (Yusuf & Ali, 2025).

Author [27] Kumawat and Joshi developed a dual-band elliptical microstrip patch antenna array for 5G applications at 28 GHz and 38 GHz. The design used Rogers RT/Duroid 5880 substrate and was simulated in CST Microwave Studio. In the first stage, a single elliptical patch produced gains of 6.81 dBi at 28 GHz and 7 dBi at 38 GHz. To obtain higher gain, the authors extended the design into a four-element multilayer array using a corporate feeding network and coaxial-to-microstrip transition. The array significantly improved the gain, reaching 11.9 dBi at 28 GHz and 12.2 dBi at 38 GHz. This shows that array configuration is effective for improving antenna performance in millimeter-wave 5G systems. However, the multilayer structure and feeding network make the design more complex, so simpler enhancement methods may still be needed for compact and practical 5G antenna designs (Kumawat & Joshi, 2021).

Author [28] Didi et al. designed a compact rectangular microstrip patch antenna with a rectangular slot for 28 GHz 5G applications. The antenna was built on Rogers RT/Duroid 5880 substrate and simulated using both HFSS and CST software to verify the results. By adding the slot to the patch structure, the antenna performance improved. It achieved a resonant frequency of 27.97 GHz, a return loss of −20.95 dB, a bandwidth of 1.06 GHz, a gain of 7.5 dB, a VSWR of 1.197, and an efficiency of 99.83 %. The study shows that slot-loading is an effective and straightforward way to improve bandwidth and impedance matching while keeping the antenna compact. However, since the work only involved simulation, practical fabrication and measurement are still needed to confirm its real-world performance.

In the author [29] Kamal et al. proposed a compact hook-shaped antenna for 28 GHz 5G millimeter-wave applications. The antenna was designed on Rogers RT/Duroid 5880 substrate, and the single element achieved about 3.59 dBi gain with high radiation efficiency. To improve the gain, the design was extended into a four-element planar array, increasing the gain to 10.3 dBi while maintaining a compact size. The fabricated prototype showed good agreement with the simulated results, which strengthens the practical value of the design. However, the array structure is more complex than a single patch antenna, so simpler compact designs may still be explored for 5G applications (Kamal et al., 2021).

Author [30] Ibrahim et al. developed a high-gain 1 × 4 slotted antenna array for 28 GHz 5G communication. The fabricated antenna achieved a measured gain of 13.1 dBi at 28 GHz, radiation efficiency of 83.05 %, and a front-to-back ratio between 15 and 20 dB. The measured results also showed good agreement with the simulation results, confirming the practical performance of the design. This study shows that combining a slotted array with an AMC reflector is effective for improving radiation characteristics in 5G millimeter-wave antennas.

The author [32] Khouyaoui et al. developed and optimized a 28 GHz rectangular microstrip patch antenna array for 5G communication applications. The antenna was designed on Rogers RT5880 substrate and transformed from a single patch element into 2 × 1 and 4 × 1 array configurations to improve gain, bandwidth, and radiation efficiency. The final 4 × 1 array achieved a very low return loss of −61 dB near 27.9 GHz, wide impedance bandwidths of 2.1 GHz and 9.3 GHz, gain of 9.04 dBi, directivity of 9.35 dBi, VSWR below 2, and radiation efficiency above 94 %. These results show that increasing the array size can significantly improve antenna performance for high-data-

rate 5G systems. However, the work was mainly simulation-based, so fabrication and experimental validation are still needed to confirm its practical performance (Khouyaoui et al., 2025).

Author [33] Paul and Saha proposed a high-gain 1 × 2 rectangular microstrip patch array antenna for upper 28 GHz 5G applications. The proposed array covered a wide frequency range from 24.722 GHz to 30.171 GHz, with a center operating frequency of 26.72 GHz. It achieved a return loss of −30.747 dB, gain of 10.98 dB, directivity of 12.30 dBi, radiation efficiency of 81 %, and VSWR within the acceptable range of 1 to 2. These results show that the 1 × 2 array structure can improve gain and bandwidth for 5G millimeter-wave communication.

Author [6] presented a hexagon patch antenna and its array configurations for 28 GHz. The design was fabricated on a Rogers RT5880 substrate with dimensions of 8 mm by 8 mm. The 1 x 2 array had a size of 10 mm by 16 mm, and the 1 x 4 array was 13 mm by 32 mm, both based on the hexagon patch element. Three configurations were implemented and simulated using CST software. The single hexagon antenna achieved a gain of 7 dBi, VSWR of 1.259, efficiency of 81 %, angular width of 165.6 degrees, and a bandwidth of 0.637 GHz. The 1 x 2 array achieved a gain of 8.9 dBi, VSWR of 1.9, efficiency of 80 %, angular width of 48.2 degrees, and bandwidth of 0.554 GHz. The 1 x 4 array provided a gain of 12 dBi, VSWR of 1.45, efficiency of 82 %, angular width of 18.8 degrees, and a bandwidth of 0.45 GHz.

The authors [34] Ermiş and Demirci investigated different rectangular microstrip antenna designs operating at 28 GHz for 5G applications. The antennas were designed on Rogers RT/Duroid 5880 substrate and analyzed using ANSYS HFSS. To improve bandwidth, the authors applied defected ground structure (DGS) and stacked patch techniques to single, 1 × 2, and 1 × 4 array antennas. The results showed that these enhancement methods increased the bandwidth of the single antenna from 1.91 GHz to 3.45 GHz, while the 1 × 2 array achieved a wide bandwidth of 7.53 GHz with a gain of 10.36 dB. The 1 × 4 array provided the highest gain of 13.8 dB with 4.53 GHz bandwidth. These findings show that DGS and stacked patch techniques can effectively improve bandwidth and gain for 28 GHz 5G antennas. However, the added structures may increase design complexity and cause slight gain reduction due to additional losses (Ermiş & Demirci, 2023).

The Author in [4] Refaat et al. designed a compact tuned reconfigurable microstrip antenna for 5G mobile communication at 28 GHz and 38 GHz. The antenna was fabricated on Rogers RT/Duroid

5880 substrate and used PIN diode switches across slits in the patch and ground plane to control the operating frequency. Depending on the switching state, the antenna can operate at 28 GHz, 38 GHz, or both bands. The measured results showed good agreement with the simulation, achieving return losses of −38.8 dB and −37.2 dB, bandwidths of 1.53 GHz and 2.21 GHz, and gains of 6.95 dBi and 5.2 dBi at 28 GHz and 38 GHz, respectively. This study shows that frequency reconfiguration is useful for improving spectrum flexibility in 5G antennas. However, the use of switching elements may increase design complexity and requires careful fabrication and biasing for practical implementation (Refaat et al., 2023).

The author [35] Mungur and Duraikannan designed and analyzed 28 GHz microstrip patch antenna array for 5G communication system . The antenna was designed on Rogers RT/Duroid 5880 substrate and comparison was made between single patch, 2 × 1 array and 4 × 1 array. Quarter-wave transformers were employed for impedance matching and reflective material enhancement was studied to improve gain. The results showed that the gain of the antenna was increased by the increase of the array element number, where the 2 × 1 array reached about 10.07 dB and the 4 × 1 array reached 13.55 dB. The Rogers RT/Duroid 5880 has also been demonstrated to perform better than Taconic TLC and FR4 substrates. The results show that the array configuration and the choice of suitable substrate are important for improving the gain and efficiency of 28 GHz 5G antennas. However, the work mainly focused on simulation, so practical fabrication and measurement would be needed to confirm real-world performance (Mungur & Duraikannan, 2018).

Author in [36] Aboshosha et al. proposed a 28 GHz four-element rectangular microstrip patch array antenna for the future 5G mobile applications. This work has tackled the investigation of millimeter-wave communication enhancement based on the array structure to support higher data rate, spectrum efficiency and coverage. The antenna was designed on low cost FR-4 substrate which is suitable for practical and low cost 5G antenna development. This shows that the proposed array can achieve an acceptable impedance matching and wideband operation around the 28 GHz band. However, the work was largely simulation based and fabrication and measurement would be necessary to validate its practical performance in real 5G systems (Aboshosha et al., 2019).

Author [37] proposed a 1 x 4 antenna array for the 28 GHz (n257) frequency band. Using an antenna array is important in 5G millimeter-wave environments to overcome challenges like path loss, multi-path fading, and improve network capacity. It is vital to assess the shortcomings of

traditional communication methods, such as limited coverage, interference, and slow data rates, which can be effectively addressed with an array. A metamaterial-loaded antenna system provides a gain of 10.81 dB, 11.76 dB directivity, and 91.4 % efficiency at 28 GHz. This design demonstrates technological strength by using planar microstrip technology on a 1.6 mm thick Rogers 5880 substrate with a relative permittivity of 2.2. The array's specific features make it suitable for integration into the millimeter-wave frequency range.

Author [38] Ullah and Tahir proposed a broadband wire hexagon antenna array for future 5G communication in the 28 GHz band. The antenna was fabricated on a thin Rogers RT/Duroid 5880 substrate and used four hexagonal wire-loop elements excited by a 4-way feed network. The measured operating band covered 25.052 GHz to 34.923 GHz, providing a wide bandwidth of 9.871 GHz. The antenna also achieved a peak gain of 12.15 dBi, measured gain of 10.12 dBi at 28 GHz, and radiation efficiency above 85%.

The author [39] Fante and Gemeda have presented a broadband rectangular microstrip patch antenna for 28 GHz 5G wireless applications. The antenna is designed on Rogers RT/Duroid 5880 and simulated using CST Studio Suite. The authors employed the inset-feed structure, quarter-wavelength impedance matching, optimized antenna dimensions, and a partial ground plane to improve impedance matching and performance. The simulation results show that the proposed antenna has the return loss of -54.49 dB, bandwidth of 1.062 GHz, gain of 7.554 dBi, VSWR of 1.011, radiation efficiency of 98 % and sidelobe level of -18.4 dB. These results show that a simple rectangular patch antenna can be optimized to provide good bandwidth, high efficiency and compact size.

Author [40] Gemeda et al. designed and analyzed a rectangular microstrip patch antenna of 28 GHz for 5G communication system . The antenna is designed on FR-4 substrate and simulated using CST software. The proposed design return loss of -38.865 db, band width of 1.046 GHZ, gain of 7.587 dBi, directivity of 7.509 dBi, VSWR of 1.023 and radiation efficiency of 98.214 %. These results show that a simple rectangular patch antenna can be competitive for 28 GHz 5G applications if properly optimized. However, the work was simulation-based, and thus, the fabrication and measurement are still required to verify its practical performance (Gemeda et al., 2021).

Author [41] Ganesh et al. have developed a hexagonal frequency reconfigurable antenna for C-band 5G. They designed the antenna with a flexible frequency configuration which is important for modern 5G systems using small and optimally allocated spectrum. The hexagonal shape gives a simple and compact radiating structure, and the frequency reconfigurable feature enables the antenna to be used in different conditions rather than having multiple fixed antennas. These results indicate that reconfigurable antennas can be designed for C-band 5G. But, the practical performance may depend on switching losses, biasing complexity, and fabrication accuracy, so they need to be tested before being deployed in the real world (Ganesh et al.,2022).

The author in [42] presents a hexagonal-shaped patch antenna for future 5G applications. The use of a defected ground structure (DGS) in the bottom ground layer helps achieve wideband operation. A substrate integrated waveguide (SIW) structure is used to enhance the radiation characteristics of the hexagonal patch antenna. The design and simulation were conducted using the 3D EM simulator Ansys HFSS 19.1. The proposed antenna has a compact size of 1.25 λ0 by 1.12 λ0 mm² and operates in the frequency range of 25.90 to 44.20 GHz with a fractional bandwidth of 52.21 %. The peak gain of the proposed antenna is 8.52 dBi over the entire operating frequency band. Its compact size and simple structure make it an excellent candidate for 5G millimeter-wave applications.

Author [43] Obot et al. designed and simulated rectangular microstrip antenna arrays to improve gain performance compared with a single patch antenna. The study first developed a single inset-fed rectangular microstrip antenna and then extended it into 2 × 1 and 4 × 1 array configurations using a parallel feed network. The antennas were designed on Rogers RT/Duroid 5880 substrate and simulated in Ansoft HFSS at 2.4 GHz. The results showed that the single patch achieved a gain of 5.26 dB, while the 2 × 1 and 4 × 1 arrays improved the gain to 9.24 dB and 10.29 dB, respectively.

The author [44] Rifat et al. developed a 1 × 4 microstrip patch array antenna for 28 GHz5G millimeter wave communication using a single patch element and then upgraded to a planar 1 × 4 array to improve the gain and radiation characteristics. The antenna was constructed on Rogers RT5880 substrate with dielectric constant of 2.2 and loss tangent of 0.0009. The antenna had a bandbreite of 27.7–28.6 GHz, a return loss of about 34.83 dB, a 96 % efficiency of 93 %, and a gain of 5.1 dBi. When converted into a 1 × 4 array, the gain was 9.74 dBi at 27.5–28.8 GHz with

a radiation efficiency of 93 %. This suggests that an array structure with a 1 4 array can improve the gain while maintaining the same efficiency in 28 GHz 5G applications. But the array is larger than a single patch element, so considerations should be taken into account compactness and feeding network optimization (Rifat et al., 2023).

Author [23] Rifat et al. developed a 1 × 4 microstrip patch array antenna for 28 GHz5G millimeter wave communication using a single patch element and then upgraded to a planar 1 × 4 array to improve the gain and radiation characteristics. The antenna was constructed on Rogers RT5880 substrate with dielectric constant of 2.2 and loss tangent of 0.0009. The antenna had a bandbreite of 27.7–28.6 GHz, a return loss of about 34.83 dB, a 96 % efficiency of 93 %, and a gain of 5.1 dBi. When converted into a 1 × 4 array, the gain was 9.74 dBi at 27.5–28.8 GHz with a radiation efficiency of 93%. This suggests that an array structure with a 1 × 4 array can improve the gain while maintaining the same efficiency in 28 GHz 5G applications. But the array is larger than a single patch element, so considerations should be taken into account compactness and feeding network optimization (Rifat et al., 2023).These results show that the stacked approach can significantly improve the gain compared with a single antenna. However, the achieved bandwidth is still limited compared with wider 5G bandwidth requirements, so further optimization may be needed for broader 5G applications (Y. Natali and M. Larasati, 2019).

The author in [45] Agarwal and Prachi proposed a high-gain linear 1 × 4 X-slotted microstrip patch antenna array for 5G mobile technology at 38 GHz. The antenna was designed on Rogers RT/Duroid 5880 substrate and simulated using CST Studio. In the single-element design, an X-shaped slot was introduced on the patch to improve impedance matching, achieving a return loss of −24.25 dB, bandwidth of 1.48 GHz, and gain of 6.98 dB. To further enhance the gain, the authors extended the design into a 1 × 4 linear array using a corporate feeding network and quarter-wave transition lines. The array achieved a gain of 13.84 dB, return loss of −15.72 dB, and bandwidth of 800 MHz. These results show that combining slot loading with array configuration can significantly improve antenna gain for millimeter-wave 5G applications. However, the array design may increase feeding complexity and reduce bandwidth compared with the single element (Agarwal & Prachi, 2020).

The author [46] examined and confirmed the performance of the hexagonal fix receiving wire in terms of straight polarization. In this paper, a hexagonal fixed reception device was effectively

designed to operate at a frequency of 2.45 GHz. The S-parameter value is -23.7962 dB, the voltage standing wave ratio (VSWR) is 1.1237, the bandwidth is 4.1102 %, the 3-D radiation far field design gain is 4.5098 dBi, the Smith chart size value is 0.0646, the phase point is 73.2778, and the reactance value is 1.0298 + j0.1279. The experimental findings align closely with the theoretical predictions.

Author in [47] In this paper, Rana and Kaur designed and fabricated a hexagonal microstrip antenna using Koch fractal curves for wireless applications. Without inset cuts, the antenna had two bands, while the inset-cut antenna has four simulated resonant frequencies at 3.36 GHz, 5.61 GHz, 8.58GHz, and 9.48 GHz. The measured results also agree well with simulation and confirmed multiband operation. It shows good return loss, VSWR, bandwidth, and gain, reaching 11.70 dB at 9.48GHz. These findings show that Koch fractal geometry and inset feeding can improve multiband performance while keeping the antenna small. It is not suitable for 28 GHz millimeter-wave 5G (Rana& Kaur, 2018).

The author in [48] Saini et al. designed a hexagonal microstrip patch antenna with CPW/coaxial feeding for wireless communication applications. The study compared a simple hexagonal patch with an L-cut hexagonal patch to improve impedance bandwidth and circular polarization performance. The antenna was designed on an FR4 substrate and simulated using HFSS, with experimental verification. The simple hexagonal patch achieved an impedance bandwidth of 65.1 MHz and an average gain of 6.6 dB, while the L-cut design improved the impedance bandwidth to 359 MHz and increased the average gain to 6.9 dB. These results show that modifying the hexagonal patch with an L-cut can improve bandwidth, gain, and circular polarization performance. However, the design operates around 3.55–3.8 GHz, so it is more suitable for lower-frequency wireless applications than 28 GHz millimeter-wave 5G systems (Saini et al., 2016).

Author in [49] Kim and Kim proposed a dual-polarized broadband microstrip patch antenna for 5G mmWave antenna modules using a low-cost FR4 substrate. To reduce the high dielectric loss of FR4 and improve bandwidth, the authors introduced an air-cavity structure, proximity L-probe feeding, and parasitic patches. The single antenna achieved a measured bandwidth of 23–29 GHz with about 5 dBi gain, while the 1 × 4 array achieved 10 –11 dBi gain and good cross-polarization suppression. The design also supported dual polarization, making it suitable for massive MIMO applications. These results show that a low-cost FR4-based antenna can still achieve wideband 5G

mmWave performance when carefully optimized. However, the structure requires accurate fabrication and careful feeding design to maintain stable performance at high frequencies (Kim & Kim, 2021).

Author [50] Dejene compared the received signal strength of femtocell systems using rectangular and circular microstrip patch antennas designed at 2.55 GHz. Both antennas were designed on an FR4 substrate and simulated using HFSS, while the indoor received signal strength was analyzed using the Multi-Wall Multi-Floor propagation model. The results showed that the rectangular patch antenna achieved a higher gain of 3.6528 dB compared with 2.924 dB for the circular patch antenna. The study also showed that received signal strength decreases as the number of walls and floors increases. Overall, the rectangular microstrip patch antenna provided better received signal strength for indoor femtocell coverage than the circular antenna. However, the work mainly focused on indoor femtocell signal strength at 2.55 GHz, so it is not directly targeted at 28 GHz millimeter-wave 5G antenna design (Dejene, 2022).

2.1. Summary of literature reviews

A review of existing literature shows that multiple methods have been employed to enhance the performance of 28 GHz microstrip antennas designed for 5G applications. These techniques include CSRR, DGS, AMC, slot loading, parasitic elements, and different array configurations [24]–[32], [34]. The reviewed works show that these techniques can improve impedance matching, bandwidth, gain, efficiency, or antenna size depending on the design structure.

However, most of the reported 28 GHz antenna designs are based on rectangular, elliptical, orthogonal, slot-loaded, or other conventional geometries. Although a 1 × 4 hexagonal microstrip antenna array operating at 28 GHz has been reported in previous work [24], its bandwidth performance is still limited. In addition, the reviewed literature does not clearly show a direct investigation of a 1 × 4 hexagonal microstrip antenna array loaded with a double circular CSRR etched into the ground plane and compared with the same baseline array without CSRR.

Therefore, the research gap addressed in this thesis is the need to improve the impedance bandwidth and matching performance of a compact 28 GHz 1 × 4 hexagonal microstrip antenna array while maintaining high realized gain. This thesis fills the gap by designing a baseline 1 × 4 hexagonal array, integrating a double circular CSRR into its ground plane, and comparing the two

designs under the same substrate, frequency, and simulation environment. This comparison helps to identify the specific effect of the CSRR on bandwidth, reflection coefficient, gain, efficiency, VSWR, and radiation characteristics.

Table 2. 1 Summary of literature reviews

Ref.	Year	Array Elements	Frequency (GHz)	Shape	Substrate	Thickness (mm)	Gain (dBi)	BW (GHz)	S_{11} (-dB)	η_{tot} (%)
[27]	2021	1 × 4	28	Elliptical patch with elliptical slot	Rogers RT5880	0.25	11.9	0.723	22.201	80.38
[49]	2021	1 × 4	28	Orthogonal	FR4	1.2	11	Not reported	27	84
[44]	2023	1 × 4	28	Rectangular	Rogers RT5880	1.575	9.74	1.3	37.23	93
[37]	2024	1 × 4	28	Rectangular	Rogers RT5880	1.6	10.81	1.357	27	91.4
[24]	2024	1 × 4	28	Hexagonal	Rogers RT5880	0.254	12	0.45	15	85

CHAPTER THREE

Microstrip Array Antenna

This chapter has three main parts. First, it explains the basics of microstrip antennas what they are made of, how they work and the common feeding methods. Second, it introduces the key performance terms and equations used to evaluate antennas, such as S_{11}, bandwidth, gain, efficiency, VSWR and radiation pattern. Third, it discusses metamaterials, focusing on SRR/CSRR and how etching a CSRR in the ground plane can improve bandwidth and efficiency for 28 GHz designs.

3.1. Microstrip Antenna Basics

Microstrip antennas are created by etching a conductive patch onto a dielectric material. This dielectric is placed over a ground plane, which provides support for the entire structure. These antennas function by generating electromagnetic waves when current flows through a feed line and reaches the patch. Conductive materials such as gold or copper are used to make the patch. Both the radiating patch and feed lines are etched onto the dielectric substrate using photoetching techniques. The patch can take various shapes, such as square, rectangular, circular, triangular, or elliptical. By altering the shape of the structure, it is possible to adjust the antenna's resonant frequency, radiation pattern, polarization, and impedance. Important factors to consider when designing a microstrip antenna include its length, width, input impedance, gain, and radiation pattern [51].

3.1.1. Advantages and Disadvantages

Advantages and Disadvantages Microstrip antennas have several advantages. These include:

1. They are lightweight, compact, and have a low profile, which makes them ideal for use in space applications where weight is a key consideration.
2. They can be designed to conform to the surfaces of missiles and spacecraft without disrupting the aerodynamics of these vehicles.
3. They are inexpensive to manufacture and are easy to produce in large quantities, making them ideal for array configurations.
4. They are also designed to work with modular systems, enabling solid-state components like oscillators and amplifiers to be directly attached to the antenna's base material.

5. The feed lines and matching networks can be fabricated at the same time as the antenna structure [52].

However, microstrip antennas also have some drawbacks:

1. Their bandwidth is typically only 1% to 3%, which limits their use in certain applications, though they can still be suitable for specific uses.
2. They suffer from relatively high losses.
3. They radiate energy into only half of the space around them.
4. They have limited power handling capability.
5. They perform poorly in end-fire radiation [52].

3.1.2. Working Principle of Single Element Rectangular MPA

A single-element rectangular microstrip patch antenna operates by exciting a metallic rectangular patch placed on a dielectric substrate with a ground plane beneath it. When RF energy is supplied through a microstrip or inset feed line, current is induced on the patch surface. The patch behaves like a resonant cavity, and radiation mainly occurs from the fringing electric fields at the open edges of the patch. At the resonant frequency, usually in the dominant TM_{10} mode, the antenna efficiently converts the guided signal into electromagnetic waves radiated into free space. The antenna performance, including resonant frequency, return loss, bandwidth, gain, and radiation efficiency, mainly depends on the patch dimensions, substrate material, substrate thickness, and feed position. Because of its simple structure, compact size, low cost, and easy fabrication, a single rectangular microstrip patch antenna is widely used as a basic element for 5G antenna design and array development.

3.1.3. Feeding Techniques

The feed technique is an important factor that greatly influences antenna features like VSWR, bandwidth, and return loss. There are two main types of feed techniques: contacting feed and non-contacting feed [54]. In the contacting feed method, RF power is sent directly to the radiating patch through a connecting component such as a microstrip wire. In the non-contacting feed system, power is transferred between the microstrip line and the radiating patch using magnetic field coupling. The four most commonly used feed methods are microstrip lines, coaxial probes (which are contacting feeds), aperture coupling, and proximity coupling (which are non-contacting feeds [55].

3.1.3.1. Microstrip-line Feed

A conductive strip is connected directly to the edge of the microstrip patch using this feeding method, as shown below. This type of feed structure allows the feed line to be etched on the same material as the patch, creating a flat and compact design. The main function of the inset cut on the patch is to align the impedance of the feed line with that of the patch, eliminating the need for extra matching parts [55]. It is important to carefully adjust both the impedance and the position of the inset to achieve this matching. The inset-fed technique is known for being simple to produce, easy to simulate, and effective for impedance matching [51]. As a result, the depth of the inset and the width of the notch play a significant role in the design of a microstrip patch antenna. Additionally, it is worth noting that the feed line can sometimes lead to unwanted radiation [54].

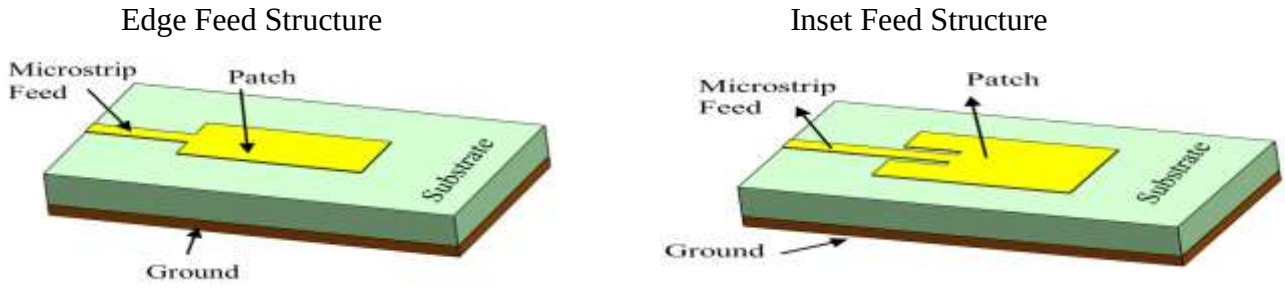


Figure 3. 1 Types of microstrip line feed.

3.1.3.2. Coaxial Feed

Coaxial feed, also known as probe feed, is frequently used to supply power to microstrip patch antennas. The inner conductor of the coaxial connector passes through the dielectric material and connects to the radiating patch, as illustrated in Figure 3.6 [55]. Meanwhile, the outer conductor is connected to the ground plane. One main advantage of this method is that it allows the feed to be positioned at a specific location. This feeding approach is straightforward to construct and generates minimal harmful radiation. However, since a hole must be drilled in the substrate and the connector extends beyond the ground plane, it is not suitable for thick substrates ($h > 0.020$ [55]). This method also has a limited bandwidth and can be challenging to match. Moreover, on thicker substrates, the longer probe length results in a more inductive input impedance, leading to impedance matching problems. When used with a thick dielectric material that offers a wide bandwidth, both the microstrip line and coaxial feed methods face several limitations, as mentioned above [55].

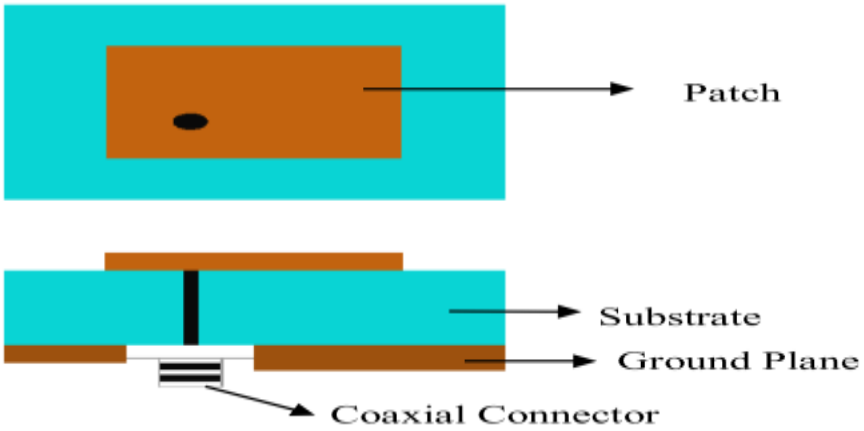


Figure 3. 2 Coaxial (Probe) feed method

3.1.3.3. Proximity Coupled Feed

This method of feeding is also referred to as the electromagnetic coupling technique. In Figure 3.7, the feed line was placed between two dielectric layers, with the topmost layer serving as the surface layer [55]. This feeding technique prevents unwanted radiation from the feed line and results in significantly improved performance because it increases the overall thickness of the microstrip patch antenna by up to 13 percent. Additionally, this approach allows the use of two distinct dielectric materials one for the patch and another for the feed line to optimize their respective functions [55].

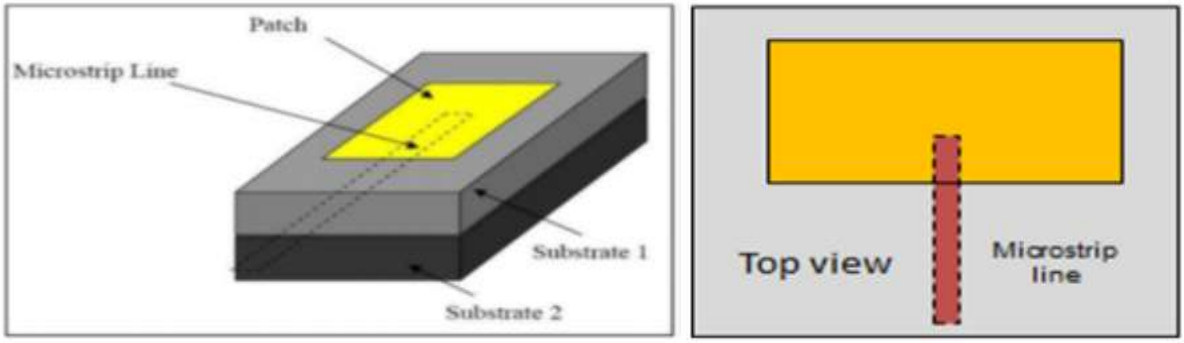


Figure 3. 3 Proximity coupling feed method

3.1.3.4. Aperture Coupled Feed

In the aperture coupled feeding technique, the input signal is transferred to the radiating patch via an aperture, which is a slot located on the ground plane of the feed line. This method differs from the conventional microstrip patch antenna in terms of its feeding structure. Figure 3.8 illustrates the aperture-coupled feed approach, where the radiating patch and the microstrip feed line are placed on separate layers, with the ground plane between them [51]. An aperture or slot in the ground plane connects the patch and the feed line. The ground plane acts as a barrier, separating the feed line from the patch and reducing unwanted radiation. A thick material with a low dielectric constant is used for the feed line at the bottom, while a material with a high dielectric constant is used for the radiator at the top of the substrate to enhance the radiation from the patch. However, the bandwidth of this feeding technique is limited [51].

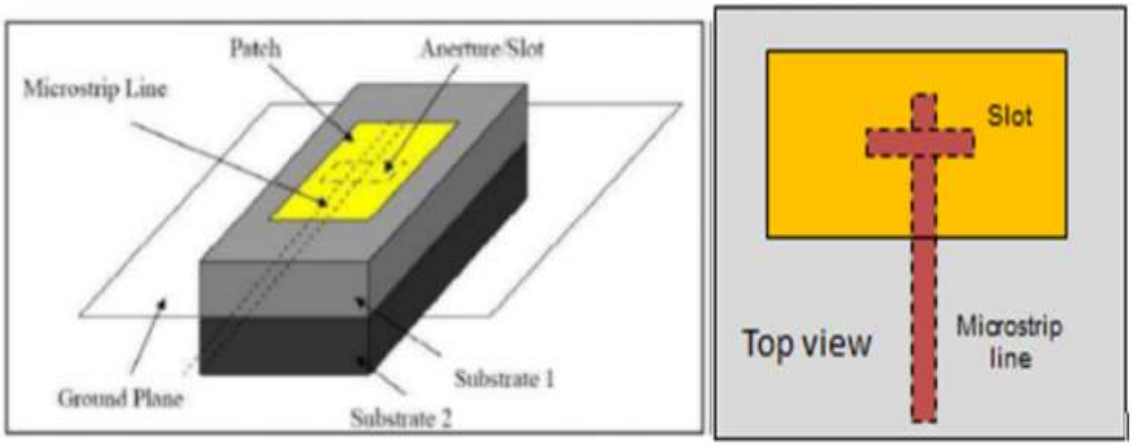


Figure 3. 4 Aperture coupled aperture feeding.

Table 3. 1 Comparison of different feeding techniques based on different characteristics

Characteristics	Microstrip line	Coaxial	Aperture coupling	Proximity coupling
Reliability	Better	Poor	Good	Good
Bandwidth	2-5	2-5	2-5	40
Bandwidth	Good	Poor	Excellent	Poor
Fabrication	Easy to fabricate	Needs soldering and drilling	Alignment is required	Alignment is required
Spurious feed radiation	More	Less	less	Minimum

3.2. Antenna parameters

Radiation pattern

A representation of an antenna's far-field radiation characteristics based on spatial coordinates, specifically the elevation angle and azimuth angle, defines its radiation pattern. This pattern is plotted using spatial coordinates [55]. Radiation intensity is the ratio of the power radiated to the unit solid angle. An "isotropic antenna" is one that radiates power uniformly in all directions. The power density S is calculated using equation 3.3 in any given direction [55].

$$\boldsymbol{S = \frac{p}{4\pi r^2}} \tag{3.3}$$

P is the total power radiated by the isotropic antenna, and r is the sphere's radius.

Equation 3.4 gives the radiation intensity for an isotropic antenna Ui [55].

$$\mathbf{Ui = r^2 S = \frac{p}{4\pi}} \tag{3.4}$$

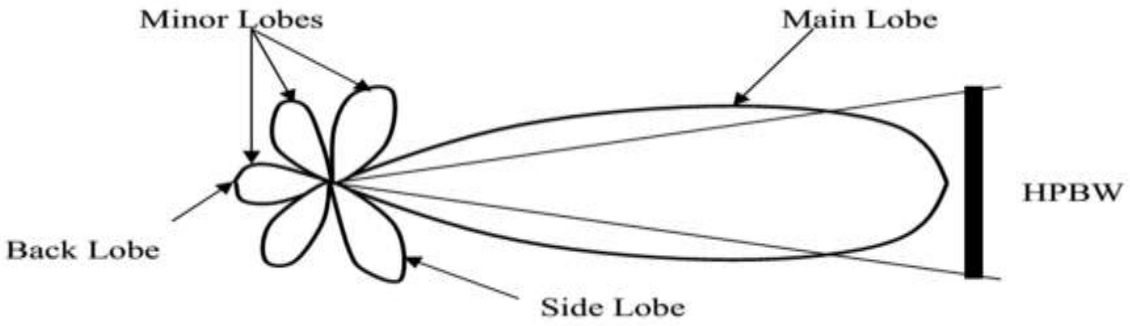


Figure 3. 5 Radiation Pattern.

Directivity

Directivity is defined as the ratio of the antenna's radiation intensity in a specific direction to the average radiation intensity across all directions. It can also be described as the ratio of the radiation intensity from an omnidirectional source in a particular direction to that of an isotropic source. Directivity is calculated using Equation 3.5 [55].

$$\mathrm{D}= \boldsymbol{\frac{4\pi U}{P} = \frac{U}{U_i}} \tag{3.5}$$

Where D represents the directivity of an antenna, P stands for the power emitted, Ui refers to the radiation intensity of an isotropic source, and U is the radiation intensity of an antenna. Equation 3.6 can be used to determine the maximum intensity when the direction of highest intensity is known [55].

$$\mathbf{D_{max}} = \frac{\mathbf{U_{max}}}{\mathbf{U_i}} = \frac{\mathbf{4\pi U_{max}}}{\mathbf{P}} \tag{3.6}$$

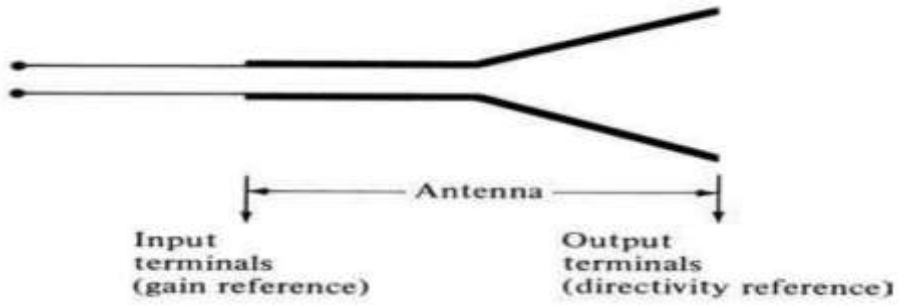
Antenna efficiency

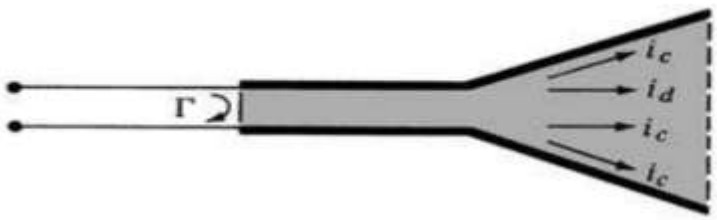
Antenna efficiency is a measure that considers both the losses at the terminals and the structure of the directional antenna. The efficiency factor accounts for wave reflections caused by impedance mismatch, as well as losses from dielectric and conduction [55]. Various efficiency factors are associated with an antenna and can be defined using Figure 3.3. The total antenna efficiency, denoted as e0, includes losses that occur at the input terminals and within the antenna's structure. These losses may be due to the following reasons, as shown in Figure 3.10(b) and 3.10(a) [55]:

1. Reflections resulting from the mismatch between the transmission line and the antenna.

2. I2R losses, which include both conduction and dielectric losses [56].

(a) Antenna reference terminals





(b) Reflection, conduction and dielectric loss

Figure 3.10 shows the reference terminals and losses of an antenna.

In general, the overall efficiency can be expressed as [56].

$$\mathbf{e_o = e_r\, e_c\, e_d} \tag{3.7}$$

where

e_o= total efficiency

$\boldsymbol{e_r}$ = $(\mathbf{1 - |\Gamma|^2})$ (dimensionless) = reflection efficiency

$\boldsymbol{e_c}$ = conduction efficiency

$\boldsymbol{e_d}$ = dielectric efficiency

Γ = The voltage reflection coefficient at the input terminals of the antenna [56].

$$\left[\Gamma = \frac{Z_{in} - Z_o}{Z_{in} + Z_o} \; where \; Z_{in} = antenna \; input \; impedance,\right]$$

$Z_o =$ the transmission line of characteristic impedance

$$\text{VSWR} = \text{Voltage standing wave ratio} = \frac{1+|\Gamma|}{1-|\Gamma|} \tag{3.8}$$

Usually, $\boldsymbol{e_c}$ and $\mathbf{e_d}$ are very difficult to compute, but it can be determined experimentally. Even with measurements, these coefficients cannot be separated, and it is usually more convenient to write equation (3-5) as [56]. $\mathbf{e_o}$ is calculated using Equation 3.9 [56].

$$\mathbf{e_o = e_r e_{cd} = e_{cd}(1 - |\Gamma|^2)} \tag{3.9}$$

where $e_{cd} = e_c\, e_d$ = Antenna radiation efficiency is a measure that connects the gain and directivity of an antenna.

Gain

Gain of an antenna, in a specific direction, is the ratio of the intensity in that direction to the radiation intensity that would occur if the power received by the antenna were spread equally

in all directions [56]. Realized gain refers to the ratio of the intensity in a particular direction to the radiation intensity that would result if the antenna's power were radiated equally in all directions. The power received by the antenna, when divided by 4π, gives the radiation intensity equivalent to the power radiated isotropically [51]. Gain is calculated using Equation 3.10 [51].

$$\mathbf{Gain} = \mathbf{4\pi}\frac{\mathbf{U(\theta_\varphi)}}{\mathbf{P_{in}}} \tag{3.10}$$

P_{in} = total input power

$U(\theta_\varphi)$ = radiation intensity

Bandwidth

The bandwidth of an antenna refers to the range of frequencies where its performance, in terms of a specific characteristic, meets a defined standard. It can be understood as the range of frequencies around a central frequency often the resonant frequency of a dipole where the antenna's properties, such as input impedance, radiation pattern, beamwidth, polarization, side lobe levels, gain, beam direction, and radiation efficiency, remain within an acceptable range compared to those at the central frequency [56]. For a broadband antenna, the bandwidth is usually expressed as the ratio of the highest to the lowest acceptable frequencies. In the case of a narrowband antenna, the bandwidth is often given as a percentage based on the difference between the upper and lower frequencies relative to the center frequency [51]. If F_o represents the center frequency, F_{min} is the lower limit of the frequency range, and F_{max} is the upper limit, the bandwidth is calculated as described in Equation (3.11) [51]**.**

$$\mathbf{BW} = \frac{\mathbf{F_{max} - F_{min}}}{\mathbf{F_o}} * \mathbf{100}\% \tag{3.11}$$

The bandwidth refers to the range of frequencies, in terms of how well the antenna performs, that meet certain specifications based on a particular standard. Figure 3.11 illustrates the bandwidth of an antenna [57].

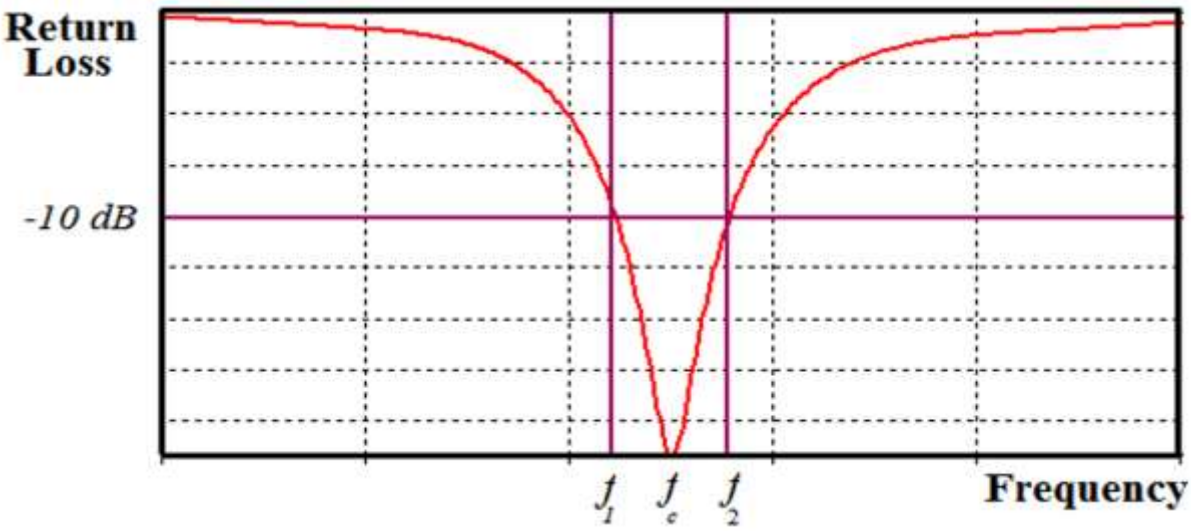


Figure 3. 6 Bandwidth of an Antenna.

Polarization

Polarization refers to the direction in which an electromagnetic wave oscillates over time and is related to the strength of the electric field vector. The polarization of the electric field is also called antenna polarization [55]**.** The most common types of polarization are linear (either horizontal or vertical) and circular (either right-hand polarization or left-hand polarization) (Sudha and Vedavathy, 2009). When the electric field vector moves back and forth along a straight line, the wave is said to be linearly polarized. In a circularly polarized wave, the electric field vector maintains a constant length but rotates in a circular motion. A left-hand circularly polarized wave rotates counterclockwise, while a right-hand circularly polarized wave rotates clockwise [58].

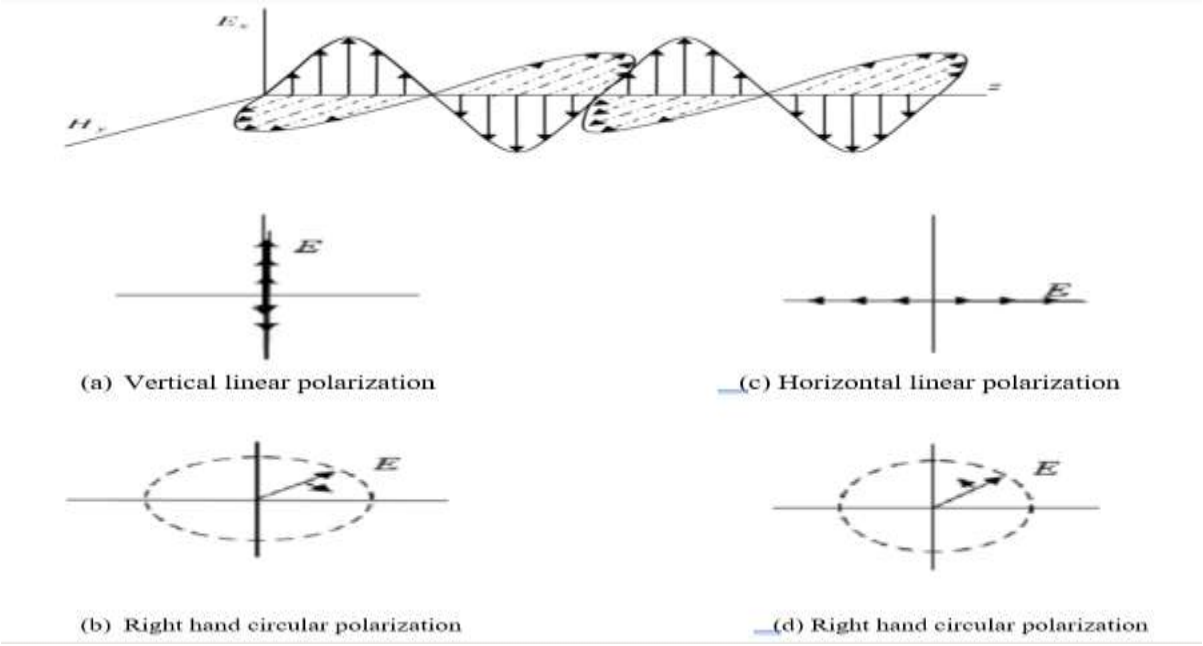


Figure 3. 7 polarization schemes.

Input Impedance

The input impedance or admittance of a microstrip radiator is an important factor; it must be precisely determined to ensure a proper match between the element and the feed [52]. Input impedance is the impedance measured at the ends of an antenna, or it can be described as the ratio of voltage to current at those two ends. It is also defined as the ratio of the relevant components of the electric and magnetic fields at a particular point. The input impedance can be calculated using equation 3.12 [55].

$$Z_{in} = R_{in} + JX_{in} \tag{3.12}$$

The antenna input impedance is denoted as Z_{in}, which consists of two parts: the antenna resistance (R_{in}) and the antenna reactance X_{in}. The reactance, X_{in}, represents the near-field power stored in the antenna and is the imaginary part of the impedance. The resistive component of the input impedance, which includes both the loss resistance and the radiation resistance, is represented by R_{in}. The power lost in the loss resistance is dissipated as heat in the antenna due to dielectric or conducting losses, whereas the power associated with the radiation resistance is radiated by the antenna [55]. The polarization schemes are illustrated in Figure [55].

Voltage Standing Wave Ratio (VSWR)

When a transmission line is connected to a load that matches its characteristic impedance, there is no reflection of the signal. However, if the transmission line is connected to a load with a different impedance (Z_L), a reflected wave is created. This reflected wave merges with the original incident wave, creating a standing wave pattern along the line. The voltage standing wave ratio (VSWR) is calculated as the ratio of the maximum voltage to the minimum voltage, as shown in equations 3.13 and 3.14. The reflection coefficient (Γ) is defined by equation 3.15 [58]. [58].

$$\mathbf{VSWR} = \left(\frac{\mathbf{V_{max}}}{\mathbf{V_{min}}}\right) \tag{3.13}$$

$$\mathbf{VSWR} = \frac{\mathbf{1 + |\Gamma|}}{\mathbf{1 - |\Gamma|}} \tag{3.14}$$

$$\Gamma = \frac{Z_L - Z_O}{Z_L + Z_O} \tag{3.15}$$

Where

Γ = Reflection coefficient

Z_L = Load impedance

Z_O = Characteristics impedance

VSWR is a key parameter in microwave devices. The ideal VSWR value is 1, which occurs when Γ equals zero [58]. This means all the power is delivered to the antenna without any reflection. However, in most applications, a VSWR of 2 or less is considered acceptable [58].

Return Loss

When assessing an antenna, return loss is an important factor to take into account. It relates to impedance matching and the principle of maximum power transfer [51]. It also serves as a measure of how effectively an antenna can transfer power from the source to itself. Return loss (RL) is the ratio of the power that reaches the antenna to the power that is reflected back from the antenna to the source. The mathematical expression for return loss is given below [51]. Return Loss is defined by equation 3.15 [51].

$$\mathbf{RL} = \mathbf{10} * \mathbf{log_{10}} \frac{P_I}{P_{ref}} (\mathbf{db}) \quad (3.16)$$

3.3. Metamaterials

Metamaterials are substances that have characteristics that do not exist in materials found in nature [51]. Metamaterials (MTM) are substances that have negative permittivity, negative permeability, or both. The most commonly used basic structures in metamaterials for improving isolation are Split-Ring Resonators (SRR), Complementary Split Ring Resonators (CSRR), or Capacitive-Loaded Loops (CLL) [51].

3.3.1. Classification of Metamaterial

Metamaterials are man-made structures designed to have specific electromagnetic properties that are not naturally present in the materials from which they are constructed [59]. One way to categorize them is by examining the signs of their effective permittivity (ε) and permeability (μ) [59].

Double positive (DPS, $\varepsilon > 0$, $\mu > 0$) [59].

These are the typical materials found in nature, also referred to as right-handed materials (RHM). In these materials, electromagnetic waves travel in the usual direction [59].

Epsilon-negative (ENG, $\varepsilon < 0$, $\mu > 0$) [59].

In this case, only the permittivity is negative [59].

These are sometimes referred to as artificial dielectrics. Due to their highly negative ε, ENG metamaterials are commonly used to reduce the size of microstrip patch antennas (MPAs) and other radio frequency components [59].

Mu-negative (MNG, $\varepsilon > 0$, $\mu < 0$) [59].

Here, only the permeability is negative, making them behave like artificial magnetic materials. MNG metamaterials can be used, for instance, to increase the gain of antennas [59].

Double negative (DNG, $\varepsilon < 0$, $\mu < 0$) [59].

Both ε and μ are negative. These materials are referred to as left-handed materials (LHM) because they allow for backward-wave propagation, where the direction of energy flow is opposite to the phase direction of the wave [59]. This distinctive characteristic results in various unique electromagnetic behaviors and potential applications. The classification of these materials is illustrated in Fig. 3.13 [59].

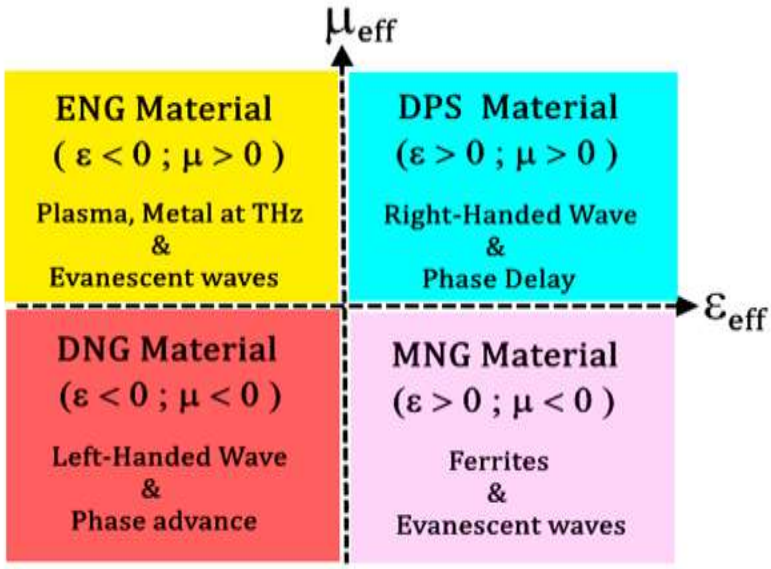


Figure 3. 8 Classification of materials based on the value of effective medium parameters.

3.3.2. Basic Properties of Metamaterial

Maxwell's first-order differential equations, specifically equations (3.17) and (3.17) [59].

$$\nabla \times \mathbf{E} = -\mathbf{j}\omega\mu\mathbf{H} \tag{3.17}$$

$$\nabla \times \mathbf{H} = -\mathbf{j}\omega\mu\mathbf{E} \tag{3.18}$$

where ω is the angular frequency.

define the electric and magnetic fields in the form of plane waves using equations (3.19) and (3.20) [60].

$$\mathbf{E} = \mathbf{E_0}\, e^{(-jk*r+j\omega t)} \tag{3.19}$$

$$\mathbf{H} = \mathbf{H_0}\, \mathbf{e}^{(-\mathbf{j}\mathbf{k}*\mathbf{r}+\mathbf{j}\omega\mathbf{t})} \tag{3.20}$$

In these equations, the wave vector is represented by k. Equations (3.21) and (3.22) take the form [60].

$$\mathbf{K} \times \mathbf{E} = \boldsymbol{\omega}\boldsymbol{\mu}\mathbf{H} \tag{3.21}$$

$$\mathbf{K} \times \mathbf{H} = -\boldsymbol{\omega}\boldsymbol{\varepsilon}\mathbf{E} \tag{3.22}$$

When both permittivity (ε) and permeability (μ) are positive, the vectors E, H, and k form a right-handed orthogonal system [60]. In such a medium, there is forward wave propagation. For simultaneous negative values of ε and μ, equations (3.23) and (3.24) can be rewritten as [60].

$$\mathbf{K} \times \mathbf{E} = -\boldsymbol{\omega}|\boldsymbol{\mu}|\mathbf{H} \tag{3.23}$$

$$\mathbf{K} \times \mathbf{H} = \boldsymbol{\omega}|\boldsymbol{\varepsilon}|\mathbf{E} \tag{3.24}$$

In this case, the vectors E, H, and k form a left-handed, mutually orthogonal system. The direction of energy flow is governed by the real part of the Poynting vector, which is defined by equation 3.15 [60].

$$\mathbf{S} = \frac{\mathbf{1}}{\mathbf{2}}\,\mathbf{E} \times \mathbf{H}^{*} \tag{3.24}$$

If both permittivity and permeability change sign at the same time, the direction of energy propagation does not change. Thus, the group velocity remains positive in both left-handed and right-handed media. The refractive index of the medium, as defined by equation 3.15 [60].

$$\mathbf{n} = \pm\sqrt{\boldsymbol{\varepsilon}\boldsymbol{\mu}} \tag{3.18}$$

Phase velocity is defined by equation 3.18 [60].

$$\boldsymbol{v_p} = \frac{\boldsymbol{c}}{\boldsymbol{n}} \tag{3.18}$$

where c is the velocity of light in vacuum.

The phase velocity is defined by equation 3.18. Left-handed materials (LHMs) are special media where both permittivity (εr) and permeability (μr) are negative. In such materials, the electric field E, magnetic field H, and wave vector k form a left-handed set instead of the usual right-handed one. In normal (right-handed) media, the refractive index is positive, so energy and phase travel in

the same direction, resulting in forward wave propagation [57]. However, in LHMs, the refractive index is negative, causing the phase velocity to be opposite to the energy flow, resulting in backward-wave propagation [57], [61]. Figure 3.14 illustrates the right-handed system on the right and the left-handed system on the left [61].

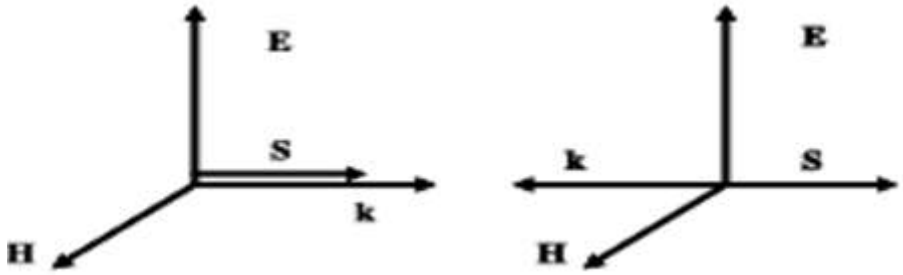


Figure 3. 9 Left: Right-Handed System and Right: Left-Handed System

3.3.3. Different types of Metamaterial Structures

To get the properties like either negative ε or negative μ, or both negative many structures are characterized till now some of them that are widely used to enhance the antenna properties are given below.

Metal thin wire structure

Such type of structure was first introduced by Pendry, 1996, for microwave range plasmonic frequency. Like metamaterial average cell size of are structures have much lesser than the guided wavelength, shows negative ε and positive μ values. The fundamental design parameters for a single rectangular MPA [55].

Split ring resonator

SRR structure was introduced by Pendry, which shows the positive ε and negative μ, characteristics of metamaterial. In case of SRR structure magnetic field remain perpendicular to the rings that generate the resonating current in rings by which magnetic dipole moment generated [62]. The topology of the SRR along with its equivalent circuit model are presented in figure 3.15 [62].



Figure 3. 10 Topology of SRR and Its Equivalent Circuit.

Complementary split ring resonator

CSRR structure can be observed as a dual of SRR structure that is replacing the metal rings by gap and remaining part or gap by metal. Figure 3.16 shows the CSRR and its equivalent circuit showing series capacitance replaced shunt inductance and vice versa [62]. The topology of the SRR along with its equivalent circuit model are presented in figure 3.15 [62].

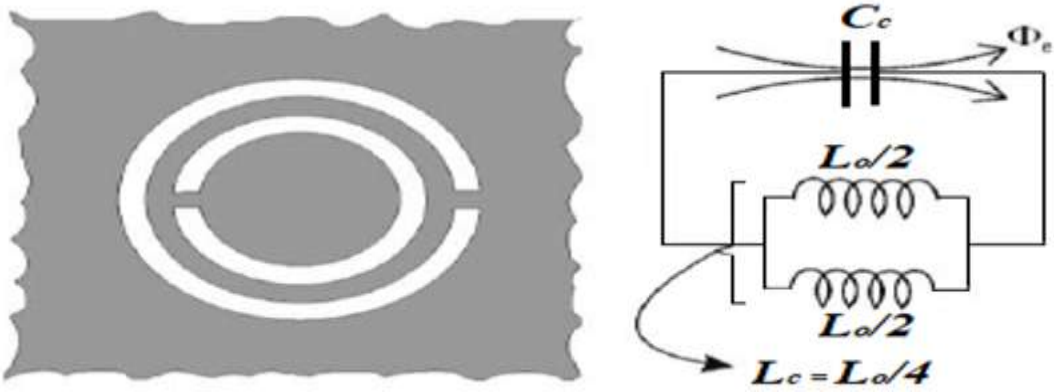


Figure 3. 11 Double circular CSRR and equivalent circuit.

3.3.4. The effects of applying metamaterials in antenna design

- The use of metamaterials to improve the gain of antennas.
- The application of metamaterials to reduce the size of antennas.
- The use of metamaterials to enhance the frequency bandwidth of antennas.

The use of metamaterials to achieve multiband performance [18].

CHAPTER FOUR

Design Hexagonal Microstrip antenna

4.1. Antenna Design Specification

In order to achieve the objective of the thesis work, antenna designing specifications play a key role. As a result, in our antenna design, the following specifications are chosen and designed to create the required antenna for 5G Application. Table 4.1 shows the design specification of the desired antenna in millimeter-wave for 5G in the frequency range of 28 GHz.

Table 4. 1 Antenna design specification for Hexagonal Microstrip Antenna

Antenna specification	Values/types
Frequency	28 GHZ
Input impedance	50 Ω
Height of substrate	0.254 mm
Dielectric constant (ε_r)	2.2
Tangent loss (tan δ)	0.0009
Dielectric material	Rogers RT/duroid 5880
Patch and Feed line	Copper
Ground plane	CSRR + Copper

The width of the hexagon, the feeder line, the ground plane, the inset length, the inset width, the conversion from a rectangular patch to a hexagonal patch, and the feed point location are determined based on the governing equations provided in chapter four.

4.2. Design Procedure

4.2.1. Design Calculations of Single Hexagonal Microstrip Patch Antenna

Patch Width (PW):

This equation is presented as an empirical approximation by Ayane Lebeta Goshu, Baye, Zenebe, and Teshome Watro Wata, as referenced in [55][51][53]. Patch Width calculated using equation 4.1 [53].

$$PW = \frac{C}{2RF\sqrt{\frac{\varepsilon_{r+1}}{2}}} \qquad (4.1)$$

$$= \frac{3*10^8 \text{m/sec}}{56\pi * 10^9\sqrt{\frac{2.2+1}{2}}} = 4.23519 \text{ mm}$$

Effective Dielectric Constant (ϵ_{eff}) and Effective Length of the Patch (PL_{eff}):

To calculate the patch length, the first step is to determine the substrate's effective permittivity using Schneider's equation [55]. Effective Dielectric Constant calculated using equation 4.1[55].

$$\boldsymbol{\epsilon_{reff}} = \frac{\boldsymbol{\epsilon_r+1}}{\boldsymbol{2}} + \frac{\boldsymbol{\epsilon_r-1}}{\boldsymbol{2}}\left(\boldsymbol{1+12\frac{h}{WP}}\right)^{-\frac{1}{2}} \quad (4.2)$$

$$\epsilon_{\text{reff}} = \frac{3.0\ +1}{2} + \frac{3.0\ -1}{2}\left(1+12\frac{0.254}{3.79}\right)^{-\frac{1}{2}}$$

$$\epsilon_{\text{reff}} = 2.0576$$

Patch Length Extension (ΔPL) and Patch Length (PL):

The patch length extension is calculated using equation 4.3 [55].

$$\boldsymbol{\Delta PL = 0.412h\frac{(\epsilon_{eff}+0.3)(3.79/h+0.264)}{(\epsilon_eff+0.258)(PW/h+0.8)}} \quad (4.3)$$

$$\Delta \text{P}L = 0.412h\frac{(\epsilon_{\text{eff}}+0.3)(3.79/h+0.264)}{(\epsilon_{\text{eff}}+0.258)(PW/h+0.8)}$$

$$\Delta \text{P}L = 0.412(0.254)\frac{(2.74\ +0.3)(3.79/0.254+0.264)}{(2.74\ +0.258)(0.254\ +0.8)}$$

$$\Delta \text{P}L = 0.1329\ mm$$

The effective length of the patch antenna is determined using equation 4.4 [55].

$$\boldsymbol{PL_{eff} = \frac{c}{2fr\sqrt{\epsilon_{eff}}} - 2\Delta PL} \quad (4.4)$$

$$PL_{eff} = \frac{3*10^8 \text{m/sec}}{56*10^9\sqrt{\epsilon_{\text{eff}}}} - 2*0.124\ mm$$

$$PL_{eff} = 3.734\ mm$$

The patch length is calculated by substituting the value of $PL_{eff} = 3.734\ mm$ and $\Delta \text{P}L = 0.1329\ mm$ and the change in patch length, ΔPL, is found to be 0.1329 mm using equation 4.5. [58]

Patch length is calculated using equation 4.5 [58] .

$$\boldsymbol{PL = PL_{eff} - 2\Delta PL} \tag{4.5}$$

$$PL = 3.24 - 2 * 0.124$$

$$PL = 3.4682\ mm$$

So equivalent rectangular patch dimension

$$W_{rect} = 4.23519\ \text{mm}$$

$$L_{rect} = 3.4682\ \text{mm}$$

Convert rectangular patch to hexagonal patch

We make a regular hexagon with the same area as the equivalent rectangle.

Equivalent area of rectangle can be calculated using equation 4.6 [63].

$$\mathbf{A_{rect} = W_{rect} * L_{rect}} \tag{4.6}$$

$$A_{rect=} 4.23519 * 3.4682$$

$$A_{rect=} 14.69\ \text{mm}^2$$

Area of regular hexagon can be calculated using equation 4.7 [63].

For a regular hexagon with side length (s)

$$\mathbf{A_{hex} = \frac{3\sqrt{3}}{2}\ s^2} \tag{4.7}$$

$A_{hex} = A_{rect}$ and solved for s.

$$s = \sqrt{\frac{2A_{rect}}{\sqrt[3]{3}}}$$

$$s = \sqrt{\frac{2*14.69}{\sqrt[3]{3}}} \qquad s = 2.376\ mm$$

Calculate flat to flat hexagon width

Calculate flat to flat hexagon width can be calculated using equation 4.8 [63].

$$\mathbf{W_{hex} = \sqrt{3} * s} \tag{4.8}$$

$$W_{hex} = \sqrt{3} * 2.376\ mm \qquad W_{hex} = 4.115\ mm$$

Ground Plane Length and Width (GPL and GPW)

Length of substrate can be calculated using equation 4.9 [51].

$$\mathbf{L_{sub,1*1} = PL + 6h} \tag{4.9}$$

$$L_{sub,1*1} = 3.4682 + 6 * 0.254$$

$$L_{sub,1*1} = 4.9922 \text{ mm}$$

Width of substrate can be calculated using equation 4.10 [51].

$$\mathbf{W_{sub,1*1} = PW + 6h} \tag{4.10}$$

$$W_{sub,1*1} = 4.23519 \text{ mm} + 6 * 0.254$$

$$W_{sub,1*1} = 5.75919 \text{ mm}$$

The position of the feed point for the patch antenna is determined by substituting the values PL = 3.4682 mm, PW = 4.23519 mm, and ϵ_{reff} = 2.0576 in equations 4.11 and 4.12 [53].

As a result, the coordinates of the feed point along the X-axis (Xf) and Y-axis (Yf) is can be calculated using equation 4.11 and 4.12 [53].

$$\mathbf{Xf = \frac{PL}{\sqrt[2]{\epsilon_{reff}}}} \tag{4.11}$$

$$Xf = \frac{3.4682}{\sqrt[2]{2.0576}} = 1.2087\text{mm}$$

$$\mathbf{Yf = \frac{PW}{2}} \tag{4.12}$$

$$Yf = \frac{4.23519}{2} = 2.1176\text{mm}$$

Width and Length of the Quarter wave Microstrip Transmission Line (W_{MTL} and L_{MTL}):

The Width of the Microstrip Transmission Line can be calculated using equation 4.13 and 4.14 [51]. for $W/h \leq 2$

$$\mathbf{W_{MTL}} = \frac{\mathbf{8e^{A}}}{\mathbf{e^{2A}-2}} \tag{4.13}$$

$$\mathbf{A} = \frac{\boldsymbol{Z_o}}{\mathbf{60}}\sqrt{\frac{\boldsymbol{\varepsilon_r+1}}{\mathbf{2}} + \frac{\boldsymbol{\varepsilon_r-1}}{\boldsymbol{\varepsilon_r+1}}\left(\mathbf{0.23} + \frac{\mathbf{0.13}}{\boldsymbol{\varepsilon_r}}\right)} \tag{4.14}$$

$$A = \frac{50}{60}\sqrt{\frac{2.2+1}{2} + \frac{2.2-1}{2.2+1}\left(0.23 + \frac{0.13}{2.2}\right)} \qquad A = 1.159$$

$$W_{MTL} = \frac{8e^{A}}{e^{2A}-2} \quad = \quad W_{MTL} = \frac{8e^{1.159}}{e^{2*1.159}-2} \quad = 0.794 \text{ mm}$$

Microstrip transmission line length (LMTL)

Compute free-space wavelength λ_O can be calculated using equation 4.15 [53].

$$\boldsymbol{\lambda_O} = \frac{\mathbf{c_O}}{\mathbf{f_O}} \tag{4.15}$$

$$\lambda_O = \frac{c_O}{f_O} \qquad \lambda_O = \frac{3*10^8}{28*10^9} \qquad \lambda_O = 10.714\ mm$$

Effective permittivity of the microstrip ϵ_{eff} can be calculated using equation 4.16 [53].

$$\boldsymbol{\epsilon_{eff}} = \frac{\boldsymbol{\varepsilon_r+1}}{\mathbf{2}} + \frac{\boldsymbol{\varepsilon_r-1}}{\mathbf{2}}\left(\frac{\mathbf{1}}{\sqrt{\mathbf{1+12\frac{h}{W}}}}\right) \tag{4.16}$$

$$\epsilon_{eff} = \frac{2.2+1}{2} + \frac{2.2-1}{2}\left(\frac{1}{\sqrt{1+12\frac{0.254}{W}}}\right)$$

$$\epsilon_{eff} = 1.871$$

Guided wavelength on the line λ_g in equations 4.17 [53].

$$\boldsymbol{\lambda_g = \frac{\lambda_0}{\sqrt{\epsilon_{eff}}}} \tag{4.17}$$

$$\lambda_g = \frac{10.714mm}{\sqrt{1.871}} \qquad \lambda_g = 7.831mm$$

Microstrip transmission line length (LMTL) as quarter-wavelength section in equations 4.18 [53].

$$\boldsymbol{L_{MTL} = \frac{\lambda_g}{4}} \tag{4.18}$$

$$L_{MTL} = \frac{7.831}{4} \qquad L_{MTL} = 1.958\,mm$$

Width and Length of the Quarter wave impedance transformer Microstrip Transmission Line (W_{QWT} and L_{QWT}):

Width of the Quarter wave impedance transformer Microstrip Transmission Line (W_{QWT}) in equation 4.19 and 4.20 [51].

$$\boldsymbol{A = \frac{Z_o}{60}\sqrt{\frac{\varepsilon_r+1}{2}} + \frac{\varepsilon_r-1}{\varepsilon_r+1}} \tag{4.19}$$

$$\boldsymbol{B = \frac{377}{2 * Z_o\sqrt{\varepsilon_r}}} \tag{4.20}$$

For $\frac{Wf}{h} < 2$

$$\boldsymbol{\frac{Wf}{h} = \frac{8e^A}{e^{2A}-2}} \tag{4.21}$$

For $\frac{Wf}{h} > 2$

$$\boldsymbol{\frac{Wf}{h} = \frac{2}{\pi}\left[B - 1\ln(2B-1) + \frac{\varepsilon_r-1}{2*\varepsilon_r}\left\{\ln(B-1) + 0.39 - \frac{0.61}{\varepsilon_r}\right\}\right]} \tag{4.22}$$

$$\boldsymbol{\frac{Wf}{h} = 1.79} \qquad \boldsymbol{wf = h * 1.79} \qquad \boldsymbol{W_{QWT}} = 0.45 \text{ mm}$$

Length of the Quarter wave impedance transformer Microstrip Transmission Line ($\boldsymbol{L_{QWT}}$)

$$\boldsymbol{L_{QWT} = \frac{\lambda_g}{4}} \qquad \boldsymbol{L_{QWT} = 1.99}$$

Length of insert feed (y):

Find input resistance at the radiating edge (R_{edge}) at 50 Ω in equations 4.23 [53].

$$\mathbf{R_{edge} = 90\frac{(\varepsilon_r)^2}{(\varepsilon_r - 1)}\left(\frac{PL}{PW}\right)^2} \quad (4.23)$$

$$\mathbf{R_{edge} = 90\frac{(2.2)^2}{(2.2-1)}\left(\frac{3.4682}{4.23519}\right)^2} \qquad \mathbf{R_{edge} = 243.36\ \Omega}$$

plugging in the values of R_{edge} and $Z_o = 50\Omega$ into equation 4.24 [53].

$$\mathbf{Z_{QT} = \sqrt{Z_o \times R_{edge}}} \quad (4.24)$$

$$\mathbf{Z_{QT} = \sqrt{50 \times 243.36} \qquad = 110.308\ \Omega}$$

Find insert feed (y) in equations 4.25 [53].

$$\mathbf{y = \frac{PL}{\pi}\cos^{-1}\left(\sqrt{\frac{Z_o}{R_{edge}}}\right)} \quad (4.25)$$

$$y = \frac{3.4682}{\pi}cos^{-1}\left(\sqrt{\frac{50\Omega}{110.308\Omega}}\right)$$

$$y = 0.92 \text{ mm}$$

4.2.2. Design Calculations of 1×2 Hexagonal Microstrip Patch Antenna Array

The single hexagonal microstrip patch antenna (MPA) has a broad radiation pattern and a moderate gain. To increase the gain and obtain a more directive beam, a planar 1×2 hexagonal MPA array is designed by combining two identical hexagonal elements along the *x*-axis. Compared with a single element, this linear array configuration improves the gain and narrows the main beam in one plane, which is suitable for 5G application at 28 GHz.

The design of the 1×2 array uses the optimized single-element hexagonal patch as the basic building block. The two elements are excited through a corporate feed network that employs 100 Ω branch lines and quarter-wave impedance transformers in order to transform the 50 Ω input impedance to the required patch input impedance and to provide in-phase excitation for both elements.

Inter-Element Spacing

The center-to-center spacing between the two elements, denoted by IS, has a strong impact on mutual coupling, side-lobe levels, and the risk of grating lobes. For a linear array, a commonly used design wavelength-based heuristic spacing rule is $0.5\ \lambda_o \leq \text{IS} \leq \lambda_o$ [64]. At 28 GHz the free-space wavelength is $\lambda_O = 10.714mm$. In this work the elements are separated by approximately 0.6 λ, which gives a good compromise between gain and side-lobe level. The chosen inter-element spacing is

$\text{IS} = 0.6\ \lambda_o \qquad \text{IS} = 0.6 * 10.714\ mm \qquad = 6.43\ mm$

Microstrip Feed Network and Quarter-Wave Transformer

The array uses a corporate feeding network implemented with microstrip lines on the same RO5880 substrate. At 28 GHz, for a substrate thickness of h=0.254 mm and target impedances of 50 Ω, 70.7 Ω and 10 0Ω, the corresponding microstrip line widths are obtained from the standard microstrip impedance equations as. 50 Ω main feed line width: $W_{50} = 0.789$ mm. 70.7 Ω quarter-wave transformer width: $W_{70} = 0.45$ mm. 100 Ω branch line width $W_{100} = 0.229$ mm. The effective permittivity of the 70.7 Ω microstrip line yields a guided wavelength $\lambda_g = 7.95$ mm. The physical length of the quarter-wave impedance transformer section is therefore $L_{QWT} = \frac{\lambda_g}{4} = 1.99\ mm$. Each patch is first connected to a 70.7 Ω line of length L_{QWT} , which transforms the 10 0Ω input resistance at the inset feed to a 50 Ω equivalent. The two transformed ports are then linked to a central 1×2 power dividers formed by a pair of 100 Ω branch lines of equal electrical length so that both patches are excited in phase. Finally, a 50 Ω main microstrip line connects the power divider to the SMA feed point.

Length and width of patch 1×2 hexagonal MPA

The length of connected 1×2 MPA array $PL_{1\times2}$ is calculated by using $PL_{1\times2}$ = PL + IS + 2LMTL [53]. Thus, by adding the values of PL =3.40451mm, IS = 6.43 mm, and LMTL = 1.958 mm together, the $PL_{1\times2}$ becomes: $PL_{1\times2}$ = 3.9364 mm + 6.43 mm + 3.916 mm = 14.2824 mm.

The width of connected 1×2 MPA array $PW_{1\times2}$ is given by $\text{PW}_{1\times2} = 2\text{PW} + \text{IS}$ [53]. hence, by adding the values of PW = 4.23519 mm and IS = 6.43 mm, then the $PW_{1\times2}$ calculated as $\text{PW}_{1\times2} = 8.4703\ \text{mm} + 6.43\ \text{mm} = 14.9\ \text{mm}$.

Ground Plane Length and Width of 1x2 hexagonal MPA array

The length and width of ground plane $GPL_{1\times2}$ and $GPW_{1\times2}$ are calculated by using $\mathrm{GPL}_{1\times2} = \mathrm{PL}_{1\times2} + 6\mathrm{h}$ and $\mathrm{GPW}_{1\times2} = \mathrm{PW}_{1\times2} + 6h$ [53]. the $PL_{1\times2}$ = 15.8064 mm, $\mathrm{PW}_{1\times2}$ = 14.9 mm, and h = 0.254 mm as follows.

$$\mathrm{GPL}_{1\times2} = \mathrm{PL}_{1\times2} + 6\mathrm{h} \quad = 14.2824\ mm + 6 * 0.254 \ = 15.8064\ mm$$

$$\mathrm{GPW}_{1\times2} = \mathrm{PW}_{1\times2} + 6h \quad = 14.9\ \mathrm{mm} + 6 * 0.254 \quad = 16.425\ \mathrm{mm}$$

4.2.3. Design 1×4 Hexagonal Microstrip Patch Antenna Array without CSRR

The single hexagonal microstrip patch antenna (MPA) has a broad radiation pattern and a moderate gain. To increase the gain and obtain a more directive beam, a 1×4 hexagonal MPA array is designed by combining four identical hexagonal elements along the *x*-axis. Compared with a single element, this linear array configuration improves the gain and narrows the main beam in one plane, which is suitable for 5G application at 28 GHz.

The design of the 1×4 array uses the optimized single-element hexagonal patch as the basic building block. The four elements are excited through a corporate feed network that employs 100 Ω branch lines and quarter-wave impedance transformers in order to transform the 50 Ω input impedance to the required patch input impedance and to provide in-phase excitation for both elements.

Inter Element Spacing

The center-to-center spacing between the four elements, denoted by IS, has a strong impact on mutual coupling, side-lobe levels, and the risk of grating lobes. For a linear array, a commonly used design wavelength-based heuristic spacing rule is $0.5\ \lambda_o \leq \mathrm{IS} \leq \lambda_o$. At 28 GHz the free-space wavelength is $\lambda_O = 10.714mm$. In this work the elements are separated by approximately 0.6 λ, which gives a good compromise between gain and side-lobe level. The chosen inter-element spacing is

$$\mathrm{IS} = 0.6\ \lambda_o \qquad \mathrm{IS} = 0.6 * 10.714\ mm \qquad = 6.43\ mm$$

Microstrip Feed Network and Quarter-Wave Transformer

The array uses a corporate feeding network that is implemented with microstrip lines on the same RO5880 substrate as the patches. At 28 GHz, with a substrate thickness of h=0.254 mm and target line impedances of 50 Ω, 70.7Ω and an approximate patch input resistance of 100 Ω, the required microstrip widths are calculated using the standard closed-form microstrip impedance equations. The 50 Ω main feed line is realized with a width of $W_{50} = 0.789$ mm, while the 70.7 Ω quarter-wave transformer section uses a narrower width of $W_{70} = 0.45$ mm. For reference, a 50 Ω microstrip line on the same substrate would have a width of $W_{50} = 0.789$ mm. this value is close to the input resistance of the inset-fed hexagonal patch and is used as a guideline when choosing the inset position.

The effective permittivity of the 70.7Ω line gives a guided wavelength of $\lambda_g = 7.95$ at 28 GHz. The physical length of each quarter-wave matching section is therefore.

$$L_{QWT} = \frac{\lambda_g}{4} = 1.99\ mm$$

Each patch is connected to the feed network through a 70.7 Ω microstrip line of length LQWTL , which transforms the approximately 100 Ω input resistance at the inset feed to an equivalent 50 Ω load as seen by the corporate network.

The two transformed ports are then combined by a 1×2 corporate power divider. This divider uses a quarter-wave transformer with characteristic impedance $Z_t = 35.4\ \Omega$ (given by $Z_t = \sqrt{50 \times 25}$) placed between the 50 Ω main trunk and the junction of the two 50 Ω branch lines, where the parallel combination of the branches presents 25 Ω. In this way, the transformer converts the 25 Ω junction impedance back to 50 Ω at the input and ensures that both patches are excited with equal amplitude and in phase. Finally, a 50 Ω main microstrip line connects the output of the corporate divider to the SMA feed point.

Length and width of patch 1×4 **hexagonal MPA**

The length of connected 1x4 MPA array $PL_{1\times4}$ is calculated by using $PL_{1\times4}$ = PL + IS + 2LMTL [53]. Thus, by adding the values of PL =3.40451mm, IS = 6.43 mm, and LMTL = 1.958 mm together, the $PL_{1\times4}$ becomes: $PL_{1\times4}$ = 3.9364 mm + 6.43 mm + 3.916 mm = 14.2824 mm.

The width of connected 1×4 MPA array $PW_{1\times4}$ is given by $PW_{1\times4} = 4PW + IS$ [53]. hence, by adding the values of PW = 4.23519 mm and IS = 6.43 mm, then the $PW_{1\times4}$ calculated as $PW_{1\times4} = 16.94076\ \text{mm} + 6.43\ \text{mm} = 23.37076\ \text{mm}$.

Ground Plane Length and Width of 1x4 hexagonal MPA array

The length and width of ground plane $GPL_{1\times4}$ and $GPW_{1\times4}$ are calculated by using $GPL_{1\times4} = PL_{1\times4} + 6h$ and $GPW_{1\times4} = PW_{1\times4} + 6h$ [53]. The $PL_{1\times4}$ = 14.2824 mm, $PW_{1\times4}$ = 23.37076 mm, and h = 0.254 mm as follows.

$$GPL_{1\times4} = PL_{1\times4} + 6h \quad = 14.2824\ \text{mm} + 6 * 0.254 \ = 15.8064\ mm$$

$$GPW_{1\times4} = PW_{1\times4} + 6h \quad = 23.37076\ \text{mm} + 6 * 0.254 \quad = 24.89476\ \text{mm}$$

4.2.4. Design 1×4 Hexagonal Microstrip Patch Antenna Array with Circular CSRR

A double CSRR was etched into the ground plane of the 1×4 microstrip patch array to create a small, carefully controlled resonance near the antenna's main resonance at 28 GHz. When the CSRR was placed where the patch edge fields are strongest, it coupled effectively to the antenna and gently reshaped the input impedance response. This produced two nearby resonances that overlap, which in turn broadened the frequency range where the matching condition $|S_{11}| < -10\ dB$ is satisfied compared with the baseline array.

Operating Frequency and Sub-Wavelength Condition

For the CSRR to function effectively as a metamaterial-inspired structure, its physical size must be significantly smaller than the guided wavelength. At the target frequency $f_O = 28\ GHZ$, the free-space wavelength λ_O is calculated as: calculated by in equation 4.15.

$$\lambda_O = \frac{c_O}{f_O} \qquad \lambda_O = \frac{3 \times 10^8}{28 \times 10^9} \qquad \lambda_O = 10.714\ mm$$

The outer radius of the CSRR (r_{out}) was set at 1.03mm. To verify the sub-wavelength condition, we examine the electrical size [55].

$$\frac{r_{out}}{\lambda_O} \tag{4.26}$$

$$= \frac{1.03}{10.714} = \mathbf{0.096}$$

As shown in (4.26), the ratio is less than 0.1, which confirms that the resonator's behavior is quasi-static.

CSRR Topology and Geometrical Parameters

A double circular CSRR is formed by etching two concentric circular slot rings into the ground plane, with each ring interrupted by a small split gap. To make the design easy to tune and improve, all key dimensions of the CSRR were defined as parameters so they could be adjusted systematically during optimization.

Primary geometric parameters (all in mm):

- r_{out}: outer radius of the outer ring
- w: slot width (etched ring thickness)
- s: spacing between the two rings (metal separation)
- g: split gap width (opening)
- $\emptyset$: split orientation angle (optional, controls coupling direction)
- y_{0ff}: placement offset beneath the patch edge (coupling control)

The relationship between the outer and inner ring radius is defined as [65].

$$\boldsymbol{r_{in,out} = r_{out} - w - s} \tag{4.27}$$

$$\boldsymbol{r_{in,in} = r_{in,out} - w} \tag{4.28}$$

Manufacturing constraint

Slot width w and gap g were constrained to meet the available fabrication limits (e.g., $w, g \geq 0.15\ mm\ or\ \geq 0.2\ mm$).

The natural frequency or resonant frequency of an LC tank circuit in equation 4.29 [66].

$$\boldsymbol{f_{CSRR} = \frac{1}{2\pi\sqrt{LC}}} \tag{4.29}$$

Where

- f_{CSRR} is the CSRR resonant frequency

- L is the equivalent inductance of the ring
- C is the equivalent capacitance of the gap

In this model:

- The effective inductance L increases with a longer current path around the ring structure (typically larger mean radius).
- The effective capacitance C increases as the split gap g becomes smaller and as inter-ring coupling (controlled by s) becomes stronger.

Accordingly, the tuning trends used in the design were:

- Increasing r_{out} $\Longrightarrow$ increases effective L and/or C $\Longrightarrow$ shifts f_{CSRR} downward.
- Increasing g reduces effective gap capacitance $\Longrightarrow$ shifts f_{CSRR} upward.
- Decreasing s increases inter-ring capacitance $\Longrightarrow$ shifts f_{CSRR} downward.

Because the CSRR is strongly influenced by near-field loading from the patch and substrate, the LC framework was used as design guidance**,** while the final resonance alignment was achieved through full-wave parametric optimization.

Table 4. 2 summarizes the key geometric dimensions used to define the double circular CSRR etched into the ground plane.

Parameter	Symbol	Value (mm)
External radius of the CSRR	(r_{ext})	1.03
Internal radius of the CSRR	(r_o)	0.63
Width of each complementation ring of the CSRR	(C)	0.2
Gap between the two complementary rings of CSRR	(d)	0.2
Split gap	(g)	0.2

4.3. Optimization Algorithm (HFSS Optimetrics)

The antenna dimensions are first calculated using standard microstrip design equations. However, at 28 GHz the final results are strongly affected by effects that equations cannot fully capture such as fringing fields, small feeding discontinuities, mutual coupling in arrays and the near-field

interaction between the patch and the CSRR in the ground plane. For this reason the design is refined using a full wave parametric optimization procedure in ANSYS HFSS Optimetrics.

HFSS Parametric Sweep and Screening & Optimization

- Inputs: $f_0 = 28\ GHZ$, $\varepsilon_r = 2.2$, h=0.254 mm, initial dimensions from analytical calculations, and a frequency sweep (24–32 GHz).

Goals: minimize dB (S_{11}) at 28 GHz, increase the bandwidth where $|S_{11}| < -10\ dB$, and maintain acceptable gain/efficiency (and isolation for arrays).

To obtain the final CSRR dimensions, a parametric sweep was performed using HFSS Optimetrics. In this process, selected CSRR parameters, including the outer radius $\boldsymbol{r_{out}}$, were varied while the other antenna dimensions were kept constant. The main purpose of the sweep was to examine how changes in the CSRR geometry affect the impedance matching of the antenna and to support the selection of the optimized CSRR dimensions. The corresponding parametric sweep plot is provided in Appendix A.

The final antenna model was checked for adaptive mesh convergence in HFSS. The convergence result shown in Appendix A indicates that the simulation converged after eight adaptive passes. The final maximum magnitude delta S was 0.016979, which is lower than the target value of 0.02. Therefore, the simulation results were considered numerically stable.

CHAPTER FIVE

Simulation Result and Discussion

In this chapter, the antenna design configurations and the corresponding simulation results are presented in the form of tables and plots. Based on these results, a detailed comparative analysis is carried out to evaluate the performance of the proposed antenna designs. This chapter is organized into three main sections. The first section describes the hexagonal shaped single microstrip patch antenna designed for single band operation. The second section focuses on the design and simulation results of the hexagonal shaped 1×2 microstrip patch antenna array. The final section presents the hexagonal shaped 1×4 microstrip patch antenna array both without metamaterial and with metamaterial along with a comprehensive discussion of the obtained simulation results.

5.1. Antenna Design Simulation Result and Discussion

5.1.1. Hexagonal Single Microstrip Patch Antenna

This section describes the design and simulation process of a single band hexagonal shaped microstrip patch antenna. The antenna is modeled and analyzed using HFSS 2024 software. Initially, the antenna dimensions are obtained from standard microstrip antenna design equations, and these dimensions are then fine-tuned through full-wave electromagnetic simulations to achieve the desired performance. The design specifications used for the single-band antenna are summarized in Table 5.1.

Figure 5.1 illustrates the hexagonal microstrip patch antenna designed to operate at a center frequency of 28 GHz. The antenna is modeled and simulated using HFSS 2024 software. A copper thickness of 0.0035 mm is used for both the radiating patch and the ground plane, while the remaining antenna dimensions are obtained from standard microstrip antenna design equations and are listed in Table 5.1. An insert feeding technique combined with a quarter-wave transformer is employed to achieve effective impedance matching. Using this antenna configuration important performance parameters such as return loss (S_{11}), gain, efficiency, VSWR, radiation pattern and radiation bandwidth are evaluated and discussed.

Table 5. 1 Calculated dimension for hexagonal single patch antenna

Designed Antenna Parameters	Values (mm)
Substrate Height	0.254
Patch Width	4.23519
Effective relative permittivity	2.0576
Effective patch length	3.734
Patch Length Extension	0.1329
Patch Length	3.4682
X-coordinate of the feed poin	1.2087
Y-coordinate of the feed poin	2.1176
50 Ω Feed Length	1.958
50 Ω Feed width	0.794
Inset feed length	0.918
Inset feed Width	0.45
Width of substrate	5.75919
Length of substrate	4.9922
Length of hexagon side	2.376
Area of regular hexagon	14.69
Flat to flat hexagon width	4.115
70 Ω matching width	0.45
70 Ω matching Length	1.99

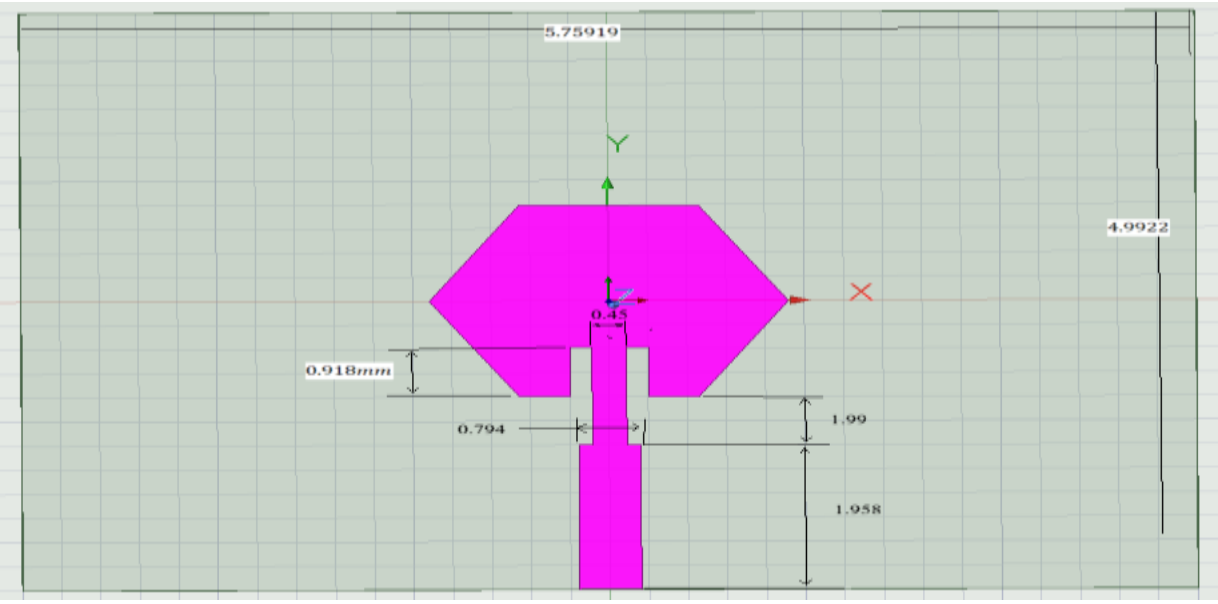


Figure 5. 1 The proposed design of single hexagonal patch antenna

Return Loss

Return loss shows how much input power is reflected back instead of being radiated. For good matching, S_{11} should be below -10 dB. In Figure 5.2, the single hexagonal patch antenna meets this condition. The S_{11} curve has a clear resonance near 28 GHz, and at about 28.0191 GHz the return loss reaches -14.4861 dB meaning most power is delivered to the antenna with limited reflection. The smooth curve around resonance also suggests stable matching, so the antenna is suitable matching, so the antenna, so the for 28 GHz 5G operation.

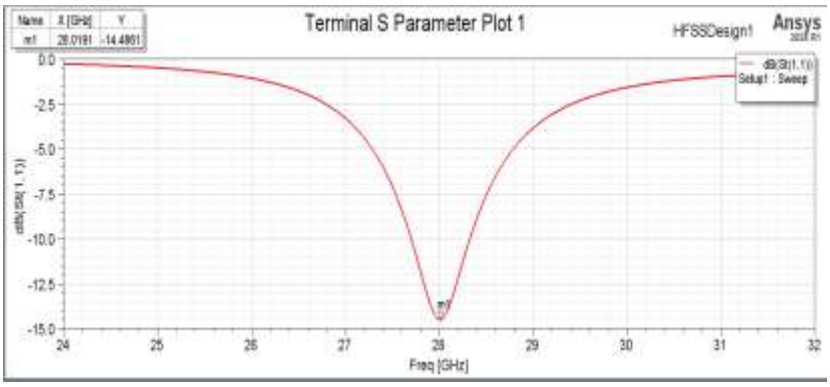


Figure 5. 2 The return loss $\mathbf{S_{11}}$ of the single band hexagonal single patch antenna

Radiation Bandwidth

Radiation bandwidth is obtained from the S_{11} curve as the frequency range where S_{11} is below -10 dB. From Figure 5.3 the lower upper cutoff frequencies are 27.7009 GHz and 28.3248 GHz respectively. Therefore, the achieved radiation bandwidth is approximately 0.6239 GHz, confirming good performance around 28 GHz.

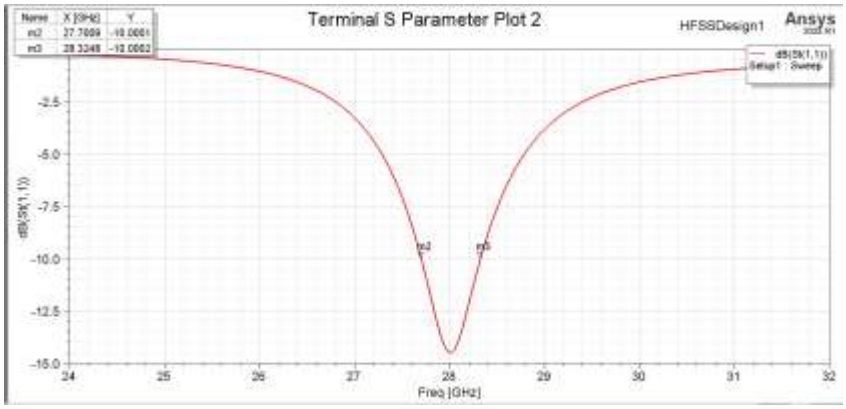


Figure 5. 3 The radiation bandwidth of the single band hexagonal single patch antenna

VSWR (Voltage Standing Wave Ratio)

The standing wave ratio (VSWR) indicates how well the antenna is matched to the connected transmission line. It represents the ratio of maximum to minimum voltage along the line and has a theoretical range of $1 < \text{VSWR} < \infty$. In most antenna designs a VSWR below 2 is acceptable and values below 1.5 are considered very good. As shown in Figure 5.11 the proposed antenna exhibits a minimum active VSWR at the operating frequency of 28.0191 GHz. The measured value VSWR value is 1.6441 which indicates good and acceptable impedance matching and efficient power transfer at the target frequency.

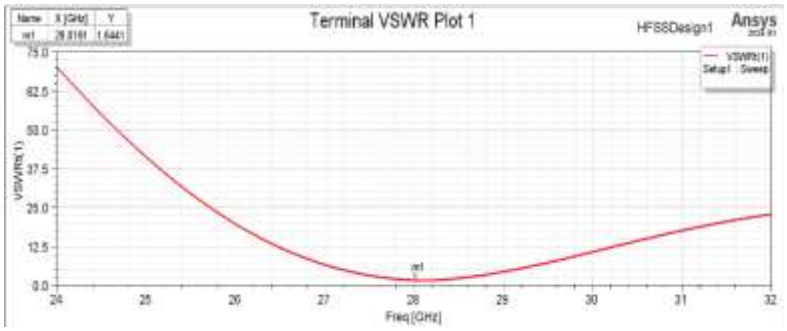


Figure 5. 4 The standing wave ratio of the single band hexagonal single patch antenna

Radiation Efficiency

Radiation efficiency shows how much of the input power is actually radiated of being lost inside the antenna. In Figure 5.5 the single hexagonal patch antenna has a radiation efficiency of about 0.9881 (98.81 %) at 28 GHz which means internal losses are very small. Total efficiency also includes mismatch losses from the feed. At 28 GHz the total efficiency is about 0.9268 (92.68 %) showing the antenna still transfers power well and is suitable for 28 GHz 5G operation.

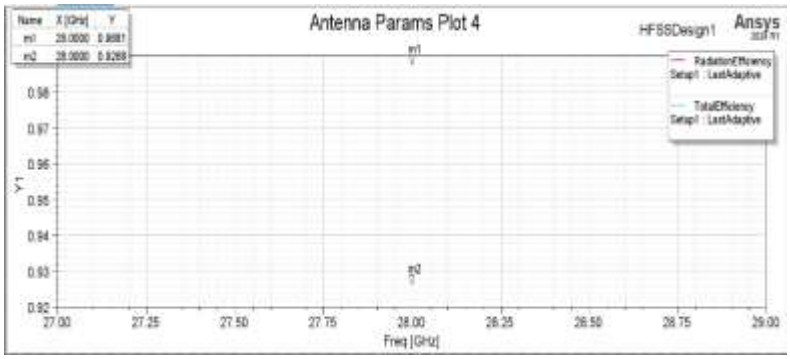


Figure 5. 5 The radiation efficiency of the single band hexagonal single patch antenna

Gain and Directivity

Gain and directivity are related directivity tells how focused the radiation is while gain also includes efficiency and losses. In Figure 5.6 the single hexagonal patch antenna shows a clear main beam in the broadside direction at 28 GHz which means it radiates mainly forward. The 3D plot gives a maximum gain of about 8.74 dBi. Based on the high efficiency $\eta_{tot} = 92.68$ the corresponding maximum directivity is about 9.09 dBi. Overall, the patterns confirm good directional radiation making the antenna suitable for 28 GHz 5G use.

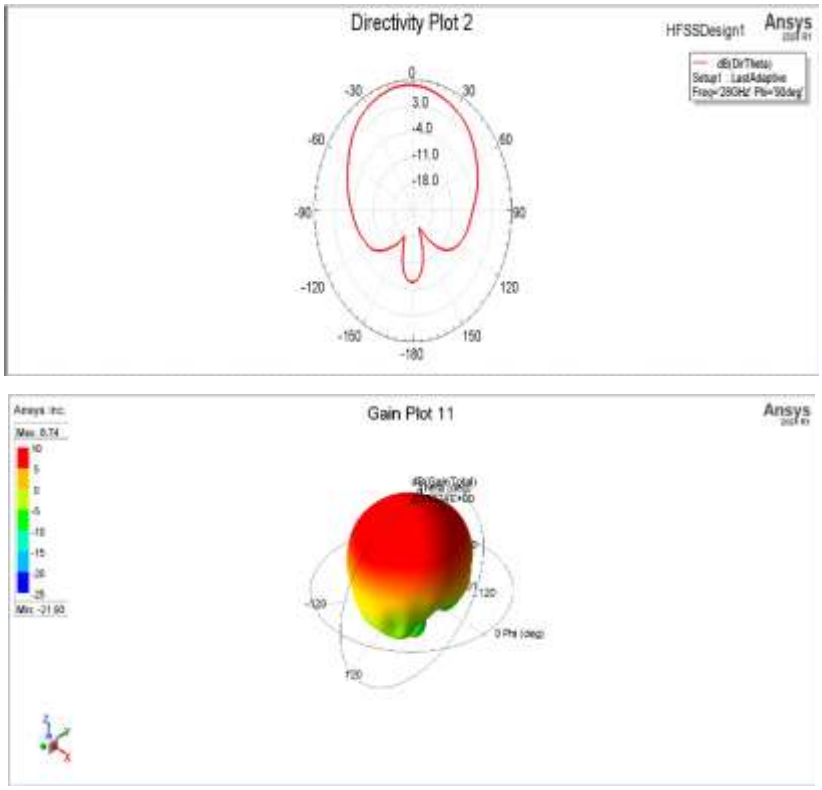


Figure 5. 6 The gain and directivity of the single band hexagonal single patch antenna

5.1.2. Hexagonal 1 × 2 microstrip patch antenna array

Figure 5.7 indicates the designed hexagonal 1 × 2 microstrip patch antenna. To design a hexagonal patch, we used copper metal for both the ground and patch. The dielectric material substrate is Rogers RT Duroid 5880 with 0.254 mm heights. We stated different antenna parameters like return loss, bandwidth, gain and efficiency. To design a hexagonal antenna, we used edge feed techniques. The dimension is shown in Table 5.2.

Table 5. 2 Calculated dimension for hexagonal 1×2 microstrip patch antenna

Designed Antenna Parameters	Values (mm)
Substrate Height	0.254
Patch Width	4.23519
Effective relative permittivity	2.0576
Effective patch length	3.734
Patch Length Extension	0.1329
Patch Length	3.4682
Branch line width	0.229
Inter-Element Spacing	6.43
50 Ω quarter-wave transformer length	1.958
50 Ω quarter-wave transformer width	0.794
Inset feed length	0.918
Inset feed Width	0.45
Width of substrate	16.425
Length of substrate	15.8064
Length of hexagon side	2.376
Area of regular hexagon	14.69
Flat to flat hexagon width	4.115
70.7 Ω quarter-wave transformer width	0.45
70.7 Ω quarter-wave transformer length	1.99

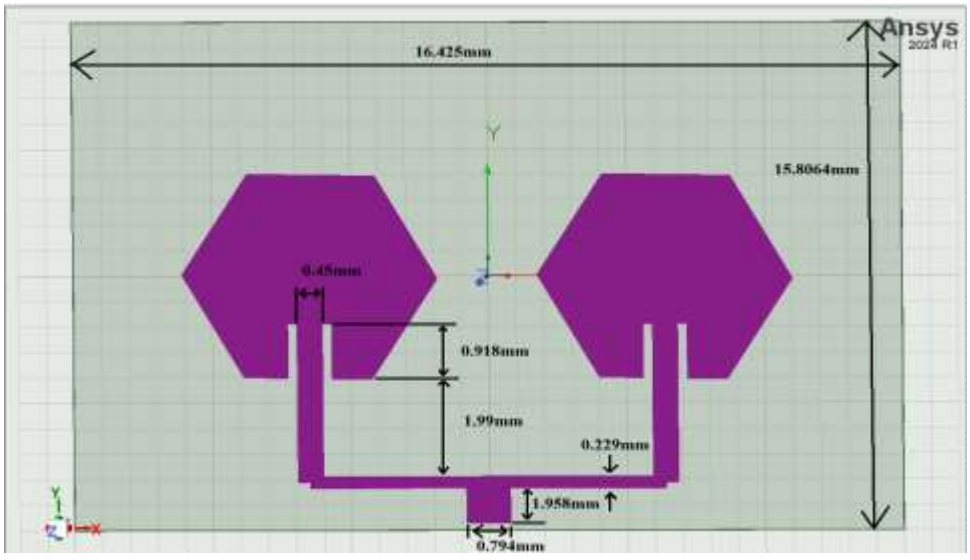


Figure 5. 7 The proposed design of single band hexagonal 1×2 MPA

Return Loss

Return loss shows how much of the input signal is reflected back from the antenna. For good power transfer the return loss should be low and an S_{11} value below -10 dB is generally considered acceptable. As illustrated in Figure 5.8 the proposed antenna exhibits a strong resonance at 28 GHz with a return loss of about -24.9984 dB. This deep notch indicates excellent impedance matching meaning most of the input power is delivered to the antenna with very little reflection. The result confirms that the antenna performs efficiently at the target frequency and is suitable for 28 GHz 5G application.

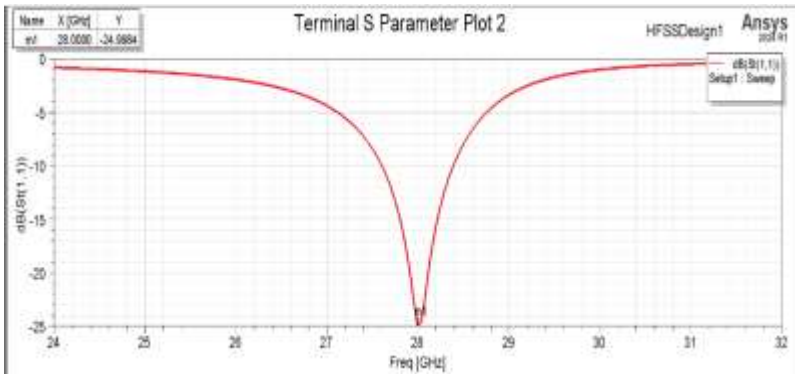


Figure 5. 8 The return loss of single band hexagonal 1×2 MPA

Radiation Bandwidth

Radiation bandwidth is the frequency range over which the antenna operates effectively defined by the region where the S_{11} value is below -10 dB. As illustrated in Figure 5.9 the lower upper cutoff frequencies are 27.6023 GHz and 28.3877 GHz respectively. Therefore, the proposed antenna achieves a radiation bandwidth of approximately 0.7854 GHz around the operating frequency of 28 GHz indicating reliable impedance matching and stable operation within the desired band.

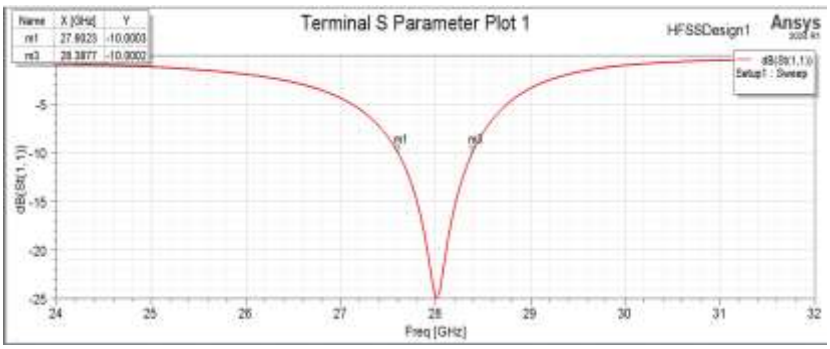


Figure 5. 9 The Radiation bandwidth of single band hexagonal 1×2 MPA

Radiation Efficiency

Radiation efficiency shows how much of the input power is actually radiated instead of being lost inside the antenna. In Figure 5.10, the 1×2 hexagonal patch antenna has a radiation efficiency of about 0.9799 (97.99 %) at 28 GHz which means the internal losses are low. Total efficiency also includes mismatch loss from the feed. At 28 GHz the total efficiency is about 0.9229 (92.29 %) showing the antenna still transfers and radiates power well making it suitable for 28 GHz operation.

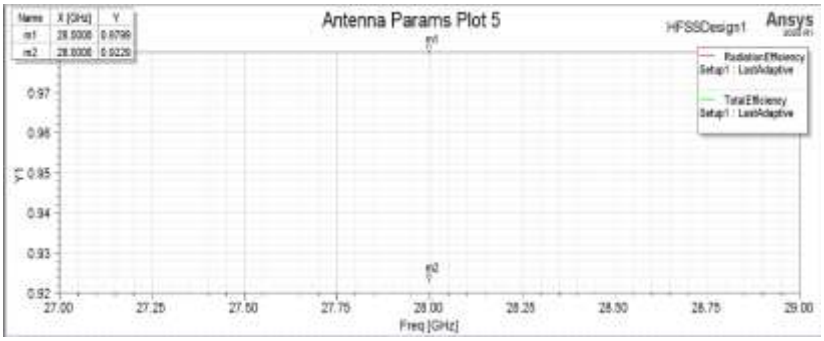


Figure 5. 10 The radiation efficiency and total efficiency of the single band hexagonal 1×2 MPA

VSWR (Voltage Standing Wave Ratio)

The standing wave ratio (VSWR) indicates how well the antenna is matched to the connected transmission line. It represents the ratio of maximum to minimum voltage along the line and has a theoretical range of $1 < \text{VSWR} < \infty$. In most antenna designs a VSWR below 2 is acceptable and values below 1.5 are considered very good. As shown in Figure 5.11 the proposed antenna exhibits a minimum active VSWR at the operating frequency of 28 GHz. The measured value VSWR value is 1.1192 which indicates good and acceptable impedance matching and efficient power transfer at the target frequency.

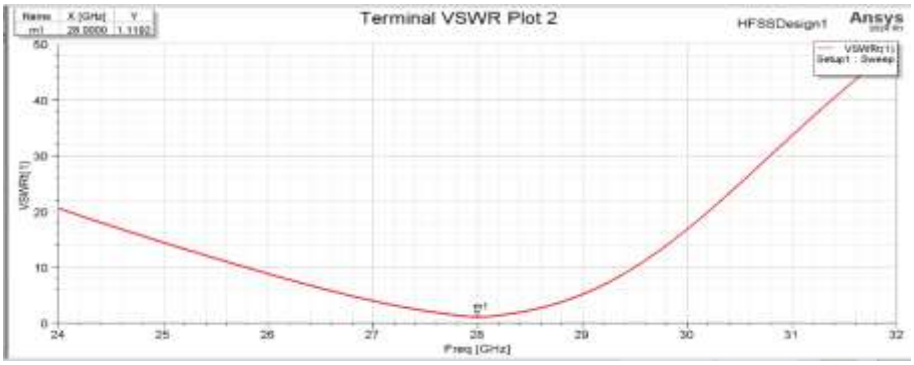


Figure 5. 11 The standing wave ratio of the single band hexagonal 1×2 MPA

Gain and Directivity

Gain and directivity are related directivity shows how focused the radiation is while gain also includes efficiency and losses. In Figure 5.12 the 1×2 hexagonal patch array has a clear main beam in the broadside direction at 28 GHz meaning it radiates mostly forward. The 3D pattern shows a maximum gain of about 10.35 dBi and the polar directivity plot confirms strong forward directivity with lower back radiation. Overall, the results show good directional performance for 28 GHz 5G use.

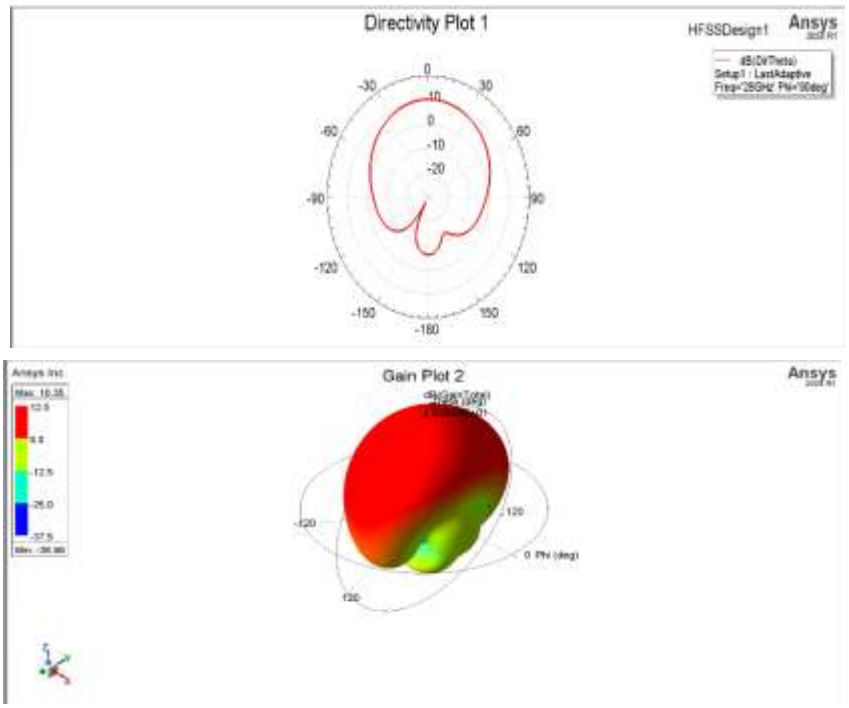


Figure 5. 12 The gain of hexagonal 1×2 MPA polar and 3D plot

5.1.3. Hexagonal 1 × 4 microstrip patch antenna array

Figure 5.13 indicates the designed hexagonal 1×4 microstrip patch antenna. To design a hexagonal patch, we used copper metal for both the ground and patch. The dielectric material substrate is Rogers RT Duroid 5880 with 0.254 mm heights. We stated different antenna parameters like return loss, bandwidth, gain and efficiency. To design a hexagonal antenna, we used edge feed techniques. The dimension is shown in Table 5.3.

Table 5. 3 Calculated dimension for hexagonal 1×4 microstrip patch antenna

Designed Antenna Parameters	Values (mm)
Substrate Height	0.254
Patch Width	4.23519
Effective relative permittivity	2.0576
Effective patch length	3.734
Patch Length Extension	0.1329
Patch Length	3.4682
Branch line width	0.789
Inter-Element Spacing	6.43
50 Ω quarter-wave transformer length	1.958
50 Ω quarter-wave transformer width	0.789
Inset feed length	0.918
Inset feed Width	0.45
Width of substrate	24.89476
Length of substrate	15.8064
Length of hexagon side	2.376
Area of regular hexagon	14.69
Flat to flat hexagon width	4.115
70.7 Ω quarter-wave transformer width	0.45
70.7 Ω quarter-wave transformer length	1.99
35.4 Ω quarter-wave transformer length	1.93
35.4 Ω quarter-wave transformer width	1.28

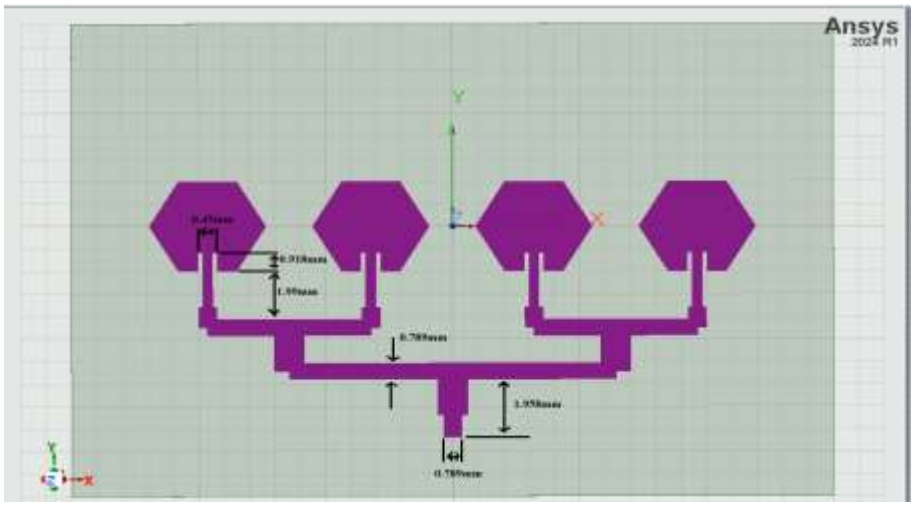


Figure 5. 13 The proposed design of single band hexagonal **1** × **4** MPA

Return Loss

Return loss describes how much of the input signal power is reflected back from the antenna instead of being radiated. For good antenna performance and efficient power transfer the return loss should be low. In practical an S_{11} value less than -10 dB is considered acceptable and indicates proper impedance matching. In the designed antenna this condition is clearly satisfied as shown in Figure 5.14. the simulated S_{11} curve exhibits a strong resonance at the operating frequency of 28 GHz where the return loss reaches about -14.6330 dB. This confirms that most of the input power is successfully delivered to the antenna with minimal reflection. The smooth shape of the S_{11} response around the resonance frequency indicates stable antenna behavior and good matching over the operating band. Therefore, the obtained return loss result demonstrates that the proposed antenna design is suitable for 28 GHz 5G applications.

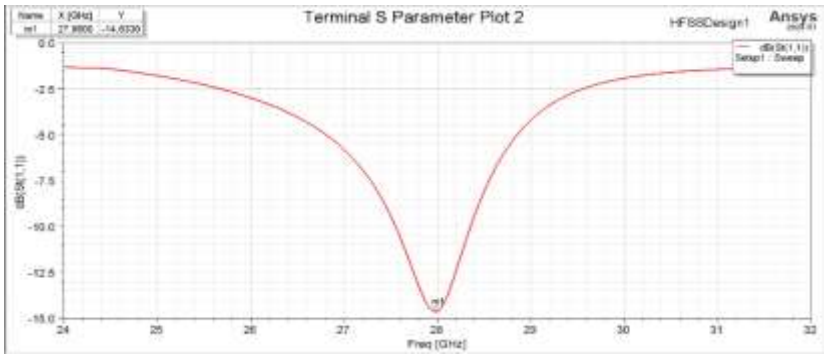


Figure 5. 14 The return loss of single band hexagonal $\mathbf{1 \times 4}$ MPA

Radiation Bandwidth

Radiation bandwidth is the frequency range over which the antenna operates effectively defined by the region where the S_{11} value is below -10 dB. As illustrated in Figure 5.15, the lower and upper cutoff frequencies are 27.5519 GHz and 28.3543 GHz respectively. Therefore, the proposed antenna achieves a radiation bandwidth of approximately 0.8024 GHz around the operating frequency of 28 GHz indicating reliable impedance matching and stable operation within the desired band.

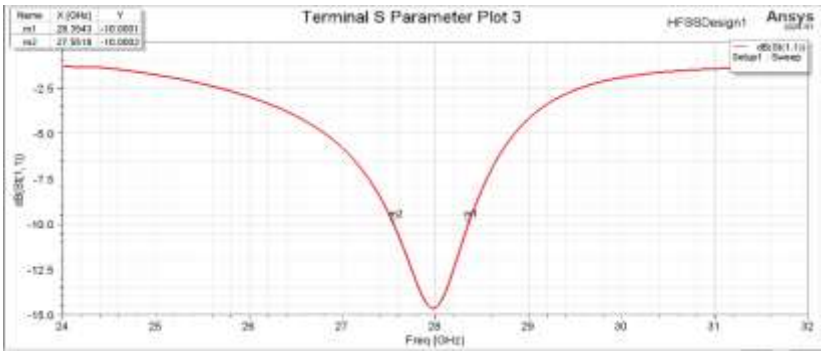


Figure 5. 15 The Radiation bandwidth of single band hexagonal $\mathbf{1 \times 4}$ MPA

Radiation Efficiency

Radiation efficiency describes how well an antenna converts the power it radiated electromagnetic waves. In other words, it shows how much of the input power is actually transmitted into free space instead of being lost inside the antenna due to material and conductor losses. Figure 5.16 presents the simulated radiation efficiency of the proposed antenna across the operating frequency range. At the operating frequency of 28 GHz the radiation efficiency is approximately 0.9674 which is equivalent to 96.74 %. This high value indicates that very little power is lost inside the antenna showing that the antenna structure and materials are highly efficiency. Total efficiency includes both radiation efficiency and losses caused by impedance mismatch between the antenna and the feeding network. At 28 GHz the total efficiency is about 0.9339 or 93.39 %. this result confirms that the antenna not only radiates power effectively but also maintains good impedance matching making it well suited for 5G millimeter-wave application.

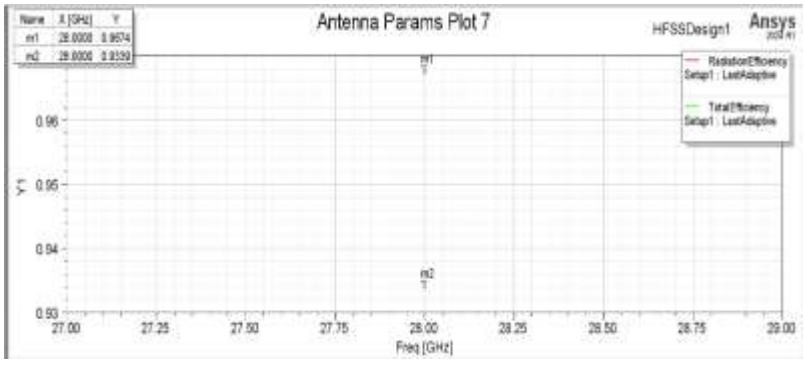


Figure 5. 16 The radiation efficiency and total efficiency of the single band hexagonal $\mathbf{1 \times 4}$ MPA

VSWR (Voltage Standing Wave Ratio)

The standing wave ratio (VSWR) indicates how well the antenna is matched to the connected transmission line. It represents the ratio of maximum to minimum voltage along the line and has a theoretical range of $1 < \text{VSWR} < \infty$. In practice a VSWR value less than 1.5 indicates good impedance matching. As shown in Figure 5.17, the proposed antenna exhibits a minimum active VSWR at the operating frequency of 28 GHz. The obtained value is 1.4574 which confirms good impedance matching and efficient power transfer at the desired frequency.

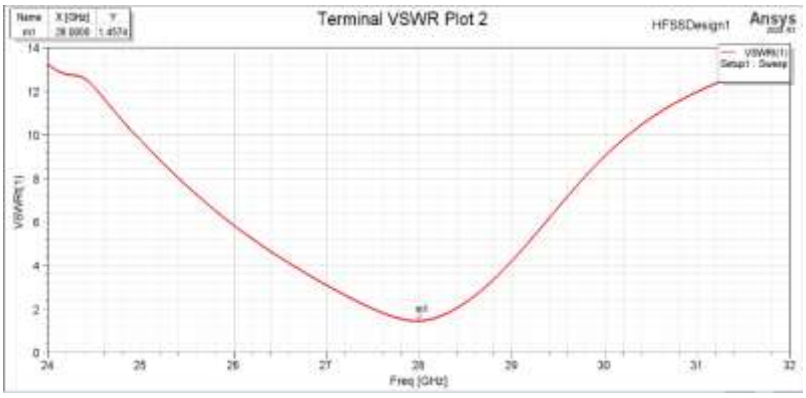
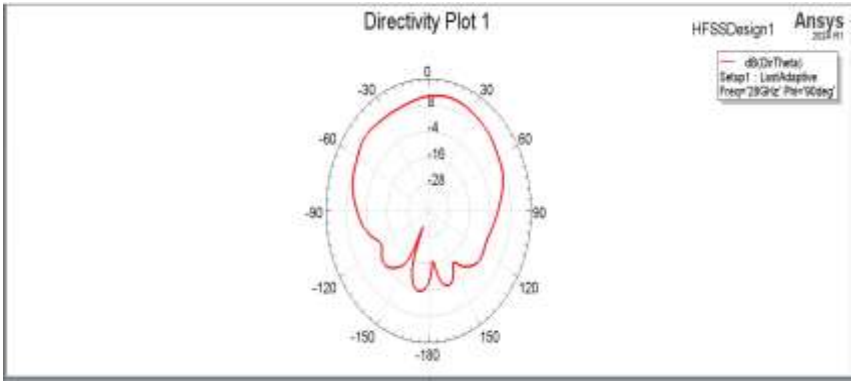


Figure 5. 17 The standing wave ratio of the single band hexagonal $\mathbf{1 \times 4}$ MPA

Gain and Directivity

Antenna gain shows how well the antenna sends energy in a specific direction compared to an ideal isotropic antenna. Directivity tells how focused the radiation is while gain also includes efficiency and losses. In Figure 5.18, the 3D gain pattern and the polar plot show a clear main beam in the broadside direction meaning the antenna radiates mainly forward. At 28 GHz the hexagonal 1×4 array reaches a maximum gain of about 12.96 dBi which confirm good directional performance fir 28 GHz 5G applications.



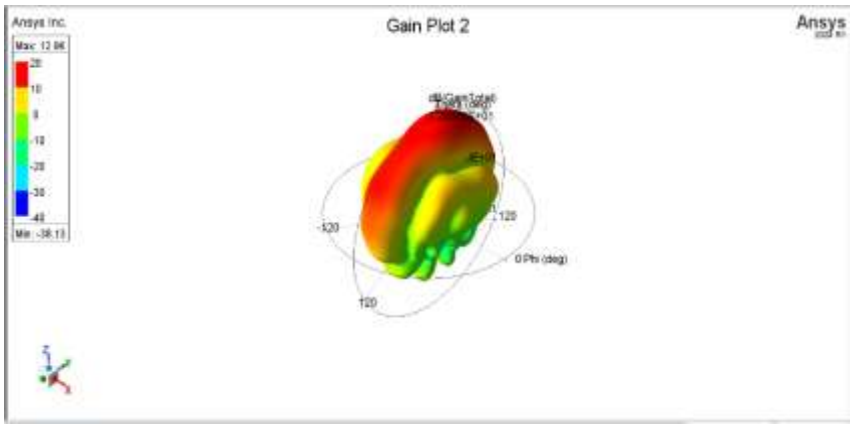


Figure 5. 18 The gain and directivity of hexagonal $\mathbf{1 \times 4}$ MPA polar and 3D plot

5.1.4. Hexagonal 1×4 microstrip patch antenna with CSRR

Figure 5,19 shows the proposed hexagonal 1×4 microstrip patch antenna array with a CSRR etched into the ground plane. Copper was used for both the patches and the ground, and the antenna was built on a Rogers RT/duroid 5880 substrate with a thickness of 0.254 mm. The design was evaluated using key performance measures such as return loss (S_{11}), bandwidth, gain, efficiency. The array was fed using a microstrip inset feed method to achieve proper matching around 28 GHz. The main geometric dimensions of the antenna and the CSRR are listed in table 5.4.

Table 5. 4 Calculated dimension for hexagonal 1×4 microstrip patch antenna with a CSRR

Designed Antenna Parameters	Values (mm)
Substrate Height	0.254
Patch Width	4.23519
Effective relative permittivity	2.0576
Effective patch length	3.734
Patch Length Extension	0.1329
Patch Length	3.4682
Branch line width	0.789
Inter-Element Spacing	6.43
50 Ω quarter-wave transformer length	1.958
50 Ω quarter-wave transformer width	0.789
Inset feed length	0.918
Inset feed Width	0.45
Width of substrate	24.89476
Length of substrate	15.8064
Length of hexagon side	2.376
Area of regular hexagon	14.69
Flat to flat hexagon width	4.115
70.7 Ω quarter-wave transformer width	0.45
70.7 Ω quarter-wave transformer length	1.99
35.4 Ω quarter-wave transformer length	1.93
35.4 Ω quarter-wave transformer width	1.28
External radius of the CSRR	1.03
Internal radius of the CSRR	0.63
Width of each complementation ring of the CSRR	0.2
Gap between the two complementary rings of CSRR	0.2
Split gap	0.2

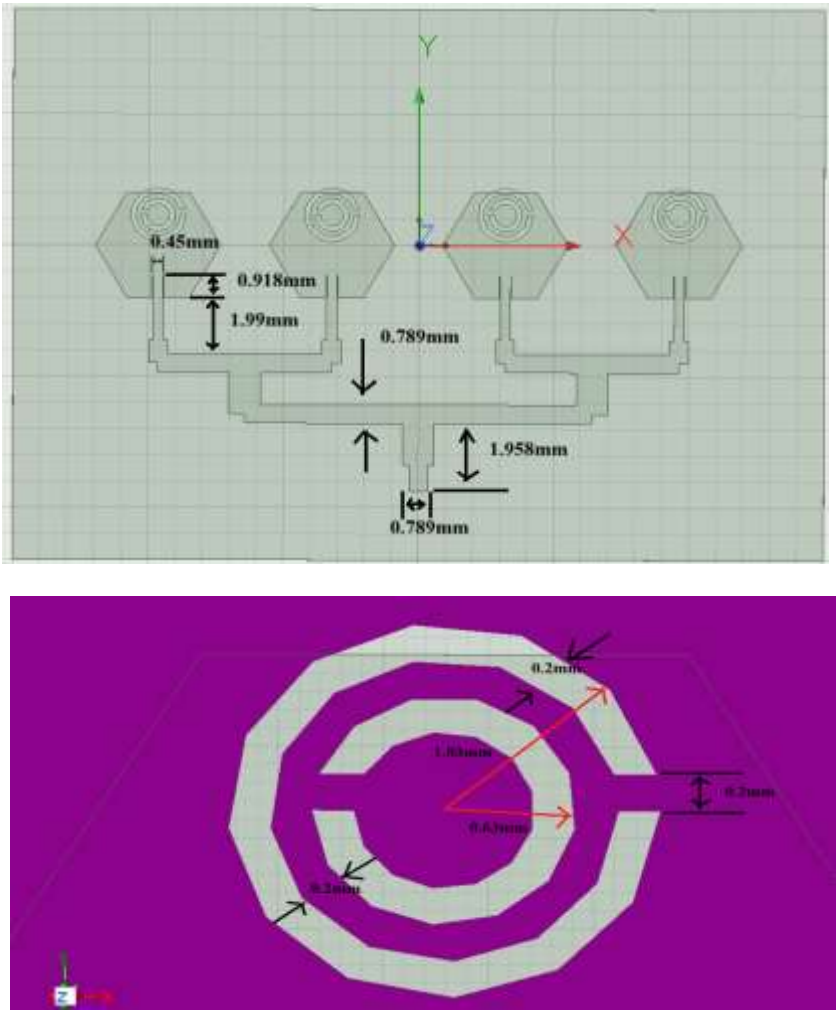


Figure 5. 19 The proposed design of single band hexagonal 1×4 MPA with a CSRR

Return Loss

Return loss shows how much of the input power is reflected back instead of being radiated. For good matching, engineers usually want S_{11} to be below -10 dB. In Figure 5.20, the proposed hexagonal 1×4 array with CSRR clearly meets this condition. The S_{11} curve has a strong resonance near 28 GHz and at about 28.01 GHz the return loss drops roughly -26.08 dB meaning very little power is reflected. The smooth shape around resonance also suggests stable matching so the antenna is suitable for 28 GHz 5G operation.

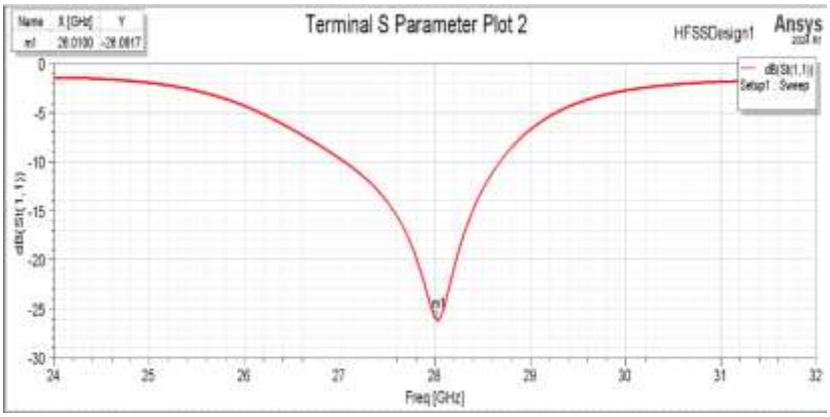


Figure 5. 20 The return loss of single band hexagonal 1×4 MPA with CSRR

The parametric sweep of the CSRR outer radius $\boldsymbol{r_{out}}$, presented in Appendix A, shows that changing $\boldsymbol{r_{out}}$ affects both the resonant frequency and the impedance matching behavior of the antenna. Based on this optimization result, $\boldsymbol{r_{out}} = 1.03\ mm$ was selected for the final design because it provides suitable matching around the target 28 GHz operating band while maintaining stable overall antenna performance.

Radiation Bandwidth

Impedance (radiation) bandwidth is the frequency range where the antenna is well matched usually defined by $S_{11} < -10\ dB$. In Figure 5.21, the lower and upper cutoff frequencies are 27.0431 GHz and 28.6811 GHz respectively. Therefore, the proposed antenna achieves a radiation bandwidth of approximately 1.638 GHz around the operating frequency of 28 GHz indicating reliable impedance matching and stable operation within the desired band.

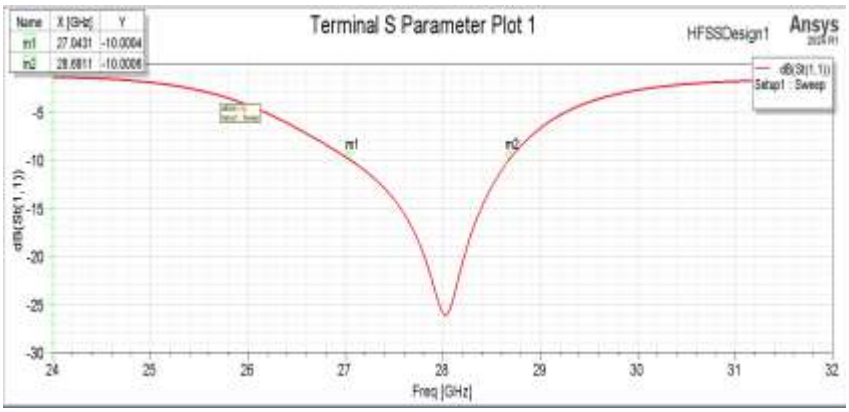


Figure 5. 21 The Radiation Bandwidth of single band hexagonal 1×4 MPA with CSRR

Radiation Efficiency

Radiation efficiency shows how much of the input power is actually radiated instead of being lost inside the antenna. As shown in Figure 5.22, the proposed hexagonal 1 × 4 array with CSRR has a radiation efficiency of about 0.9908 (99.08 %) at 28 GHz, which means internal losses are very small. Total efficiency also includes mismatch losses from the feed. At 28 GHz, the total efficiency is about 0.9883 (98.83 %) indicating the antenna is well matched and radiates very efficiently for 28 GHz 5G operation.

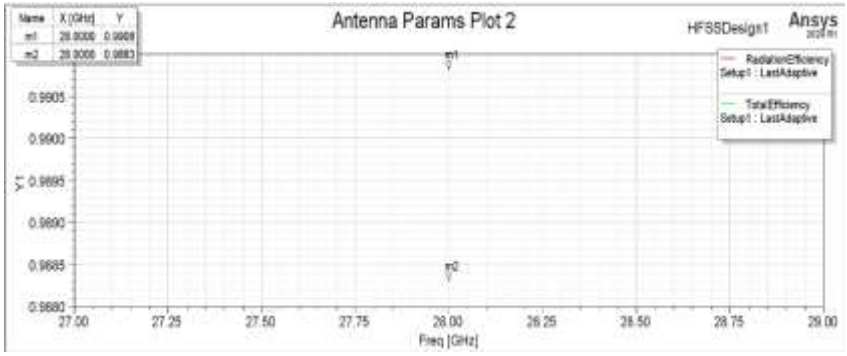


Figure 5. 22 The radiation efficiency and total efficiency of single band hexagonal 1×4 MPA with CSRR

VSWR (Voltage Standing Wave Ratio)

VSWR shows how well the antenna is matched to the feed line. A value close to 1 means very little power is reflected and values below about 1.5 are usually considered good. In Figure 5.23, the proposed hexagonal 1 × 4 array with CSRR reaches its minimum VSWR near 28 GHz. At about 28.01 GHz the VSWR is 1.1045 which indicates excellent matching and efficient power transfer at the target frequency.

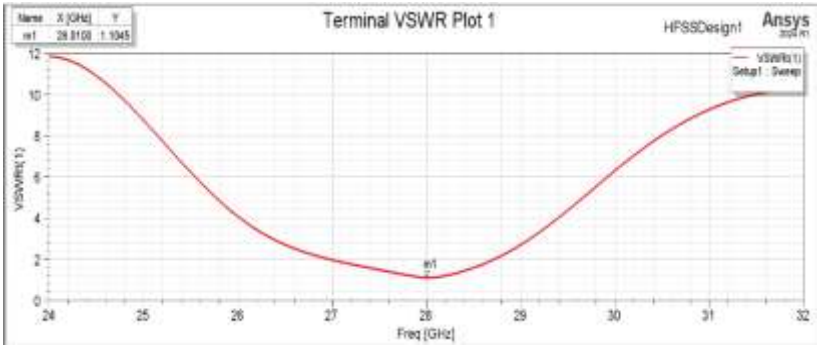


Figure 5. 23 The standing wave ratio of single band hexagonal 1×4 MPA with CSRR

Gain and Directivity

Antenna gain shows how well the antenna sends energy in a specific direction compared to an ideal isotropic antenna. Directivity tells how focused the radiation pattern is while gain also includes efficiency and losses. In Figure 5.24 3D gain plot and the polar pattern show a clear main beam pointing in the broadside direction. At 28 GHz the proposed hexagonal 1×4 array with CSRR reaches a maximum gain of about 12.88 dBi which confirms good directional performance for 28 GHz 5G use.

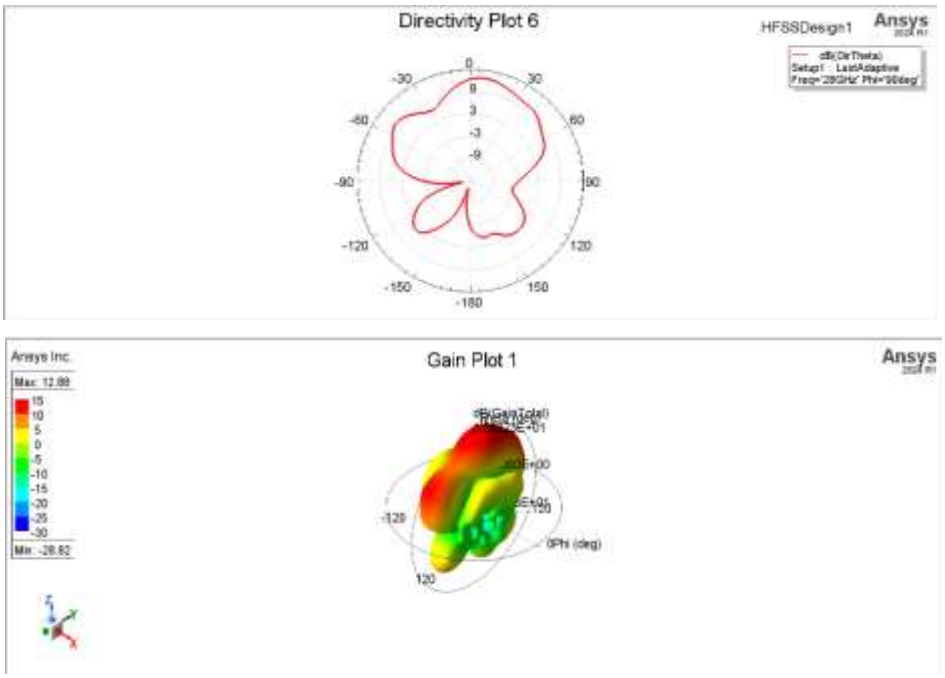


Figure 5. 24 The gain and directivity of hexagonal 1×4 MPA with CSRR polar and 3D plot

Surface current distribution

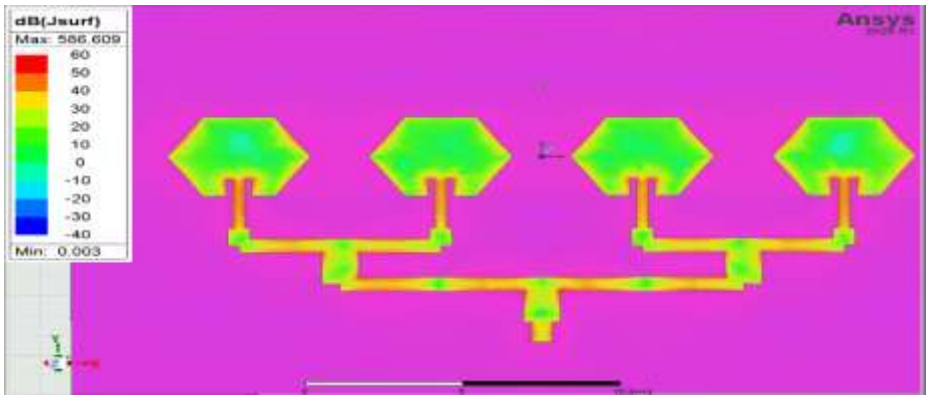


Figure 5. 25 Surface current distribution of the 1 × 4 hexagonal MPA array without CSRR at 28 GHz.

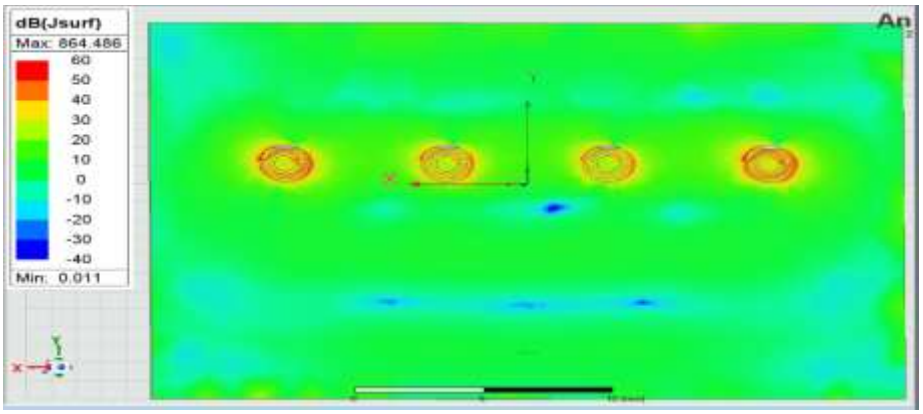


Figure 5. 26 Surface current distribution of the 1 × 4 hexagonal MPA array with CSRR at 28 GHz.

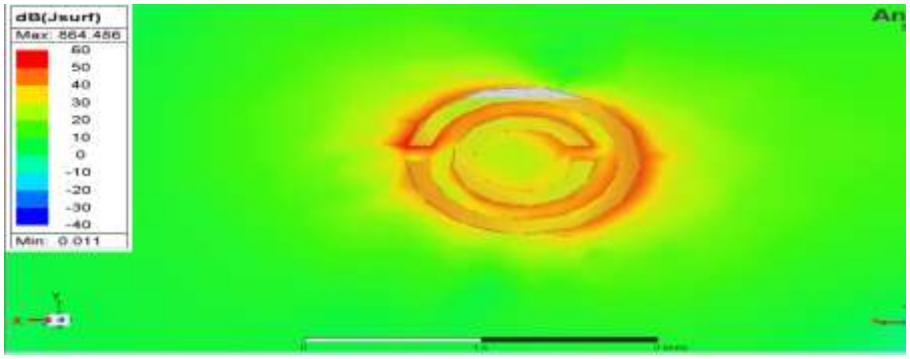


Figure 5. 27 Enlarged surface current distribution around the CSRR rings and split-gap region at 28 GHz.

The surface current distribution was examined to explain how the CSRR affects the antenna performance. For the conventional 1 × 4 hexagonal array without CSRR, the current is mainly concentrated along the corporate feed network and the patch-feed connection areas. However, after the CSRR is introduced into the ground plane, additional current concentration appears around the CSRR rings and split-gap regions at 28 GHz.

This shows that the CSRR is not only a structural modification, but it is electromagnetically coupled with the antenna. As a result, it affects the input impedance response of the antenna and helps create an additional resonance near the operating frequency. Therefore, the improvement in impedance bandwidth is mainly related to the CSRR-induced resonance, while the optimization process helps tune the final antenna response around 28 GHz.

A fabrication tolerance check was performed by changing the CSRR split gap around its final value. As shown in Appendix A, a ±0.05 mm change in g slightly affects the resonance position and S_{11}. However, the antenna still keeps acceptable matching near 28 GHz, which indicates that the proposed design can tolerate small fabrication variations.

5.1.5. Comparison of Single, 1 × 2 , and 1 × 4 Hexagonal Arrays with and Without CSRR

Table 5.5 compares the performance of the designed hexagonal antenna single element, 1 × 2 array and 1 × 4 array with and without the CSRR. The results show that adding the CSRR mainly improves the impedance bandwidth, reflection coefficient, and total efficiency. The realized gain, however, remains almost unchanged, with only a small decrease from 12.96 dBi to 12.88 dBi.

Table 5. 5 Comparison of Single, 1×2, and 1×4 Hexagonal Arrays With/Without CSRR

Ref.	Array Elements	Frequency (GHz)	Shape	Substrate	Thickness (mm)	Gain (dBi)	BW (GHz)	S_{11} (-dB)	η_{tot} (%)
This research	Single	28	hexagonal	Rogers RT5880	0.254	8.74	0.62	14.486	92.68
This research	1 × 2	28	hexagonal	Rogers RT5880	0.254	10.35	0.785	24.998	92.29
This research	1 × 4 without CSRR	28	hexagonal	Rogers RT5880	0.254	12.96	0.802	14.633	93.39
This research	1 × 4 with CSRR	28	hexagonal	Rogers RT5880	0.254	12.88	1.638	26	98.83

Table 5. 6 Percentage Improvement of Single, 1×2, and 1×4 Hexagonal Arrays With/Without CSRR

Ref.	Array Elements	Frequency (GHz)	Shape	Substrate	Thickness (mm)	Gain (%)	BW (%)
This research	Single	28	hexagonal	Rogers RT5880	0.254	0.0	0.0
This research	1 × 2	28	hexagonal	Rogers RT5880	0.254	18.42	26.613
This research	1 × 4 without CSRR	28	hexagonal	Rogers RT5880	0.254	48.28	29.035
This research	1 × 4 with CSRR	28	hexagonal	Rogers RT5880	0.254	47.37	164.19

5.2. Performance Comparison with Related Works

Table 5.6 compares the proposed 28 GHz 1×4 hexagonal array with other published 1×4 array antenna. Most of the referenced designs operate in a single band around 28 GHz but they use different shaped slot/ground modifications and substrate thicknesses which affects bandwidth and gain.

In this work, two versions are included to show the effect of CSRR. The baseline 1×4 hexagonal array (without CSRR) achieves about 12.96 dBi gain with about 0.8 GHz bandwidth $S_{11} = 14.63$ dB , and total efficiency around 93.39 %**.** After adding the double circular CSRR in the ground the antenna keeps a similar gain (=12.88 dBi) but the bandwidth increases strongly to about $1.638\ GHz$ $(27.04 - 28.68$ GHz), with better matching $(S_{11} = -26$dB) and higher total efficiency $(= 98.83$ %).

Overall, the comparison shows that CSRR integration mainly improves bandwidth and impedance matching while maintaining high realized gain, making the design suitable for 28 GHz 5G applications.

CHAPTER SIX

Conclusion and Future Work

6.1. Conclusion

This thesis discusses the design, simulation and performance analysis of a 28 GHz hexagonal microstrip patch antenna array for 5G application. Since 5G requires high data speed and wide bandwidth in the millimeter wave band the antenna must be small in size but still give high gain, good matching (S_{11}), wide bandwidth and high efficiency. The antenna performance is evaluated using key parameters such as return loss (S_{11}), bandwidth, gain and total efficiency.

First, a single hexagonal patch antenna was designed on Rogers RT/duroid 5880 substrate with thickness 0.254 mm. The simulation results show a gain of 8.74 dBi, bandwidth of 0.62 GHz, S_{11} of -14.486 dB and total efficiency of 92.68 %. Next, the design was extended to a 1×2 hexagonal array, which improved the performance. This 1×2 array achieved a gain of 10.35 dBi, bandwidth of 0.8 GHz, S_{11} of -24.998 dB and total efficiency of 92.29 %.

After that, a 1×4 hexagonal array without CSRR was designed to increase gain further. It achieved a gain of 12.96 dBi, bandwidth of 0.8 GHz, S_{11} of -14.633 dB total efficiency of 93.39 %. Finally, to improve bandwidth while keeping high gain, a complementary split ring resonator (CSRR) was added by cutting it into the ground plane of the 1×4 array. The final 1×4 array with (CSRR) achieved a gain of 12.88 dBi, a much higher bandwidth of 1.638 GHz, S_{11} of -26 dB and a very high total efficiency of 98.83 %.

All antenna designs were simulated using ANSYS HFSS. The final 1×4 CSRR-integrated array has a compact overall size of $30\ \text{mm} \times 21\ \text{mm} \times 0.254\ \text{mm}$, making it suitable for 28 GHz mmWave 5G systems. The results show that adding CSRR in the ground plane greatly improves bandwidth and efficiency, while keeping the gain almost the same, proving that the proposed design is a good option for 5G communication applications.

6.2. Future Work

In this work, a 28 GHz 1 × 4 hexagonal microstrip patch array was designed using a CSRR etched in the ground plane to increase bandwidth while keeping high realized gain for 5G applications. Although the antenna was evaluated using return loss, bandwidth, gain and efficiency there are still important areas that can be improved in future studies. The following research directions are recommended:

- Multi CSRR distribution under the 1 × 4 array instead of using one CSRR arrangement future work should place one tuned CSRR under each element (or use scaled CSRRs) and also test CSRRs between elements. This can create multiple nearby resonances that overlap and help widen the band further.
- Change the feeding technique: the current design uses a microstrip inset feed. Future studies can test other feeding methods such as corporate feed networks, aperture coupled or proximity coupled feeding which may improve matching and bandwidth at 28 GHz.
- Hybrid metamaterial approach: in addition to CSRR it is recommended to combine CSRR with other metamaterial structure such as AMC/HIS reflectors, EBG surfaces or DGS. A hybrid approach may improve bandwidth and gain together but the interaction between resonators should be studied carefully.
- MIMO/5G extension: future work should extend the design to dual polarized arrays or a 2 × 4 configuration and evaluate MIMO metrics such as ECC, diversity gain and channel capacity to confirm 5G system suitability.
- Experimental validation: the design should be fabricated and tested by measuring s parameters, radiation patterns and gain in an anechoic chamber. Simulation and measurement results should be compared and any differences should be explained using fabrication tolerance and material loss effects.

Reference

[1] N. Jayarenjini and C. Unni, “Hexagonal shaped microstrip patch antenna for satellite and military applications,” *Int. J. Eng. Adv. Technol.*, vol. 7, no. 5, pp. 101–105, 2018.

[2] K. Dinakaran, A. Anandkumar, M. Kathirvelu, N. Lavanya, S. Vanitha, and M. Indraja, “Design of hexagonal microstrip patch antenna,” *AIP Conf. Proc.*, vol. 2965, no. 1, pp. 1–8, 2024, doi: 10.1063/5.0212540.

[3] M. S. Rana, S. I. Islam, S. Al Mamun, L. K. Mondal, M. T. Ahmed, and M. M. Rahman, “An S-Band Microstrip Patch Antenna Design and Simulation for Wireless Communication Systems,” *Indones. J. Electr. Eng. Informatics*, vol. 10, no. 4, pp. 945–954, 2022, doi: 10.52549/ijeei.v10i4.4141.

[4] S. A. Refaat, H. A. Mohamed, A. M. Abdelhady, and A. S. S. Mohra, “A 28/38 GHz tuned reconfigurable antenna for 5G mobile communications,” *Indones. J. Electr. Eng. Comput. Sci.*, vol. 31, no. 1, pp. 248–258, 2023, doi: 10.11591/ijeecs.v31.i1.pp248-258.

[5] M. M. Soliman, M. L. Hakim, M. J. Uddin, M. M. A. Faisal, and A. Rahaman, “Optimization of Design Parameters of Microstrip Patch Antenna at 28 GHz and 38 GHz for 5G Applications,” *3rd IEEE Int. Conf. Telecommun. Photonics, ICTP 2019*, vol. 8, no. 10, pp. 341–352, 2019, doi: 10.1109/ICTP48844.2019.9041770.

[6] S. Pokhrel, “No TitleΕΛΕΝΗ,” *Αγαη*, vol. 15, no. 1, pp. 37–48, 2024.

[7] A. J. A. Al-Gburi, Z. Zakaria, I. M. Ibrahim, and E. B. A. Halim, “Microstrip Patch Antenna Arrays Design for 5G Wireless Backhaul Application at 3.5 GHz,” *Lect. Notes Electr. Eng.*, vol. 865, no. January, pp. 77–88, 2022, doi: 10.1007/978-981-16-9781-4_9.

[8] S. S. Al-Bawri, M. T. Islam, T. Shabbir, G. Muhammad, M. D. Shabiul Islam, and H. Y. Wong, “Hexagonal shaped near zero index (NZI) metamaterial based MIMO antenna for millimeter-wave application,” *IEEE Access*, vol. 8, pp. 181003–181013, 2020, doi: 10.1109/ACCESS.2020.3028377.

[9] M. Pant, L. Malviya, and V. Choudhary, “Performance Improvement of 28 GHz Antenna

Array for Fifth-Generation Wireless Communication System," *Lect. Notes Electr. Eng.*, vol. 777, pp. 371–380, 2022, doi: 10.1007/978-981-16-2761-3_35.

[10] M. Alsharari, R. Agravat, S. Lavadiya, A. Armghan, K. Aliqab, and S. K. Patel, "Design and development of hexagonal-shaped copper and liquid metamaterial-loaded superstrate patch antenna for 5G, WLAN, tracking and detection applications," *Ain Shams Eng. J.*, vol. 16, no. 1, 2025, doi: 10.1016/j.asej.2024.103236.

[11] R. H. Mahmud, "Terahertz Microstrip Patch Antennas For The Surveillance Applications," *Kurdistan J. Appl. Res.*, vol. 5, no. 1, pp. 16–27, 2020, doi: 10.24017/science.2020.1.2.

[12] A. G. S. A. Gaid, M. A. M. Ali, A. Saif, and W. A. A. Mohammed, "Design and analysis of a low profile, high gain rectangular microstrip patch antenna for 28 GHz applications," *Cogent Eng.*, vol. 11, no. 1, p., 2024, doi: 10.1080/23311916.2024.2322827.

[13] A. B. Devarapalli and T. Moyra, "Design of a Metamaterial Loaded W-shaped Patch Antenna with FSS for Improved Bandwidth and Gain," *Silicon*, vol. 15, no. 4, pp. 2011–2024, 2023, doi: 10.1007/s12633-022-02123-6.

[14] Y. S. H. Khraisat, "Design of 4 elements rectangular microstrip patch antenna with high gain for 2.4 GHz applications," *Mod. Appl. Sci.*, vol. 6, no. 1, pp. 68–74, 2012, doi: 10.5539/mas.v6n1p68.

[15] S. Basu, A. Srivastava, and A. Goswami, "□ Dual Frequency Hexagonal Microstrip Patch Antenna," *Int. J. Sci. Res. Publ.*, vol. 3, no. 11, pp. 1–9, 2013, [Online]. Available: www.ijsrp.org

[16] S. Palanisamy, B. Thangaraju, O. I. Khalaf, Y. Alotaibi, S. Alghamdi, and F. Alassery, "A novel approach of design and analysis of a hexagonal fractal antenna array (Hfaa) for next-generation wireless communication," *Energies*, vol. 14, no. 19, pp. 1–18, 2021, doi: 10.3390/en14196204.

[17] N. Vikram, R. S. Sabeenian, M. Nandhini, and V. Visweeshwaran, "Design and Implementation of Microstrip Patch Antenna for Biomedical Application," *Lect. Notes*

Networks Syst., vol. 471, pp. 613–620, 2023, doi: 10.1007/978-981-19-2535-1_47.

[18] W. Jan Krzysztofik and T. Nghia Cao, "Metamaterials in Application to Improve Antenna Parameters," *Metamaterials and Metasurfaces*, 2019, doi: 10.5772/intechopen.80636.

[19] M. S. Alshulle and A. Omar, "Scientific International Conference in Science & Engineering Metamaterial Based Microstrip Patch Antenna Design for 5G / WiFi Wireless Technology applications .," no. January 2014, pp. 288–292, 2024.

[20] B. Ajewole, P. Kumar, and T. Afullo, "A Microstrip Antenna Using I-Shaped Metamaterial Superstrate with Enhanced Gain for Multiband Wireless Systems," *Micromachines*, vol. 14, no. 2, 2023, doi: 10.3390/mi14020412.

[21] J. Colaco and R. B. Lohani, "Metamaterial based multiband microstrip patch antenna for 5G wireless technology-enabled IoT devices and its applications," *J. Phys. Conf. Ser.*, vol. 2070, no. 1, 2021, doi: 10.1088/1742-6596/2070/1/012116.

[22] F. Dad, "Performance Analysis of Micro Strip Patch Antenna at 2.4 GHz using Metamaterial," *Int. J. Eng. Work.*, vol. 06, no. 09, pp. 269–274, 2019, doi: 10.34259/ijew.19.609269274.

[23] Y. Natali and M. Larasati, "Gain Enhancement Using Stub and Stacked Hexagon Microstrip Antenna for 5G Communication," *Proc. - 2019 Int. Conf. Radar, Antenna, Microwave, Electron. Telecommun. ICRAMET 2019*, pp. 49–52, 2019, doi: 10.1109/ICRAMET47453.2019.8980392.

[24] R. A. Kadhim, "Hexagon-shaped Patch and Array Antenna at 28GHz for Improving the Performance of 5G Technology," vol. 32, no. 3, 2024.

[25] O. Darboe, J. Kenyatta, F. Manene, D. Konditi, D. Bernard, and O. Konditi, "A 28 GHz Rectangular Microstrip Patch Antenna for 5G Applications," *Int. J. Eng. Res. Technol.*, vol. 12, no. 6, pp. 854–857, 2019, [Online]. Available: http://www.irphouse.com

[26] M. A. Yusuf and M. H. Ali, "A Bandwidth-Enhanced Compact Microstrip Rectangular Patch Antenna Based on CSRRS for 5G Applications," vol. 32, no. 2, 2025.

[27] P. Kumawat and S. Joshi, “A Novel Dual-Band Orthogonal Polarized Elliptical Patch Antenna Array for 5G Applications,” vol. 65, no. 3, pp. 184–190, 2021, doi: 10.37398/JSR.2021.650322.

[28] S. E. Didi, I. Halkhams, M. Fattah, Y. Balboul, S. mazer, and M. El Bekkali, “Design of a microstrip antenna patch with a rectangular slot for 5G applications operating at 28 GHz,” *Telkomnika (Telecommunication Comput. Electron. Control.*, vol. 20, no. 3, pp. 527–536, 2022, doi: 10.12928/TELKOMNIKA.v20i3.23159.

[29] M. M. Kamal *et al.*, “A novel hook-shaped antenna operating at 28 ghz for future 5g mmwave applications,” *Electron.*, vol. 10, no. 6, pp. 1–10, 2021, doi: 10.3390/electronics10060673.

[30] A. A. Ibrahim, H. Zahra, O. M. Dardeer, N. Hussain, S. M. Abbas, and M. A. Abdelghany, “Slotted Antenna Array with Enhanced Radiation Characteristics for 5G 28 GHz Communications,” *Electron.*, vol. 11, no. 17, pp. 1–13, 2022, doi: 10.3390/electronics11172664.

[31] S. Talari and P. Chandra Sekhar, “A High Gain Dual Band Hexagonal Metamaterial Inspired Antenna for 5G Applications,” *Eng. Technol. Appl. Sci. Res.*, vol. 14, no. 6, pp. 18029–18035, 2024, doi: 10.48084/etasr.8575.

[32] I. Khouyaoui, M. Hamdaoui, M. Elbathaoui, and J. Foshi, “Optimizing Rectangular Patch Antenna Arrays for Enhanced 5G Communication,” *EPJ Web Conf.*, vol. 330, pp. 5–10, 2025, doi: 10.1051/epjconf/202533004004.

[33] M. M. Soliman, A. Z. M. Imran, and K. S. Ullah, “Highly Efficient 2×2 Antenna Array at 28 GHz and 38 GHz for 5G Applications,” *ICIET 2019 - 2nd Int. Conf. Innov. Eng. Technol.*, pp. 23–24, 2019, doi: 10.1109/ICIET48527.2019.9290692.

[34] S. Ermiş and M. Demirci, “Improving the Performance of Patch Antenna by Applying Bandwidth Enhancement Techniques for 5G Applications,” *Teh. Glas.*, vol. 17, no. 3, pp. 305–312, 2023, doi: 10.31803/tg-20220819001236.

[35] D. Mungur and S. Duraikannan, “Design and Analysis of 28 GHz Millimeter Wave

Antenna Array for 5G Communication Systems," *J. Sci. Technol. Eng. Manag. Res. Innov. ISSN*, vol. 1, no. 3, p. 10, 2018.

[36] A. Aboshosha, M. B. El-Mashade, and E. A. Hegazy, "Design and Analysis of Rectangular Microstrip Patch Array Antenna on 28 GHz Band for Future of 5G," *Res. Anthol. Dev. Optim. 5G Networks Impact Soc.*, vol. 17, pp. 25–43, 2021, doi: 10.4018/978-1-7998-7708-0.ch002.

[37] M. J. Uddin, "Performance Analysis of Microstrip Patch Antenna Array for 28GHz Submitted By Md Golam Rabbani Nayeem T191069 Department of Electronic & Telecommunication Engineering," 2024.

[38] H. Ullah and F. A. Tahir, "A broadband wire hexagon antenna array for future 5G communications in 28 GHz band," *Microw. Opt. Technol. Lett.*, vol. 61, no. 3, pp. 696–701, 2019, doi: 10.1002/mop.31613.

[39] K. A. Fante and M. T. Gemeda, "Broadband microstrip patch antenna at 28 GHz for 5G wireless applications," *Int. J. Electr. Comput. Eng.*, vol. 11, no. 3, pp. 2238–2244, 2021, doi: 10.11591/ijece.v11i3.pp2238-2244.

[40] M. Tegegn Gemeda, K. A. Fante, H. L. Goshu, and A. L. Goshu, "Design and Analysis of a 28 GHz Microstrip Patch Antenna for 5G Communication Systems," *Int. Res. J. Eng. Technol.*, pp. 881–886, 2021, [Online]. Available: www.irjet.net

[41] M. Ganesh, N. S. Raghava, and T. Sabapathy, "Design a hexagonal shape frequency reconfigurable antenna for new C-band 5G applications," *2022 IEEE Int. Conf. Electron. Comput. Commun. Technol. CONECCT 2022*, pp. 2–6, 2022, doi: 10.1109/CONECCT55679.2022.9865714.

[42] A. Dixit, A. Kumar, and A. Kumar, "A wideband SIW hexagonal patch antenna for 5G millimeter-wave applications," *2021 IEEE Indian Conf. Antennas Propagation, InCAP 2021*, pp. 248–251, 2021, doi: 10.1109/InCAP52216.2021.9726457.

[43] A. B. Obot, G. A. Igwue, and K. M. Udofia, "Design and Simulation of Rectangular Microstrip Antenna Arrays for Improved Gain Performance," *Int. J. Networks Commun.*,

vol. 2019, no. 2, pp. 73–81, 2019, doi: 10.5923/j.ijnc.20190902.02.

[44] C. This and T. Views, “1 × 4 Patch Array Antenna for 28GHz 5G Millimeter-wave Communication,” pp. 12–13, 2023, doi: 10.1109/ICCIT60459.2023.10441552.

[45] S. Agarwal, “High Gain Linear 1 × 4 X-slotted Microstrip Patch Antenna Array for 5G Mobile Technology,” no. 2, pp. 2–7, 2020.

[46] V. Prakasam and N. B. Reddy, “Hexagonal Shaped Micro-strip Patch Antenna Design for 2.45 GHz WLAN System,” *Proc. 6th Int. Conf. Inven. Comput. Technol. ICICT 2021*, pp. 13–18, 2021, doi: 10.1109/ICICT50816.2021.9358687.

[47] S. B. Rana and H. Kaur, “Design and fabrication of hexagonal antenna for wireless applications,” *Int. J. Inf. Technol.*, vol. 12, no. 2, pp. 447–452, 2020, doi: 10.1007/s41870-018-0234-9.

[48] A. M. Saini Tech Student and A. Kushwaha, “Design of Hexagonal Microstrip Patch Antenna with CPW Feeding & Comparison Analysis with other Patch Antenna,” *Int. J. Rev. Electron. Commun. Eng.*, vol. 4, no. April, pp. 20–23, 2016, [Online]. Available: http://ijrece.org

[49] S. Kim, “Design and Analysis of Dual Polarized Broadband Microstrip Patch Antenna for 5G mmWave Antenna Module on FR4 Substrate,” no. April, pp. 64306–64316, 2021, doi: 10.1109/ACCESS.2021.3075495.

[50] H. Dejene, “Study on received signal strength of femtocell with circular and rectangular microstrip patch antenna designed at 2.55 GHz,” *Sci. Tech. J. Inf. Technol. Mech. Opt.*, vol. 22, no. 2, pp. 348–354, 2022, doi: 10.17586/2226-1494-2022-22-2-348-354.

[51] “Multiband Phased Array Antenna for 5G Mobile Handsets Multiband Phased Array Antenna for 5G Mobile Handsets,” 2022.

[52] a T. Submitted, I. N. Partial, O. F. The, R. For, and T. H. E. Degree, “DESIGN , TESTING AND ASSEMBLY OF RECTANGULAR PATCH ANTENNA Master of Technology in Department of Electrical Engineering National Institute of Technology DESIGN , TESTING AND ASSEMBLY OF RECTANGULAR PATCH ANTENNA

Master of Technology in Department of Elect," 2007.

[53] S. R. Patch and C. Systems, "Jimma University School of Postgraduate Program Jimma Institute of Technology," 2021.

[54] B. Institut Dresden, S. Author, and M. Tascioglu, "Theoretical Analysis, Simulation and Development of Antenna Arrays for mm-Wave Systems," no. May, 2021.

[55] T. Watro Wata, "Design and Performance Analysis of PIFA Microstrip Antenna Array at mmWave for MIMO Cellular Radio Communication," no. January, 2022, doi: 10.13140/RG.2.2.19015.27047.

[56] A. SYNAK, "Erasmus Student Exchange Project: Design and Implementation of Uhf Patch Antenna," 2014, [Online]. Available: https://core.ac.uk/download/41813223.pdf

[57] M. Moftah and H. Yousiff, "Size Reduction of Square Microstrip Patch Antenna by Using Metamaterials Structure," no. July, 2018.

[58] KITUR STANLEY KIBET [B.Ed., "Design and Fabrication of Aperture Coupled Microstrip," 2013.

[59] T. P. Dave, "Design and Analysis of Compact Microstrip Patch Antenna for LTE Applications Using Metamaterials," *Gujarat Technol. Univ.*, no. 149997111015, 2020.

[60] R. Rani, P. Kaur, and N. Verma, "Metamaterials and their applications in patch antenna: A review," *Int. J. Hybrid Inf. Technol.*, vol. 8, no. 11, pp. 199–212, 2015, doi: 10.14257/ijhit.2015.8.11.17.

[61] V. Subramanian, "DESIGN OF METAMATERIAL BASED PATCH ANTENNA DEPARTMENT OF ELECTRICAL ENGINEERING INDIAN INSTITUTE OF TECHNOLOGY MADRAS CHENNAI – 600036," no. May, 2014.

[62] "Circular Patch Partial and Slotted Ground with rectangular CSRR Metamaterial Antenna for Wireless Application Thesis Master of Technology," 2018.

[63] R. Kumar Yadav, J. Kishor, and R. Lal Yadava, "Design of Hexagonal Patch Antenna for Mobile Wireless System Design of Hexagonal Patch Antenna for Mobile Wireless

Systems," *Ijstm, 2011*, vol. 2, no. 4, pp. 34–38, 2011, [Online]. Available: www.ijstm.com

[64] A. J. Wiley, *ANTENNA THEORY ANALYSIS AND DESIGN THIRD EDITION*.

[65] F. Falcone *et al.*, "Effective Negative- " Stopband Microstrip Lines Based on Complementary Split Ring Resonators," vol. 14, no. 6, pp. 280–282, 2004.

[66] R. Baee, G. Dadashzadeh, and F. G. Kharakhili, "Using of CSRR and its Equivalent Circuit Model in Size Reduction of Microstrip Antenna," pp. 457–460, 2007.

Appendix A
HFSS Model Construction and Meshing Setup

HFSS 3D Model Views

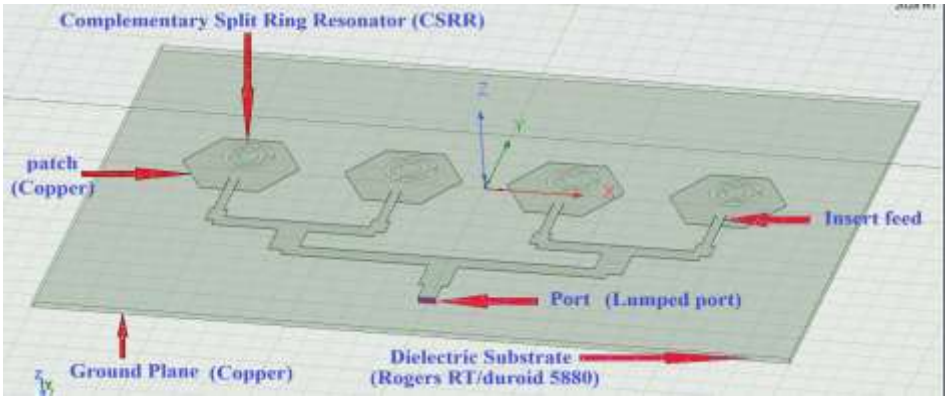


Figure A. 1 Overall 3D model of the hexagonal MPA array (patch, substrate, ground, feed network, and CSRR)

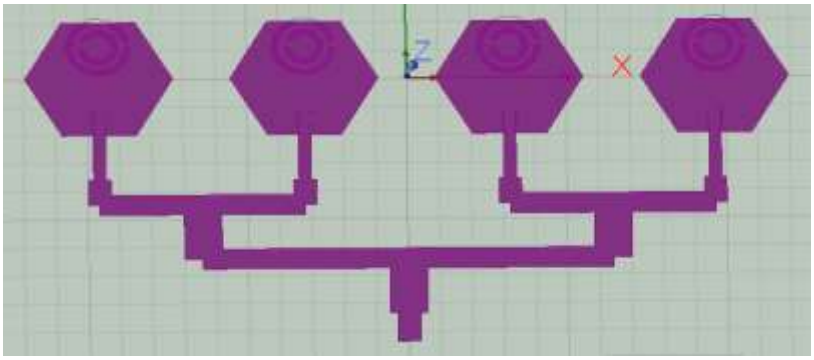


Figure A. 2 Top view of the hexagonal MPA array (patch and feed network)

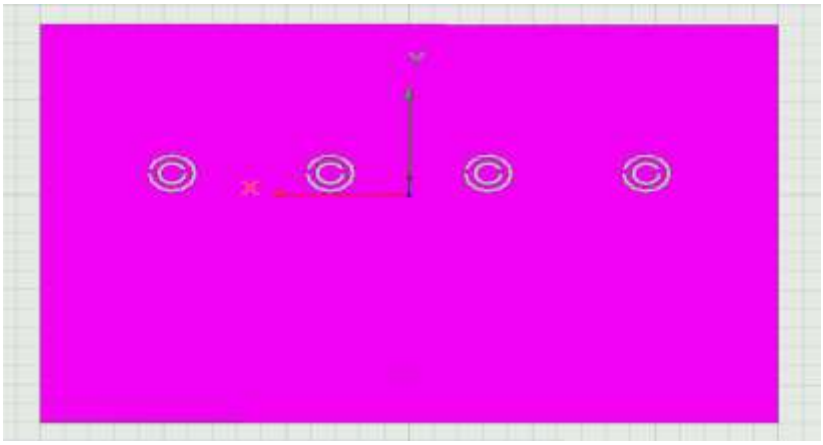


Figure A. 3 Bottom view of the antenna (ground plane and CSRR structure)

A.2 HFSS Mesh Distribution and Refinement Views

This appendix provides supplementary HFSS simulation results and model views that support the antenna design and analysis presented in the main chapters. It includes 3D geometry and meshing views of the proposed 1 × 4 hexagonal microstrip patch antenna with the double circular CSRR structure. These figures are added to clearly demonstrate how the model was constructed and how the meshing strategy was applied during the simulation.

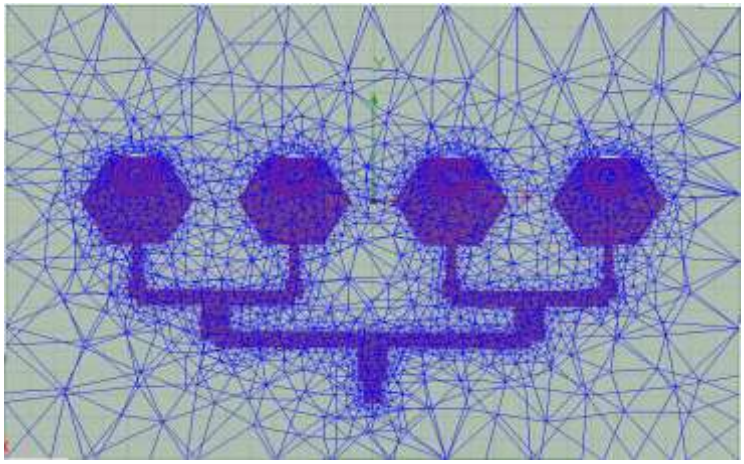


Figure A. 4 Global Mesh Distribution Over the Hexagonal Patch Geometry

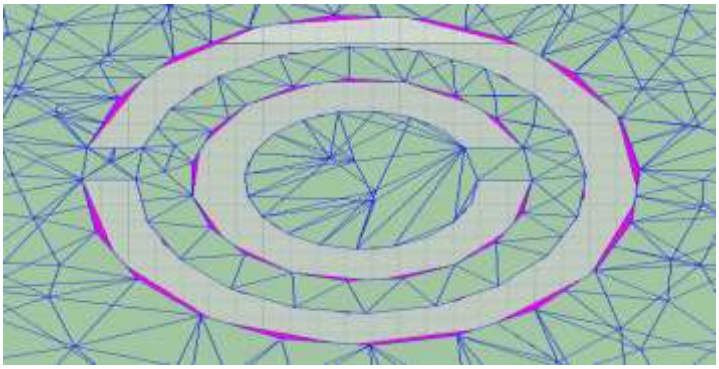


Figure A. 5 Localized Mesh Refinement on the CSRR Unit Cells.

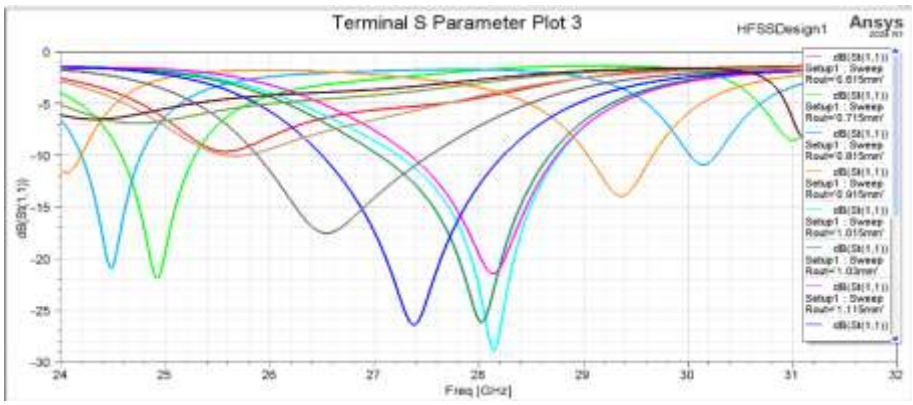


Figure A. 6 Parametric analysis of CSRR outer radius r_{out} on the reflection coefficient $\mathbf{S_{11}}$ of the proposed 1 × 4 CSRR-loaded hexagonal microstrip antenna array

Figure A.6 shows the HFSS parametric sweep performed to study the effect of changing the CSRR outer radius r_{out}. This sweep was used during the optimization process to examine how r_{out} influences the antenna response and supports the selection of the final CSRR dimensions.

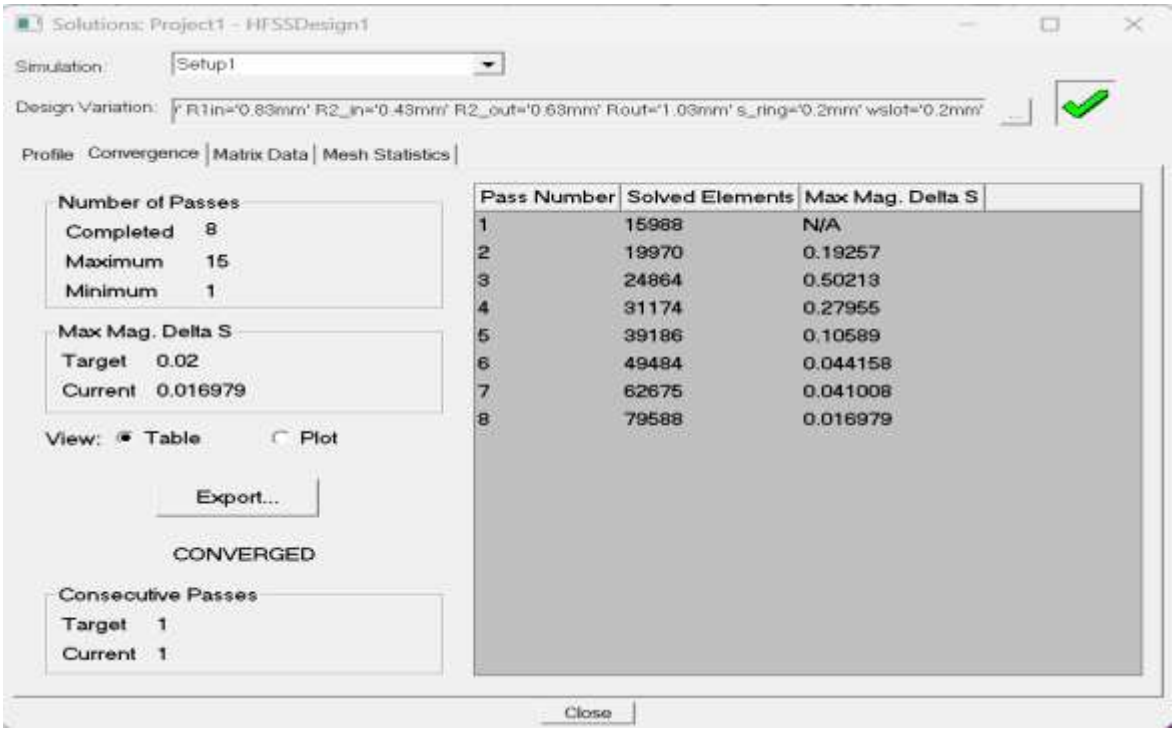


Figure A. 7 HFSS adaptive mesh convergence result for the final 1 × 4 CSRR-loaded hexagonal microstrip antenna array

Figure A.7 presents the adaptive mesh convergence result of the final antenna model. The simulation converged after eight adaptive passes, with a final maximum magnitude delta S of 0.016979, which is below the target value of 0.02. This confirms that the HFSS result is stable enough for final antenna performance analysis.

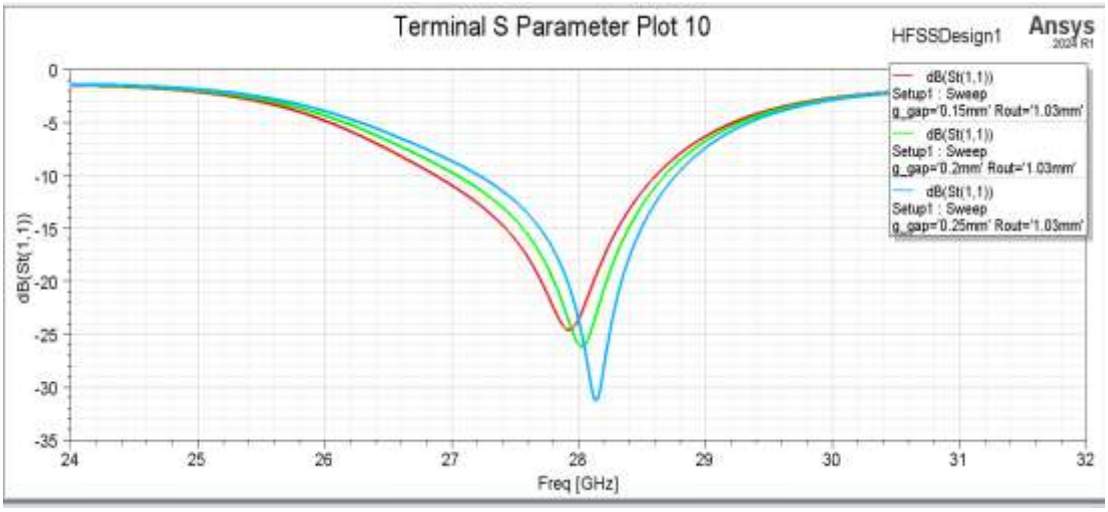


Figure A. 8 Fabrication tolerance analysis of the CSRR split gap g and its effect on the reflection coefficient $\mathbf{S_{11}}$

Figure A.8 shows the fabrication tolerance analysis of the CSRR split gap **g**. The gap was changed from 0.15 mm to 0.25 mm while $\boldsymbol{r_{out}}$ was kept constant at 1.03 mm. The result indicates that small gap variations slightly affect the resonant frequency and $\mathbf{S_{11}}$ depth, but the antenna still keeps good impedance matching around the desired 28 GHz band.

Appendix B

HFSS simulation setup and Optimized Antenna Dimensions

Table 6. 1 HFSS Simulation Settings Used in This Work

Setting Category	Parameter	Value used
Solution setup	Solution type	Driven Modal
Frequency setup	Center frequency	28 GHz
Frequency setup	Sweep range	24-32 GHz
Boundary conditions	Radiation/PML	Radiation boundary
Mesh configuration	Convergence criteria	Enabled
Excitation/port	Port type	Lumped port
Mesh configuration	Adaptive meshing	Enabled
Mesh configuration	Max adaptive passes	15
Simulation accuracy	Mesh refinement region	CSRR + feed region
Mesh configuration	Maximum element length	1.6mm
Mesh configuration	Maximum delta S	0.02
Frequency setup	Sweep type	Interpolating

Table 6. 2 Initial Calculated and Optimized Values of the Proposed Single Hexagonal MPA

Designed Antenna Parameters	Initial Values (mm)	Optimized Values (mm)
Length of Inset Feed	0.918	1.0256
Width of Inset Feed	0.45	0.44
Length of hexagon side	2.376	2.29
Flat to flat hexagon width	4.115	3.969
Width of substrate	5.759	15
Length of substrate	4.992	12
Insert feed gap	0.2	0.28
Inter-Element Spacing	5.35	6.43
50 Ω Feed width	0.794	0.7
50 Ω Feed length	1.958	3
70.7 Ω matching width	0.45	0.44
70.7 Ω matching length	1.99	1.006

Table 6. 3 Initial Calculated and Optimized Values of the Proposed 1×2 Hexagonal MPA Array.

Designed Antenna Parameters	Initial Values (mm)	Optimized Values (mm)
Length of Inset Feed	0.918	1.084
Width of Inset Feed	0.45	0.453
Length of hexagon side	2.376	2.31
Flat to flat hexagon width	4.115	4.001
Width of substrate	16.425	15
Length of substrate	15.8064	10
50 Ω quarter-wave transformer width	0.789	0.789
50 Ω quarter-wave transformer length	1.958	0.685
70.7 Ω quarter-wave transformer width	0.45	0.453
70.7 Ω quarter-wave transformer length	1.99	2.006

Table 6. 4 Initial Calculated and Optimized Values of the Proposed 1×4 Hexagonal MPA Array.

Designed Antenna Parameters	Initial Values (mm)	Optimized Values (mm)
Length of Inset Feed	0.918	0.823
Width of Inset Feed	0.45	0.38
Length of hexagon side	2.376	2.29
Flat to flat hexagon width	4.115	3.966
Width of substrate	24.89476	30
Length of substrate	15.8064	21
Branch line width	0.789	0.7
50 Ω quarter-wave transformer width	0.789	0.7
50 Ω quarter-wave transformer length	1.958	1
70.7 Ω quarter-wave transformer width	0.45	0.38
70.7 Ω quarter-wave transformer length	1.99	1.627
35.4 Ω quarter-wave transformer width	1.281	1.17
35.4 Ω quarter-wave transformer length	1.93	1.59

Table 6. 5 Initial Calculated and Optimized Values of the Proposed 1×4 Hexagonal MPA Array with CSRR.

Designed Antenna Parameters	Initial Values (mm)	Optimized Values (mm)
Length of Inset Feed	0.918	0.8466
Width of Inset Feed	0.45	0.38
Length of hexagon side	2.376	2.317
Flat to flat hexagon width	4.115	4.013
Width of substrate	24.89476	30
Length of substrate	15.8064	21
Branch line width	0.789	0.7
50 Ω quarter-wave transformer width	0.789	0.7
50 Ω quarter-wave transformer length	1.958	1
70.7 Ω quarter-wave transformer width	0.45	0.38
70.7 Ω quarter-wave transformer length	1.99	1.6035
35.4 Ω quarter-wave transformer width	1.281	1.17
35.4 Ω quarter-wave transformer length	1.93	1.59
External radius of the CSRR	Initial trial value in HFSS Optimetrics	1.03
Internal radius of the CSRR	Initial trial value in HFSS Optimetrics	0.63
Width of each complementation ring of the CSRR	Initial trial value in HFSS Optimetrics	0.2
Gap between the two complementary rings of CSRR	Initial trial value in HFSS Optimetrics	0.2
Split gap	Initial trial value in HFSS Optimetrics	0.2